

SATURABLE NONLINEARITY AND STABLE
MULTI-DIMENSIONAL OPTICAL SOLITONS

A Dissertation

Presented to the Faculty of the Graduate School

of Cornell University

in Partial Fulfillment of the Requirements for the Degree of

Doctor of Philosophy

by

Yi-Fan Chen

May 2005

© 2005 Yi-Fan Chen

ALL RIGHTS RESERVED

SATURABLE NONLINEARITY AND STABLE MULTI-DIMENSIONAL OPTICAL SOLITONS

Yi-Fan Chen, Ph.D.

Cornell University 2005

Stable multi-dimensional optical solitons have been predicted to exist in saturable instantaneous Kerr-like nonlinear systems for many years. The experimental observation of these objects is interesting scientifically and can have important applications. However, to date no experimental observation has been reported.

The prospects of realizing these predicted phenomena depend on the accessibility of the nonlinear parameters in a physical feasible system. To address this question, we first develop a systematic way of determining the nonlinear properties of materials based on the previously developed spectrally-resolved two-beaming coupling measurement. This new method is used to measure the nonlinear properties of several materials. The results are used to assess the prospects of producing stable multi-dimensional optical solitons in saturable instantaneous Kerr-like nonlinear systems. We conclude that the prospects for producing three-dimensional solitons are poor. However, it is more likely to succeed in producing stable two-dimensional optical solitons.

BIOGRAPHICAL SKETCH

Yi-Fan Chen was born in Taipei, Taiwan in 1972. He started his undergraduate study in National Taiwan Ocean University, Keelung, Taiwan in 1990, majoring in Electrical Engineering. He transferred to National Cheng Kung University, Tainan, Taiwan and changed his major to Physics in 1992. In 1995, he received a B.S. in physics (*summa cum laude*) from National Cheng Kung University and joined the Taiwanese Navy to serve his two-year mandatory military service. While in the navy, he was a second lieutenant overseeing quality control in a vessel maintenance facility. In 1997, after completing his military service, he was admitted into the M.S. program in Physics at National Tsing Hua University, Hsinchu, Taiwan. He earned his degree in 1999. The same year he was admitted into the Ph.D. program in Applied Physics at California Institute of Technology (Caltech), Pasadena, CA, U.S. One year later, he transferred to the Applied Physics Ph.D. program at Cornell University, Ithaca, NY, U.S. and started working under Professor Frank Wise's guidance since 2001. During his graduate studies, he has been involved in research activities related to laser frequency stabilization, laser optical phase control, biophysics, micro-/nano-fabrication, nonlinear wave propagation, optical solitons, and negative refraction phenomena.

“If you would be a real seeker after truth, it is necessary that at least once in your life you doubt, as far as possible, all things.”— René Descartes (1596-1650)

ACKNOWLEDGEMENTS

I am indebted to many people in my Ph.D. study and in the preparation of this dissertation. First and foremost, I would like to thank my advisor, Professor Frank Wise, for his patient guidance, his sincere advices, his dedication to science and science education, and his insightful understanding of scientific subjects. Under his guidance, becoming an independent researcher from a graduate student has been a very wonderful experience. He is a great scientist, a mentor, and a friend. I also would like to thank Professor Alexander Gaeta and Professor Michal Lipson for serving on my committee. Their suggestions and advices have undoubtedly made this a better dissertation. I also owe it to Professor Boris Malomed for making me think harder and learn more on many subjects related to solitons.

Thank you also goes to Kale Beckwitt, from whom I have learned a lot of experimental tricks and the inspiring discussions between us always brought interesting discoveries. I hope all is going well for him at Intel. Omer Ilday also taught me many things in both experiments and theories. His research in MIT has been making important progress and there is no doubt that he will continue to move forward. I have also enjoyed some of the best and exciting scientific conversations with Peer Fischer. His witty comments on a wide variety of subjects were the best refresher in our often long and mind-bending discussions. I wish him best of luck for his experiments in Rowland Institute. I am also in debt to Jeffrey Harbold. Jeff's humor has always helped me through the dark moments. His valuable suggestions were also one main reason that my job hunting was relatively smooth. It is good to see that he is enjoying his new career and new life in Southern California. The dissertation was proofread by Stephen Clark. I thank him for pointing out many errors and helping me make the dissertation easier to read.

I also would like to say thank you to Hyungsik Lim, whose proposals to go to a movie were often seconded by me. He was also the person who introduced to me the exciting sport of skiing. These outside-the-lab activities have enriched my life in Ithaca. I also want to thank Byung-Ryool Hyun, Jeffrey Moses, Joel Buckley, Andy Chang, Lyuba Kouznetsova, and Shian Zhou. Together they create a enjoyable and dynamic office environment.

The primary support for this work was provided by the National Science Foundation. The samples used in this work were from Dr. Bruce Aitken at Corning Corporation and Dr. Jas Sanghera at Naval Research Laboratory. Many thanks for their generosity.

I can't express how grateful I am to my parents. They have always been extremely supportive. They always try their best to provide me the opportunities to go further and higher.

Last but not least, my deepest gratitude goes to my wife, Yi, for her support and endurance. She is always understanding, caring, calming and strong. Life without her would be unimaginable.

TABLE OF CONTENTS

1	Introduction	1
1.1	A brief history of the soliton	3
1.2	Four classes of solitons	8
1.3	Organization of the dissertation	11
2	Spectrally-resolved two-beam coupling beyond the small phase shift approximation	13
2.1	Introduction	13
2.2	Beyond small phase approximation	18
2.3	Comparison of linear approximation, second-order approximation and numerical simulation	27
2.4	Conclusions	39
3	Measurement of fifth- and seventh-order nonlinearities of glasses	40
3.1	Introduction	40
3.2	Spectrally-resolved two-beam coupling with high-order nonlinearities	42
3.3	Experimental results	56
3.4	Conclusions	63
3.5	Acknowledgements	64
4	Criteria for the experimental observation of multi-dimensional optical solitons in saturable media*	65
4.1	Introduction	65
4.2	Theoretical analysis of the necessary conditions for the existence of two- and three-dimensional solitons	69
4.3	Measurements of nonlinear parameters of glasses	78
4.4	Stability windows for the two- and three-dimensional solitons	79
4.5	Conclusions	83
4.6	Acknowledgements	84
5	Future directions	85
A	Simulation code	90
	Bibliography	119

*Most of the results presented in this chapter have been published in [19].

LIST OF FIGURES

2.1	A typical SRTBC setup. The beam out of the pulsed laser is split into the probe-beam and the pump-beam. The ratio between pump- and probe-beam is somewhat arbitrary but should be at least 5 : 1 for Pump : Probe. After the sample the probe beam is split again. The two-photon absorption (TPA) coefficient β and instantaneous Kerr nonlinearity n_2 can then be extracted from the integrated signal and spectrally-resolved signal respectively.	14
2.2	The pump-beam induces a nonlinear phase shift upon the probe-beam. Depending on the sign of the nonlinearity of the material and the relative delay, the induced phase has a different temporal shape, which results in different spectral shift.	16
2.3	The nonlinear phase shift is detected in the spectral domain using a monochromater. As the delay varies, the induced spectral shift changes and the transmission through the monochromater also changes. This produces a typical SRTBC bipolar signal trace, as shown in the inset.	17
2.4	A two-dimensional data matrix of SRTBC. As indicated in the figure, the simulation parameters are $\tilde{\alpha} = 0$, $\tilde{\beta} = 0$, $\tilde{\gamma} = 0.05$, and $I_{p0} = 1$. This corresponds to a nonlinear phase shift $\Delta\phi_{NL} = 0.05$. The detuning is in the unit of FWHM PSD. The time delay is in the unit of half-width at (1/e)-maximum of the intensity profile. A SRTBC signal trace can be obtained from sectioning the data matrix along a fixed detuning.	29
2.5	Another two-dimensional data matrix of SRTBC. Here, the simulation parameters are $\tilde{\alpha} = 0$, $\tilde{\beta} = 0$, $\tilde{\gamma} = 0.3$, and $I_{p0} = 1$. This corresponds to a nonlinear phase shift $\Delta\phi_{NL} = 0.3$. Similar to Fig. 2.4, the detuning is in the unit of FWHM PSD. The time delay is in the unit of half-width at (1/e)-maximum of the intensity profile.	30
2.6	SRTBC signal traces produced by a linear approximate expression, a second-order approximate expression, and numerical simulation. The parameters used are $\tilde{\alpha} = 0$, $\tilde{\beta} = 0.02$, $\tilde{\gamma} = 0.05$, and $I_{p0} = 1$. The corresponding nonlinear phase shift $\Delta\phi_{NL} = 0.05$. The frequency detuning is 1 FWHM PSD, and the time delay is in the unit of half-width at (1/e)-maximum of the field profile. The approximate expressions agree with numerical simulation well. . .	32

2.7	SRTBC signal traces produced by a linear approximate expression, a second-order approximate expression, and numerical simulation with parameters of 10 times the magnitude of those in Fig. 2.6. The parameters used are $\tilde{\alpha} = 0$, $\tilde{\beta} = 0.2$, $\tilde{\gamma} = 0.5$, and $I_{p0} = 1$. The corresponding nonlinear phase shift $\Delta\phi_{NL}$ is 0.5. The frequency detuning is 1 FWHM PSD, and the time delay is in the unit of half-width at (1/e)-maximum of the field profile. It is clear that linear approximate expression breaks down. On the contrary, second-order approximate expression agrees with numerical simulation relatively well.	33
2.8	Nonlinear phase shift (and thus intensity) dependence of the SRTBC signal trace peak/valley magnitude predicted by a linear approximate expression, a second-order approximate expression, and numerical simulation. The frequency detuning is 1.5 FWHM PSD. While the second-order approximate expression agrees with the numerical simulation better than linear approximate simulation, at large nonlinear phase shift, the deviation of both approximate expressions is significant.	35
2.9	Nonlinear phase shift dependence of the SRTBC signal size (peak-valley). The frequency detuning is 1.5 FWHM PSD. The same data in Fig. 2.8 is presented here differently, with the SRTBC trace peak-valley amplitude plotted.	36
2.10	Nonlinear phase shift (and thus intensity) dependence of the SRTBC signal trace peak/valley magnitude predicted by a linear approximate expression, a second-order approximate expression, and numerical simulation. The frequency detuning is 0.5 FWHM PSD. While the second-order approximate expression agrees with the numerical simulation well up to a nonlinear phase shift ~ 0.5 , at large nonlinear phase shift, the deviation of both approximate expressions become significant.	37
2.11	Nonlinear phase shift dependence of the SRTBC signal size (peak-valley). The frequency detuning is 0.5 FWHM PSD. The same data in Fig. 2.10 is presented here in differently, with the SRTBC trace peak-valley amplitude plotted.	38
3.1	Numerical calculation is used to determine the dependence of the signal on pump-beam intensity in the presence of $\chi^{(3)}$ alone. Inset: SRTBC signals calculated for the indicated nonlinear phase shifts. The time delay is in the units of the pulse duration.	43
3.2	Extension of SRTBC to higher-order nonlinearities: The model including higher-order nonlinear effects is used to predict the SRTBC signal. Shown here is the effect of a self-defocusing $\chi^{(5)}$ on a self-focusing $\chi^{(3)}$. The time delay is in the units of the pulse duration.	57

3.3	Intensity dependence of the SRTBC signal magnitude (peak-valley) for various values of self-focusing $\chi^{(3)}$ and for a self-focusing $\chi^{(3)}$ with a self-defocusing $\chi^{(5)}$	58
3.4	Intensity dependence of the (a) SRTBC signal magnitude (normalized peak-valley transmission difference) and (b) nonlinear absorption signal of As_2S_3 . Insets show examples of SRTBC and nonlinear absorption traces (symbols) along with the best fit theoretical curves. The time delay is given in units of the pulse duration.	61
4.1	The operation window for the 2D solitons, as predicted on the basis of the experimentally-measured characteristics of the glass. The hatched area is the window neglecting loss. The shaded area is the dramatically reduced (but definitely existing) window found with loss taken into account.	80
4.2	The operation window for 3D solitons. The meaning of the hatched area is the same as in the 2D case, i.e., it shows the window obtained neglecting loss. When loss is taken into account, the window vanishes completely.	82
5.1	The refractive index and absorption/gain for a noninverted Lorentz oscillator (solid line) and an inverted Lorentz oscillator (dashed line). For a give frequency, the sign of the dispersion properties for an inverted Lorentz oscillator will be opposite to that of a noninverted oscillator.	87

LIST OF TABLES

- 3.1 Measured n_2 , $|n_4/n_2|$, and α_2 . For sapphire, both n_4 and α_2 are under the detection limit and upper-limits are given. For all samples, a self-defocusing $n_4(< 0)$ is observed. 62

Chapter 1

Introduction

Unlike 170 years ago when the soliton was first discovered, today nonlinear science is considered one of the most important frontiers in understanding the fundamentals of nature. Soliton's status as a hallmark of nonlinear science has been firmly established. It took many years for people to understand that nonlinear effects in general and solitons in particular are not just unimportant mathematical curiosities, but are an important path to understanding nature. From biology to metrology to plasma physics to optics, nonlinear effects and solitons all play important roles (c.f. [1]). In fact, the understanding of the soliton gained since its discovery has helped to enable many important technological breakthroughs, such as the prediction of tsunamis and optical communications, just to name a few.

Although great progress has been made both in the theoretical understanding and in experimental demonstrations in the past 50 years, soliton research is still a young field. There remain a wide range of systems to be explored and new systems continue to be discovered in different areas of physics. Novel theories and experimental approaches are being developed to apply to these new territories. All these have been accelerated by the explosion of computational power in the past 20 years. Calculation unthinkable 20 years ago can now be carried out on personal computers in the matter of minutes. It is also this abundance of computational power that enables soliton researchers to expand the horizon to include systems that are not exactly-solvable. The study of which requires large amount of numerical simulation. One example of these systems is the optical quadratic nonlinear system.

Among the many important questions that remain to be answered in optical soliton research is: How does one make a stable three-dimensional (3D) optical soliton? A stable 3D optical soliton is a localized electromagnetic wave confined in all three spatial dimensions and in time which propagates stably. Such an object has been predicted to exist theoretically in optical systems with appropriate nonlinear properties. But it has not been observed experimentally to date. The question by itself is scientifically important. Moreover, the answer to this question could also start another technology revolution in telecommunications and computation [2]. Recent development in the optical quadratic nonlinear system has been very encouraging [3]. Important progress has been made towards answering this question and more research efforts are being invested in this direction.

Additionally, theoretical study has shown that a saturable instantaneous Kerr nonlinear system also supports stable 3D optical solitons [4]. The saturation of instantaneous Kerr nonlinearities occurs due to the existence of higher-order nonlinearities such as $\chi^{(5)}$ and $\chi^{(7)}$. Theoretical predictions require that these higher-order nonlinearities be of “appropriate” magnitude. It is then natural to ask if such an “appropriate” amount of higher-order nonlinearities can be found in real materials. The main focus of this work is to investigate the prospects of experimentally realizing stable 3D optical solitons in a saturable instantaneous Kerr nonlinear system. In order to answer this question, we develop a systematic way of determining the higher-order nonlinearities of materials based on spectrally-resolved two-beam coupling (SRTBC). We utilize the developed method to measure several materials and assess the prospects of realizing the goal of producing stable 3D optical solitons.

To provide the needed context for the subject, a brief history of the soliton and

a simple classification of different types of solitons are given in the following two sections.

1.1 A brief history of the soliton

It is generally accepted that the first documented record of solitons was made by John Scott Russell, a Scottish engineer, in August 1834 (c.f. [5]; most historical accounts in this section are according to Filippov [1], Remoissenet [5], and Gesztesy and Holden [6]). He observed a smooth well-defined heap of water that detached itself from the prow of a barge when the barge was brought to rest. The heap propagated without changing shape and speed for over two miles along the Union Canal linking Edinburgh with Glasgow. He described the event in the following terms: *“I was observing the motion of a boat which was rapidly drawn along a narrow channel by a pair of horses, when the boat suddenly stopped-not so the mass of water in the channel which it had put in motion; it accumulated round the prow of the vessel in a state of violent agitation, then suddenly leaving it behind rolled forward with great velocity, assuming the form of a large solitary elevation, a rounded, smooth and well-defined heap of water, which continued its course along the channel apparently without change of form or diminution of speed. I followed it on horseback, and overtook it still rolling on at a rate of some eight or nine miles an hour, preserving its original figure some thirty feet long and a foot to a foot and a half in height. Its height gradually diminished, and after a chase of one or two miles I lost it in the windings of the channel. Such, in the month of August 1834, was my first chance interview with that singular and beautiful phenomenon which I have called Wave of Translation,... ”* [7]

Russell’s observations were followed by numerous water-tank experiments and

he established the following important properties for these “solitary waves”:

- (1) An isolated solitary wave has a constant velocity and does not change its shape
- (2) The dependence of the velocity v on the canal depth h and the height of the wave y_0 , is given by the relation

$$v = \sqrt{g(y_0 + h)} \quad (1.1)$$

where g is the gravity acceleration. The formula is valid for $y_0 < h$.

- (3) Depending on the relation between its height and length, an initial elevation of water might evolve into one or more solitary waves.
- (4) There exists only solitary elevations (humps); solitary cavities (depression) are never observed. An initial depression is transformed into an oscillatory wave, not a solitary depression.

Unfortunately, Russell’s report went unnoticed on the continent, and even more unfortunately, in England, two distinguished scientists— Airy and Stokes – read his paper carefully and severely criticized it. They concluded that what Russell had described was impossible according to their own theories on nonlinear shallow-water waves. The controversy had a chilling effect and the solitary wave was forgotten by most people. More than two decades had passed before a resolution to the controversy was provided.

It later became clear that the controversy arose from neglecting dispersion, a crucial factor for soliton formation, in both Airy’s and Stokes’ calculation. This was pointed out and Russell’s claim was confirmed independently by French scientist Joseph Valentine de Boussinesq (1871), Lord Rayleigh (1876) and Saint-Venant (1885). Nevertheless, these new developments appeared insufficient to overcome the criticism and establish the final truth, partly due to the very high prestige of Airy and Stokes. It would have to wait until 1895 for the controversy to be com-

pletely resolved when Dutch scientist Diderik Johannes Korteweg and his student Gustav de Vries reexamined and summarized all previous considerations on the subject. They confirmed that Airy's and Stokes' opinions were incorrect and introduced a simpler modelling equation for the shallow water wave, the now famous KdV equation. From the KdV equation, they derived a solution which was exactly Russell's solitary wave.

While the work of Korteweg and de Vries did resurrect solitons as a scientific reality, the general scientific community would not pay much attention to the subject and it remained an unimportant curiosity in the mathematical structure in nonlinear wave theory for many decades more. However, a remarkable discovery made by E. Fermi, J. Pasta and S. Ulam (FPU) in their study in the heat transport problem in 1955 revived the interest in the KdV equation and solitons.

At first glance, the problem that FPU considered at first sight had nothing to do with solitons, it was related to heat transport. More specifically, the subject was how a system starting with energy concentrating in a single normal mode reached thermal equilibrium – the equipartition of all possible normal modes. It was obvious that a purely linear system (e.g., a crystal in which the interaction between atoms is purely harmonic) would never reach thermal equilibrium, since all modes were independent of each other. Debye suggested in 1914 that the nonlinearity of the atomic interaction caused the modes to exchange energy and resulted in thermal equilibrium. FPU in 1955 attempted to verify Debye's conjecture by using computer simulation for a one-dimensional lattice. They had expected to observe equipartition of energy between modes and thermal equilibrium eventually. However, much to their surprise, they did not find that the energy spreaded throughout different modes, in stead, they observed that the energy distribution returned

almost back to the originally excited mode periodically. This surprise later led N. Zabusky and M. Kruskal to consider the problem using the KdV equation and succeeded in explaining the recurrence phenomenon by soliton collision. Their work prepared the ground for the breakthrough by Gardner et al. in 1967, who introduced the inverse-scattering approach to exactly solve the KdV equation. The next year, Lax introduced the whole hierarchy of nonlinear evolution of the KdV type. In the same year (1968), Zakharov introduced the nonlinear Schrodinger equation (NLSE) to describe the time evolution of the envelope of weakly nonlinear deep-water wave trains. These “envelope solitons” or “group solitons” were further studied and Zakharov and Shabat later (1971) solved the equation exactly also using the inverse-scattering method. The solutions were verified experimentally later by Yuen and Lake (1975). At roughly the same period of time, the parallel development took place in the field of the electromagnetic wave. Hasegawa and Tappert showed theoretically that the envelope of a light wave propagating in an optical fiber can also be described by NLS. They predicted the existence of bright solitons, which now are under investigation and have also made important impacts on modern optical telecommunications.

The third main class of soliton is the Frenkel-Kontorova (FK) soliton introduced in 1938. This soliton is described by the Sine-Gordon equation and is sometimes called a Sine-Gordon (SG) soliton. Yakov Il'ich Frenkel and T. A. Kontorova first connected the dislocation in the crystalline structure of solids with the concept of soliton. In many systems the Sine-Gordon equation (or its relatives) describes the interaction and evolution of the defects of the crystalline structure and solitons are the localized solutions to such systems. These also include the magnetic domain walls which are closely related to the soliton solution. One of the most striking

difference of this type of soliton from the other two types (the KdV soliton and the envelope soliton) is its persistence. For the KdV soliton and the envelope soliton, the presence of dissipative effects in general destroy the solitons completely. However, for a FK soliton, it is possible that the dissipative effects only “stop” the movement of the soliton, and the soliton becomes at rest, but can exist eternally in principle. For example, a defect (dislocation) can exist for as long as the host crystal exists. This third type of soliton is less familiar to wave scientists but is very important in solid state physics. It is sometimes also referred as a topological soliton for the obvious reason.

The above summarizes some of the most important milestones in the development in soliton study up to 1980. One common property among the systems mentioned is that they are all integrable systems [8]. A system that is integrable can be solved exactly using the inverse scattering transform (IST) and analytical solutions can be obtained. To mathematicians, these are the systems where the word “soliton” can be used in its most strict sense: *a soliton is a localized exact solution of a nonlinear wave equation, its shape and speed do not change during the propagation, and will not be altered by a collision with other solitons.* Although these integrable systems are valuable models, the real world is full of effects such as loss mechanisms, external driving forces, defects, etc. These effects make the systems non-integrable and perturb the original soliton states. As a result, the solitary objects can no longer exist eternally and become meta-stable. It is then more practical to relax the definition of soliton to include all meta-stable, localized and finite energy states that are the outcomes of the balance between nonlinear and linear effects.

This extended definition allows us to include one more class of nonlinear system

that is *not* integrable: the quadratic nonlinear system. Many important theoretical and experimental developments in the study of solitons have been made in this system during the past 20 years. The optical quadratic nonlinear system is especially promising for its potential of achieving the long-sought realization of stable multi-dimensional optical solitons. The key to producing stable multi-dimensional optical solitons is the saturation of the third-order nonlinearity $\chi^{(3)}$. Ordinarily this would require higher-order nonlinearities such as $\chi^{(5)}$, $\chi^{(7)}$, etc, as mentioned previously. However, an alternative was suggested by Stegeman et al in 1993 [9]. As they pointed out, the nonlinear response of an optical quadratic nonlinear system (with only $\chi^{(2)}$) can mimic that of a saturable $\chi^{(3)}$ system through a process called “cascading”. Many theoretical and experimental works have been done since [3] and the first experimental demonstration of two dimensional spatio-temporal solitons appeared in 1999 (Liu et al.)[10].

In the next section, we will briefly introduce the nonlinear equations underlying the above mentioned four classes of solitons: KdV soliton, Envelope soliton, FK soliton, and quadratic soliton.

1.2 Four classes of solitons

(i) KdV soliton

This is the first discovered soliton. The key equation for this class of soliton is

$$u_t + \frac{1}{4}u_{xxx} - \frac{2}{3}uu_x = 0. \quad (1.2)$$

Some example systems are the shallow water wave and nerve pulse transportation.

(ii) Envelope soliton

The envelope soliton is probably the most familiar to optical scientists. The equa-

tion that describes the system is usually called the nonlinear Schrödinger equation (NLSE) due to its similarity to the Schrödinger equation. The general form of NLSE is

$$u_t + \frac{i}{2}u_{xx} - i|u|^2u = 0. \quad (1.3)$$

This equation describes systems such as the nonlinear optical fiber with only instantaneous third-order nonlinearity $\chi^{(3)}$. The evolution of deep water waves can also be described by this equation. The stationary solutions in this system are “envelope solitons”, which consist of a hyperbolic secant envelope with modulation at the imposed carrier frequency. More generally speaking, the NLSE is a special case of a broader class of equation, the Ablowitz-Kaup-Newell-Segur (AKNS) hierarchy:

$$\begin{aligned} u_t + \frac{i}{2}u_{xx} - iu^2v &= 0 \\ v_t - \frac{i}{2}v_{xx} + iuv^2 &= 0. \end{aligned} \quad (1.4)$$

It is easy to see that when $v = u^*$, the AKNS equation reduces to the familiar NLSE.

The stationary soliton solutions of the NLSE become unstable if the equation is extended to more than one dimension:

$$u_t + \frac{i}{2}\nabla_d^2 u - i|u|^2u = 0, \quad (1.5)$$

where $d > 1$. But this instability can be eliminated if the nonlinear term in the NLSE is generalized to include higher-order nonlinear effects, which could saturate the third-order nonlinearity [4]. The generalized NLSE takes the form:

$$u_t + \frac{i}{2}u_{xx} - if(|u|^2)u = 0. \quad (1.6)$$

For a material with cubic-quintic nonlinearity, $f(|u|^2) = \alpha|u|^2 - \beta|u|^4$. For a material with saturable nonlinearity, we have $f(|u|^2) = \eta|u|^2/(1 + \gamma|u|^2)$. The generalized NLSE becomes important when the optical field in a material is strong enough so that the higher-order nonlinearities become non-negligible. The magnitude of these higher-order nonlinear effects determine the intensity threshold beyond which the stationary soliton solutions become stable. However, the unavoidable accompanying nonlinear loss limits the maximum intensity that can be used, since the higher the intensity, the faster the energy decay due to the nonlinear loss. Does a “window of parameters” exist between these conflicting requirements? This is the question the present work tries to answer.

(iii) FK soliton

The key equation that describes this class of soliton is the Sine-Gordon equation:

$$u_{xt} - \sin(u) = 0. \quad (1.7)$$

Some of the examples of this family of solitons are dislocations in crystalline structure and magnetic domain walls.

(iv) Quadratic soliton

The quadratic system can be described by the following coupled equations:

$$\begin{aligned} iu_t + u_{xx} - u + vu^* &= 0, \\ 2iv_t + \delta v_{xx} - \gamma v + \frac{1}{2}u^2 &= 0. \end{aligned} \quad (1.8)$$

As mentioned in the previous section, this system has gained a lot of attention among optical scientists due to its potential for achieving a large and saturable nonlinearity through the cascading process [9].

1.3 Organization of the dissertation

Among the four classes of solitons introduced in the previous section, the more relevant ones to optical sciences are envelope solitons (described by NLSE) and quadratic solitons. These two classes of solitons provide two different approaches to achieve the goal of experimentally producing stable multi-dimensional solitons: saturable third-order nonlinearity through cascading $\chi^{(2)}$ (quadratic system) and saturable third-order nonlinearity through higher-order nonlinearities (generalized NLSE). This work will focus on the latter.

In order to assess the prospects of using higher-order nonlinearities to stabilize multi-dimensional solitons, we need to develop a systematic way of measuring these quantities. Spectrally-resolved two-beam coupling (SRTBC) is a technique originally developed for measuring the third-order nonlinearity [11] with high sensitivity. We extend this technique and use it to measure higher-order nonlinearities.

The magnitude of higher-order nonlinearities are generally much smaller than third-order effect. In order to observe these effects, high-intensity optical fields must be used. Prior studies with SRTBC have all been limited to relatively low intensity and to the small nonlinear phase shift range. In this range, the signal size is proportional to the optical field intensity for a fixed third-order nonlinearity. Naïvely, one would expect that higher-order nonlinear effects manifest themselves as the deviation from a straight line in the signal size vs. intensity relation. As discussed in Chapter 2, this is not the case. For a nonlinear system with only instantaneous third-order nonlinearity, the signal size is not proportional to the intensity at high intensities in general. Thus the deviation from a straight line itself is not a guarantee that higher-order nonlinear effects are present. This observation leads to the work discussed in Chapter 3, where the SRTBC model is extended

to include higher-order nonlinearities. With the extended technique, we are able to determine the higher-order nonlinear parameters for several glass materials. Chapter 4 is where we assess the prospects of stabilizing multi-dimensional solitons through higher-order nonlinearities. In Chapter 5, we propose some interesting ideas which could point to future directions of research on multi-dimensional optical solitons.

To summarize, the new results presented in this work are (i) The extension of SRTBC theory to include arbitrary large signals and higher-order nonlinearities in the analysis; (ii) The first measurements of seventh-order nonlinearities in transparent glasses; (iii) The first systematic investigation on the attainable physical parameter space for multi-dimensional solitons experiments with nonlinear loss taken into account.

Chapter 2

Spectrally-resolved two-beam coupling beyond the small phase shift approximation

The conventional spectrally-resolved two-beam coupling experiment assumes a small nonlinear phase shift and uses an approximate expression in which the signal size is proportional to the phase shift. We show that as the nonlinear phase shift becomes large, the signal-size will not increase proportionally to the intensity and the usual approximate expression should be replaced with either a more accurate approximate expression or numerical simulation.

2.1 Introduction

Spectrally-resolved two-beam coupling (SRTBC) is a simple way to determine the magnitude and the sign of $\text{Re}[\chi^{(3)}]$ (proportional to the nonlinear refractive index n_2) and $\text{Im}[\chi^{(3)}]$ (proportional to the two-photon absorption coefficient β). As demonstrated in [11], this technique can achieve high sensitivity and can detect a nonlinear phase shift as small as 3×10^{-6} rad. A typical setup is shown in Fig. 2.1. It is essentially a pump-probe detection setup. The pump- and probe-beam cross at the sample and the instantaneous Kerr nonlinearity causes cross-phase modulation, which affects the probe-beam spectrum. The change can then be detected and analyzed to gain knowledge of the material instantaneous Kerr nonlinearity. In our experiments, the interaction range of the pump- and probe-

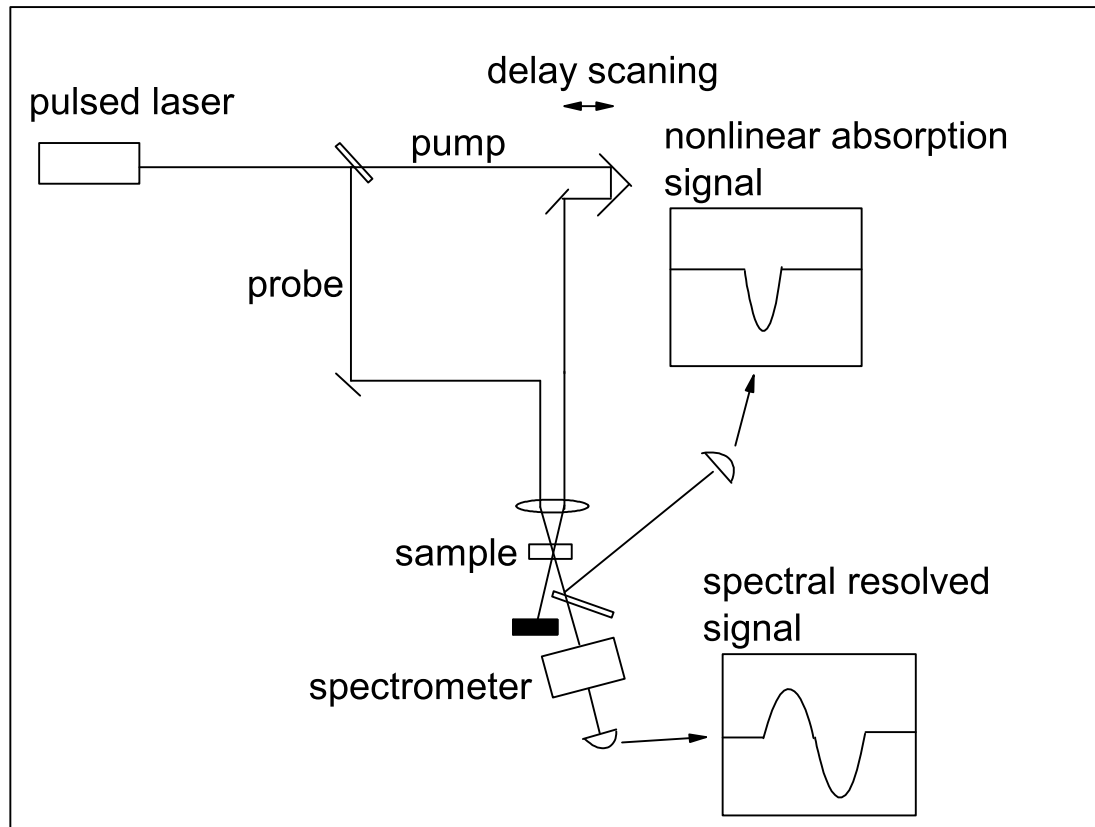


Figure 2.1: A typical SRTBC setup. The beam out of the pulsed laser is split into the probe-beam and the pump-beam. The ratio between pump- and probe-beam is somewhat arbitrary but should be at least 5 : 1 for Pump : Probe. After the sample the probe beam is split again. The two-photon absorption (TPA) coefficient β and instantaneous Kerr nonlinearity n_2 can then be extracted from the integrated signal and spectrally-resolved signal respectively.

beam is usually short (\sim mm) and for the typical pulse width (\sim 100 fs) we use in the experiments. The effects of group-velocity dispersion (GVD) can be safely ignored in the analysis.

To gain some intuitive understanding of the mechanism of SRTBC, Fig. 2.2 and Fig. 2.3 illustrate what happens in the time and frequency domain during the pump-probe interaction for a material with positive instantaneous Kerr nonlinearity ($n_2 > 0$). The intensity profile of the pump-beam creates a nonuniform refractive index profile in time for the probe-beam. As a result, a time-dependent nonlinear phase is imposed on the probe-beam:

$$\phi_{NL}(L, t) = \frac{4\pi n_2 I_{pump}(t)L}{\lambda_0}, \quad (2.1)$$

where $I_{pump}(t)$ is the pump-beam intensity, L is the interaction length, and λ_0 is the probe-beam center wavelength in vacuum. We know that the probe-beam time- and space-dependency can be described by:

$$u(L, t) = u_0(t - t_0) \exp\left[i\left(\frac{2\pi n_0}{\lambda_0}\right)L + \phi_{NL}(L, t) - \omega_0 t\right], \quad (2.2)$$

where n_0 is the linear refractive index of the material and $u_0(t - t_0)$ is a Gaussian profile centered at t_0 . Since the energy is concentrated around t_0 , we expand $\phi_{NL}(L, t)$ around t_0 :

$$\begin{aligned} \phi_{NL}(L, t) &= \phi_{NL}(L, t_0) + \left.\frac{d\phi_{NL}(L, t)}{dt}\right|_{t=t_0} (t - t_0) \\ &= \phi_{NL}(L, t_0) + \frac{4\pi n_2 L}{\lambda_0} \left.\frac{dI_{pump}(t)}{dt}\right|_{t=t_0} (t - t_0) \end{aligned} \quad (2.3)$$

Substitute Eqn. 2.3 into Eqn. 2.4, we get

$$u(L, t) = u_0(t - t_0) \exp\left[i[\phi_0 - (\omega_0 + \delta\omega)(t - t_0)]\right], \quad (2.4)$$

where $\phi_0 = (2\pi n_0 L / \lambda_0) + \omega_0 t_0 + \phi_{NL}(L, t_0)$ and

$$\delta\omega = \frac{4\pi n_2 L}{\lambda_0} \frac{dI_{pump}(t)}{dt} \quad (2.5)$$

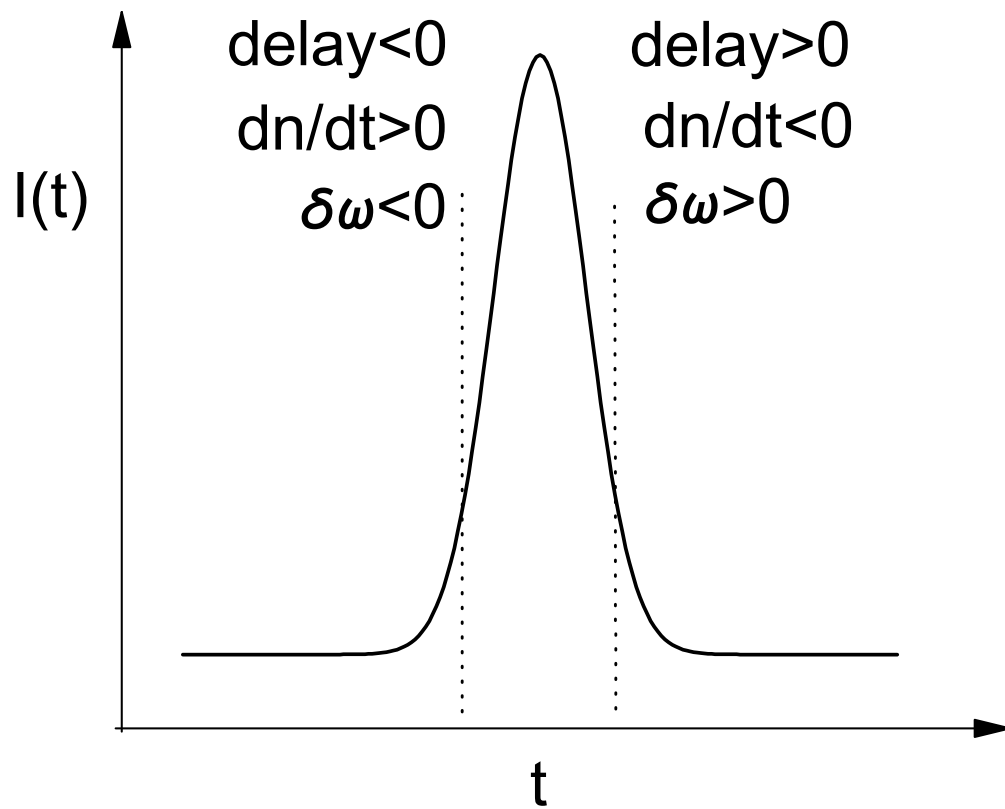


Figure 2.2: The pump-beam induces a nonlinear phase shift upon the probe-beam. Depending on the sign of the nonlinearity of the material and the relative delay, the induced phase has a different temporal shape, which results in different spectral shift.

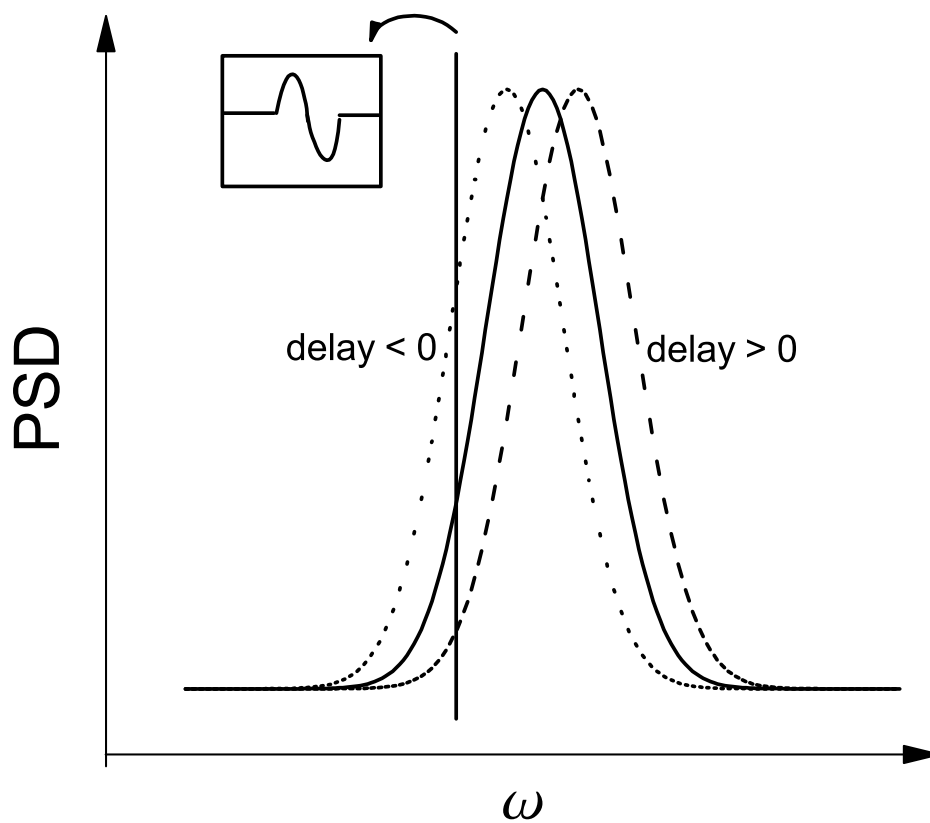


Figure 2.3: The nonlinear phase shift is detected in the spectral domain using a monochromator. As the delay varies, the induced spectral shift changes and the transmission through the monochromator also changes. This produces a typical SRTBC bipolar signal trace, as shown in the inset.

is the frequency shift. From Fig. 2.2 we can see that for a material with a positive instantaneous Kerr nonlinearity, the probe-beam with negative time delay relative to the pump-beam will experience a negative frequency shift. On the contrary, if the delay is positive, it will experience a positive frequency shift. It can also be seen from Eqn. 2.5 that the frequency shift is proportional to the magnitude of the instantaneous Kerr nonlinearity n_2 and the amplitude of the pump-beam intensity. As illustrated in Fig. 2.3, the typical SRTBC bipolar signal is obtained through selecting a specific component of the spectrum.

2.2 Beyond small phase approximation

Although the explanation of the mechanism of SRTBC described in the previous section can provide some intuition and a working picture, a more mathematical rigorous description is needed for more accurate analysis as well as for extending the model beyond the small phase shift limit. The equations describing the nonlinear interaction of pump- and probe-beam for material with only instantaneous third-order nonlinearity ($\chi^{(3)}$) have been previously derived [11, 12]:

$$\begin{aligned}
 \frac{\partial I_p}{\partial z} + \frac{1}{v} \frac{\partial I_p}{\partial t} &= -(\alpha + \beta I_p) I_p, \\
 \frac{\partial \phi_p}{\partial z} + \frac{1}{v} \frac{\partial \phi_p}{\partial t} &= \frac{\omega_0}{c} n_2 I_p, \\
 \frac{\partial I_s}{\partial z} + \frac{1}{v} \frac{\partial I_s}{\partial t} &= -(\alpha + 2\beta I_p) I_s, \\
 \frac{\partial \phi_s}{\partial z} + \frac{1}{v} \frac{\partial \phi_s}{\partial t} &= 2 \frac{\omega_0}{c} n_2 I_p,
 \end{aligned} \tag{2.6}$$

where $I_{p(s)}$ and $\phi_{p(s)}$ are the intensity and the phase of the temporal envelope of the pump (probe) beam. α is the linear absorption coefficient, and β is the TPA coefficient. n_2 is the instantaneous Kerr nonlinearity and v is the group velocity. An expression for small-phase shift SRTBC signal (relative transmittance) for a

Gaussian pulse $E(t) \sim \exp(-t^2/t_0^2)$ has also been given previously [11]:

$$\begin{aligned} \frac{\Delta T}{T} &= \frac{2}{\sqrt{3}} \exp(\delta^2 t_0^2/6) \exp(-2\tau^2/3t_0^2) \\ &\times [2(\omega_0 n_2 L I_{p0}/c) \sin(2\delta\tau/3) - \beta L I_{p0} \cos(2\delta\tau/3)], \end{aligned} \quad (2.7)$$

where I_{p0} is the peak intensity of the pump-beam, τ is the probe-beam delay relative to pump-beam and $\delta = \omega - \omega_0$ is the detuning of the monochrometer from the center frequency. The expression is valid for small phase shift (i.e. when $\Delta\phi \equiv \omega_0 I_{p0} n_2 L/c$ is less than ~ 0.1). Here, we extend the expression to include the case when the phase shift is larger.

Starting from Eqns. 2.6, we first introduce the transformation:

$$\begin{aligned} \hat{z} &= z \\ \hat{t} &= t - \frac{z}{v}. \end{aligned} \quad (2.8)$$

This changes the time frame to the ‘‘moving frame’’ with the velocity of the group velocity and simplifies the equations:

$$\begin{aligned} \frac{\partial I_p}{\partial \hat{z}} &= -(\alpha + \beta I_p) I_p, \\ \frac{\partial \phi_p}{\partial \hat{z}} &= \frac{\omega_0}{c} n_2 I_p, \\ \frac{\partial I_s}{\partial \hat{z}} &= -(\alpha + 2\beta I_p) I_s, \\ \frac{\partial \phi_s}{\partial \hat{z}} &= 2\frac{\omega_0}{c} n_2 I_p. \end{aligned} \quad (2.9)$$

We can further normalize \hat{z} to the total interaction length L through the following transformation:

$$\begin{aligned} \hat{z} &= L\xi, \\ \tilde{\alpha} &= L\alpha, \\ \tilde{\beta} &= L\beta, \\ \tilde{\gamma} &= \frac{L\omega_0 n_2}{c}. \end{aligned} \quad (2.10)$$

We now have:

$$\begin{aligned}
\frac{\partial I_p}{\partial \xi} &= -(\tilde{\alpha} + \tilde{\beta} I_p) I_p, \\
\frac{\partial \phi_p}{\partial \xi} &= \tilde{\gamma} I_p, \\
\frac{\partial I_s}{\partial \xi} &= -(\tilde{\alpha} + 2\tilde{\beta} I_p) I_s, \\
\frac{\partial \phi_s}{\partial \xi} &= 2\tilde{\gamma} I_p.
\end{aligned} \tag{2.11}$$

Although the equations seem complicated, they are actually analytically solvable.

We proceed as follows:

$$\left(\frac{\partial \xi}{\partial I_p} \right)_t = \left(\frac{\partial I_p}{\partial \xi} \right)_t^{-1} = \frac{-1}{\tilde{\alpha} I_p + \tilde{\beta} I_p^2}. \tag{2.12}$$

The above equation can be solved, we get

$$\xi = \tilde{F}(\hat{t}) - \frac{1}{\tilde{\alpha}} \left[\ln I_p - \ln(\tilde{\alpha} + \tilde{\beta} I_p) \right], \tag{2.13}$$

where

$$\tilde{F}(\hat{t}) = \frac{1}{\tilde{\alpha}} \left[\ln I_p(\xi = 0, \hat{t}) - \ln(\tilde{\alpha} + \tilde{\beta} I_p(\xi = 0, \hat{t})) \right] \tag{2.14}$$

is determined by the initial launched pump-pulse shape $I_p(\xi = 0, \hat{t})$. From Eqn. 2.13,

we have

$$-\tilde{\alpha}(\xi - \tilde{F}(\hat{t})) = \ln\left(\frac{I_p}{\tilde{\alpha} + \tilde{\beta} I_p}\right), \tag{2.15}$$

which yields

$$\exp\left[\tilde{\alpha}(\xi - \tilde{F}(\hat{t}))\right] = \tilde{\beta} + \frac{\tilde{\alpha}}{I_p}. \tag{2.16}$$

More explicitly, we have

$$\begin{aligned}
I_p(\xi, \hat{t}) &= \frac{\tilde{\alpha}}{\exp[\tilde{\alpha}(\xi - \tilde{F}(\hat{t}))] - \tilde{\beta}} \\
&= \frac{\tilde{\alpha}}{e^{\tilde{\alpha}\xi} \left[\tilde{\beta} + \frac{\tilde{\alpha}}{I_p(\xi = 0, \hat{t})} \right] - \tilde{\beta}}
\end{aligned} \tag{2.17}$$

Using Eqn. 2.17, it is then straightforward to calculate $\phi_p(\xi, \hat{t})$, $\phi_s(\xi, \hat{t})$ and $I_s(\xi, \hat{t})$.

Direct integration of $I_p(\xi, \hat{t})$ yields:

$$\begin{aligned}
\phi_p(\xi, \hat{t}) &= \tilde{\gamma} \int I_p(\xi, \hat{t}) d\xi = \int \frac{\tilde{\alpha}\tilde{\gamma}}{e^{\tilde{\alpha}\xi} \left[\tilde{\beta} + \frac{\tilde{\alpha}}{I_p(\xi=0, \hat{t})} \right] - \tilde{\beta}} d\xi \\
&= \int \frac{\tilde{\alpha}\tilde{\gamma}}{\tilde{\beta}} \left(\frac{\hat{G}e^{\tilde{\alpha}\xi}}{\hat{G}e^{\tilde{\alpha}\xi} - \tilde{\beta}} - 1 \right) d\xi \\
&= \frac{\tilde{\gamma}}{\tilde{\beta}} \left[\ln(\hat{G}e^{\tilde{\alpha}\xi} - \tilde{\beta}) - \tilde{\alpha}\xi \right] - \frac{\tilde{\gamma}}{\tilde{\beta}} \ln(\hat{G} - \tilde{\beta}) + \phi_p(\xi=0, \hat{t}) \\
&= \frac{\tilde{\gamma}}{\tilde{\beta}} \left[\ln(\hat{G}e^{\tilde{\alpha}\xi} - \tilde{\beta}) - \tilde{\alpha}\xi \right] - \frac{\tilde{\gamma}}{\tilde{\beta}} \ln \left(\frac{\tilde{\alpha}}{I_p(\xi=0, \hat{t})} \right) \\
&\quad + \phi_p(\xi=0, \hat{t}).
\end{aligned} \tag{2.18}$$

We have used the notation

$$\hat{G} \equiv \tilde{\beta} + \frac{\tilde{\alpha}}{I_p(\xi=0, \hat{t})}. \tag{2.19}$$

Similarly,

$$\begin{aligned}
\phi_s(\xi, \hat{t}) &= 2\tilde{\gamma} \int I_p(\xi, \hat{t}) d\xi \\
&= \int \frac{2\tilde{\alpha}\tilde{\gamma}}{\tilde{\beta}} \left(\frac{\hat{G}e^{\tilde{\alpha}\xi}}{\hat{G}e^{\tilde{\alpha}\xi} - \tilde{\beta}} - 1 \right) d\xi \\
&= \frac{2\tilde{\gamma}}{\tilde{\beta}} \left[\ln(\hat{G}e^{\tilde{\alpha}\xi} - \tilde{\beta}) - \tilde{\alpha}\xi \right] - \frac{2\tilde{\gamma}}{\tilde{\beta}} \ln(\hat{G} - \tilde{\beta}) + \phi_s(\xi=0, \hat{t}) \\
&= \frac{2\tilde{\gamma}}{\tilde{\beta}} \left[\ln(\hat{G}e^{\tilde{\alpha}\xi} - \tilde{\beta}) - \tilde{\alpha}\xi \right] - \frac{2\tilde{\gamma}}{\tilde{\beta}} \ln \left(\frac{\tilde{\alpha}}{I_p(\xi=0, \hat{t})} \right) \\
&\quad + \phi_s(\xi=0, \hat{t}).
\end{aligned} \tag{2.20}$$

For I_s , we have the following:

$$\frac{\left(\frac{\partial I_s}{\partial \xi} \right)}{I_s} = -(\tilde{\alpha} + 2\tilde{\beta}I_p), \tag{2.21}$$

which yields

$$\ln I_s(\xi, \hat{t}) = -\tilde{\alpha}\xi - 2\tilde{\beta} \int I_p(\xi, \hat{t}) d\xi$$

$$\begin{aligned}
&= -\tilde{\alpha}\xi - 2\left[\ln(\widehat{G}e^{\tilde{\alpha}\xi} - \tilde{\beta}) - \tilde{\alpha}\xi\right] + 2\ln\left(\frac{\tilde{\alpha}}{I_p(\xi=0, \hat{t})}\right) \\
&\quad + \ln I_s(\xi=0, \hat{t}), \tag{2.22}
\end{aligned}$$

or equivalently,

$$\begin{aligned}
I_s(\xi, \hat{t}) &= I_s(\xi=0, \hat{t}) \frac{e^{\tilde{\alpha}\xi} \left(\frac{\tilde{\alpha}}{I_p(\xi=0, \hat{t})}\right)^2}{(\widehat{G}e^{\tilde{\alpha}\xi} - \tilde{\beta})^2} \\
&= I_s(\xi=0, \hat{t}) \frac{e^{\tilde{\alpha}\xi} \left(\frac{\tilde{\alpha}}{I_p(\xi=0, \hat{t})}\right)^2}{\left(e^{\tilde{\alpha}\xi} \frac{\tilde{\alpha}}{I_p(\xi=0, \hat{t})} - \tilde{\beta}(1 - e^{\tilde{\alpha}\xi})\right)^2} \tag{2.23}
\end{aligned}$$

One simple way to verify expressions Eqn. 2.17, Eqn. 2.18, Eqn. 2.20 and Eqn. 2.23 is by taking the limit $\tilde{\beta} \rightarrow 0$. We then have

$$\begin{aligned}
\lim_{\tilde{\beta} \rightarrow 0} I_p(\xi, \hat{t}) &= \lim_{\tilde{\beta} \rightarrow 0} \frac{\tilde{\alpha}}{e^{\tilde{\alpha}\xi} \left[\tilde{\beta} + \frac{\tilde{\alpha}}{I_p(\xi=0, \hat{t})}\right] - \tilde{\beta}} = I_p(\xi=0, \hat{t}) e^{-\tilde{\alpha}\xi} \\
\lim_{\tilde{\beta} \rightarrow 0} \phi_p(\xi, \hat{t}) &= \lim_{\tilde{\beta} \rightarrow 0} \left\{ \frac{\tilde{\gamma}}{\tilde{\beta}} \left[\ln(\widehat{G}e^{\tilde{\alpha}\xi} - \tilde{\beta}) - \tilde{\alpha}\xi \right] - \frac{\tilde{\gamma}}{\tilde{\beta}} \ln\left(\frac{\tilde{\alpha}}{I_p(\xi=0, \hat{t})}\right) \right\} \\
&\quad + \phi_p(\xi=0, \hat{t}) \\
&= \lim_{\tilde{\beta} \rightarrow 0} \left\{ \frac{\tilde{\gamma}}{\tilde{\beta}} \ln\left[\frac{(\widehat{G}e^{\tilde{\alpha}\xi} - \tilde{\beta})e^{-\tilde{\alpha}\xi} I_p(\xi=0, \hat{t})}{\tilde{\alpha}}\right] \right\} \\
&\quad + \phi_p(\xi=0, \hat{t}) \\
&= \lim_{\tilde{\beta} \rightarrow 0} \left\{ \frac{\tilde{\gamma}}{\tilde{\beta}} \ln\left[\frac{\tilde{\beta}(1 - e^{-\tilde{\alpha}\xi}) I_p(\xi=0, \hat{t}) + \tilde{\alpha}}{\tilde{\alpha}}\right] \right\} \\
&\quad + \phi_p(\xi=0, \hat{t}) \\
&= \lim_{\tilde{\beta} \rightarrow 0} \left\{ \left[\frac{\tilde{\gamma}(1 - e^{-\tilde{\alpha}\xi}) I_p(\xi=0, \hat{t})}{\tilde{\alpha} + \tilde{\beta}(1 - e^{-\tilde{\alpha}\xi}) I_p(\xi=0, \hat{t})} \right] \right\} \\
&\quad + \phi_p(\xi=0, \hat{t}) \\
&= \phi_p(\xi=0, \hat{t}) + \frac{\tilde{\gamma}}{\tilde{\alpha}} (1 - e^{-\tilde{\alpha}\xi}) I_p(\xi=0, \hat{t}) \\
\lim_{\tilde{\beta} \rightarrow 0} I_s(\xi, \hat{t}) &= \lim_{\tilde{\beta} \rightarrow 0} I_s(\xi=0, \hat{t}) \frac{e^{\tilde{\alpha}\xi} \left(\frac{\tilde{\alpha}}{I_p(\xi=0, \hat{t})}\right)^2}{\left(e^{\tilde{\alpha}\xi} \frac{\tilde{\alpha}}{I_p(\xi=0, \hat{t})} - \tilde{\beta}(1 - e^{\tilde{\alpha}\xi})\right)^2}
\end{aligned}$$

$$\begin{aligned}
&= I_s(\xi = 0, \hat{t})e^{-\tilde{\alpha}\xi} \\
\lim_{\tilde{\beta} \rightarrow 0} \phi_s(\xi, \hat{t}) &= \lim_{\tilde{\beta} \rightarrow 0} \frac{2\tilde{\gamma}}{\tilde{\beta}} \left[\ln(\hat{G}e^{\tilde{\alpha}\xi} - \tilde{\beta}) - \tilde{\alpha}\xi \right] - \frac{2\tilde{\gamma}}{\tilde{\beta}} \ln \left(\frac{\tilde{\alpha}}{I_p(\xi = 0, \hat{t})} \right) \\
&\quad + \phi_s(\xi = 0, \hat{t}) \\
&= \phi_s(\xi = 0, \hat{t}) + \frac{2\tilde{\gamma}}{\tilde{\alpha}} (1 - e^{-\tilde{\alpha}\xi}) I_p(\xi = 0, \hat{t}). \tag{2.24}
\end{aligned}$$

The result is consistent with the result from directly solving Eqn. 2.11 with $\tilde{\beta} = 0$.

With the expressions Eqn. 2.17, Eqn. 2.18, Eqn. 2.20 and Eqn. 2.23, we are ready to write down the probe beam field after the propagation of the distance L , $E_s(1, \hat{t})$.

$$\begin{aligned}
E_s(1, \hat{t}) &\propto [I_s(1, \hat{t})]^{1/2} \exp[i\phi_s(1, \hat{t})] \\
&= [I_s(0, \hat{t})]^{1/2} \frac{e^{\tilde{\alpha}/2} \tilde{\alpha}}{I_p(0, \hat{t})(\hat{G}e^{\tilde{\alpha}} - \tilde{\beta})} \\
&\quad \times \exp[i\phi_s(0, \hat{t})] \exp\left\{ i \frac{2\tilde{\gamma}}{\tilde{\beta}} \left[\ln \frac{(\hat{G} - \tilde{\beta}e^{-\tilde{\alpha}}) I_p(0, \hat{t})}{\tilde{\alpha}} \right] \right\} \\
&= [I_s(0, \hat{t})]^{1/2} \exp[i\phi_s(0, \hat{t})] \exp(-\tilde{\alpha}/2) \frac{\exp\left[i \frac{2\tilde{\gamma}}{\tilde{\beta}} \ln\left(1 + \frac{\tilde{\beta}}{\tilde{\alpha}}(1 - e^{-\tilde{\alpha}}) I_p(0, \hat{t})\right) \right]}{\left(1 + \frac{\tilde{\beta}}{\tilde{\alpha}}(1 - e^{-\tilde{\alpha}}) I_p(0, \hat{t})\right)} \tag{2.25}
\end{aligned}$$

The SRTBC signal trace can then be calculated:

$$\frac{\Delta T}{T} = \left| \frac{\mathcal{F}[E_s(1, \hat{t})]}{\mathcal{F}[E_s(0, \hat{t})]} \right|^2 - 1, \tag{2.26}$$

where $\mathcal{F}[\cdot]$ denotes Fourier transform.

We have derived the most general expression for the SRTBC trace and using Eqn. 2.25 and Eqn. 2.26 one can predict the SRTBC trace for arbitrary initial pulse shape and initial phase. Although this expression contains all possible cases, it is complicated and involves integration. In many cases, a simpler algebraic expression is more desirable. We will derive such an expression now.

For simplicity, we define:

$$\Theta \equiv \frac{\tilde{\beta}(1 - e^{\tilde{\alpha}})}{\tilde{\alpha}} I_p(0, \hat{t}) \quad (2.27)$$

We can expand Eqn. 2.25 in Θ

$$\begin{aligned} E_s(1, \hat{t}) &= E_s(0, \hat{t}) e^{-\tilde{\alpha}/2} \frac{\exp[i\frac{2\tilde{\gamma}}{\tilde{\beta}} \ln(1 + \Theta)]}{1 + \Theta} \\ &= E_s(0, \hat{t}) e^{-\tilde{\alpha}/2} (1 - \Theta + \Theta^2 - \Theta^3 + \dots) \exp[i\frac{2\tilde{\gamma}}{\tilde{\beta}} \ln(1 + \Theta)] \\ &= E_s(0, \hat{t}) e^{-\tilde{\alpha}/2} (1 - \Theta + \Theta^2 - \Theta^3 + \dots) \\ &\quad \times \left\{ 1 + \left[\frac{i2\tilde{\gamma}}{\tilde{\beta}} \left(\Theta - \frac{\Theta^2}{2} + \frac{\Theta^3}{3} - \dots \right) \right] + \frac{1}{2!} \left[\frac{i2\tilde{\gamma}}{\tilde{\beta}} \left(\Theta - \frac{\Theta^2}{2} + \frac{\Theta^3}{3} - \dots \right) \right]^2 \right. \\ &\quad \left. + \frac{1}{3!} \left[\frac{i2\tilde{\gamma}}{\tilde{\beta}} \left(\Theta - \frac{\Theta^2}{2} + \frac{\Theta^3}{3} - \dots \right) \right]^3 + \dots \right\} \end{aligned} \quad (2.28)$$

On the other hand we also have

$$e^{-\tilde{\alpha}/2} = 1 - \frac{\tilde{\alpha}}{2} + \frac{\tilde{\alpha}^2}{2!2^2} - \frac{\tilde{\alpha}^3}{3!2^3} + \dots \quad (2.29)$$

With the above expansion Eqn. 2.29 we can rewrite $E_s(1, \hat{t})$:

$$\begin{aligned} E_s(1, \hat{t}) &= E_s(0, \hat{t}) \left(1 - \frac{\tilde{\alpha}}{2} + \frac{\tilde{\alpha}^2}{2!2^2} - \frac{\tilde{\alpha}^3}{3!2^3} + \dots \right) (1 - \Theta + \Theta^2 - \Theta^3 + \dots) \\ &\quad \times \left\{ 1 + \left[\frac{i2\tilde{\gamma}}{\tilde{\beta}} \left(\Theta - \frac{\Theta^2}{2} + \frac{\Theta^3}{3} - \dots \right) \right] + \frac{1}{2!} \left[\frac{i2\tilde{\gamma}}{\tilde{\beta}} \left(\Theta - \frac{\Theta^2}{2} + \frac{\Theta^3}{3} - \dots \right) \right]^2 \right. \\ &\quad \left. + \frac{1}{3!} \left[\frac{i2\tilde{\gamma}}{\tilde{\beta}} \left(\Theta - \frac{\Theta^2}{2} + \frac{\Theta^3}{3} - \dots \right) \right]^3 + \dots \right\} \end{aligned} \quad (2.30)$$

Furthermore,

$$\begin{aligned} \frac{(1 - e^{-\tilde{\alpha}})}{\tilde{\alpha}} &= \frac{1 - \left(1 - \tilde{\alpha} + \frac{\tilde{\alpha}^2}{2!} - \frac{\tilde{\alpha}^3}{3!} + \dots \right)}{\tilde{\alpha}} \\ &= 1 - \frac{\tilde{\alpha}}{2!} + \frac{\tilde{\alpha}^2}{3!} - \dots \end{aligned} \quad (2.31)$$

So we have

$$\Theta = \tilde{\beta} I_p(0, \hat{t}) \left(1 - \frac{\tilde{\alpha}}{2!} + \frac{\tilde{\alpha}^2}{3!} - \dots \right). \quad (2.32)$$

Expanding Eqn. 2.30 and keeping the lowest two orders of $\tilde{\alpha}$, $\tilde{\beta}$ and $\tilde{\gamma}$ (and thus of Θ , since Θ is the order of $\tilde{\beta}$):

$$\begin{aligned}
E_s(1, \hat{t}) &= E_s(0, \hat{t}) \left(1 - \frac{\tilde{\alpha}}{2} + \frac{\tilde{\alpha}^2}{2!2^2}\right) (1 - \Theta + \Theta^2) \\
&\quad \times \left(1 + \frac{i2\tilde{\gamma}}{\tilde{\beta}}\Theta - \frac{i\tilde{\gamma}}{\tilde{\beta}}\Theta^2 - \frac{2\tilde{\gamma}^2}{\tilde{\beta}^2}\Theta^2\right) + \dots \\
&= E_s(0, \hat{t}) \left(1 - \frac{\tilde{\alpha}}{2} - \Theta + \frac{i2\tilde{\gamma}}{\tilde{\beta}}\Theta + \frac{\tilde{\alpha}^2}{8} + \Theta^2 - \frac{i\tilde{\gamma}}{\tilde{\beta}}\Theta^2 - \frac{2\tilde{\gamma}^2}{\tilde{\beta}^2}\Theta^2 + \frac{\tilde{\alpha}}{2}\Theta - \frac{i\tilde{\alpha}\tilde{\gamma}}{\tilde{\beta}}\Theta - \frac{i2\tilde{\gamma}}{\tilde{\beta}}\Theta^2 + \dots\right) \\
&= E_s(0, \hat{t}) \left[1 - \frac{\tilde{\alpha}}{2} - \tilde{\beta}I_p(0, \hat{t}) + 2i\tilde{\gamma}I_p(0, \hat{t}) + \tilde{\alpha}\tilde{\beta}I_p(0, \hat{t}) - i2\tilde{\alpha}\tilde{\gamma}I_p(0, \hat{t}) \right. \\
&\quad \left. + \frac{\tilde{\alpha}^2}{8} + \tilde{\beta}^2(I_p(0, \hat{t}))^2 - i3\tilde{\beta}\tilde{\gamma}(I_p(0, \hat{t}))^2 - 2\tilde{\gamma}^2(I_p(0, \hat{t}))^2 + \dots\right] \quad (2.33)
\end{aligned}$$

We now assume the pulses are Gaussian and initial phase is zero:

$$\begin{aligned}
E_p(0, \hat{t}) &= E_{p0}e^{-\hat{t}^2/t_0^2} \\
E_s(0, \hat{t}) &= E_{s0}e^{-(\hat{t}-\tau)^2/t_0^2} \quad (2.34)
\end{aligned}$$

and

$$\begin{aligned}
I_p(0, \hat{t}) &= I_{p0}e^{-2\hat{t}^2/t_0^2} \\
I_s(0, \hat{t}) &= I_{s0}e^{-2(\hat{t}-\tau)^2/t_0^2} \quad (2.35)
\end{aligned}$$

With these, we obtain the expression for $E_s(1, \hat{t})$

$$\begin{aligned}
E_s(1, \hat{t}) &= E_{s0} \left\{ \left(1 - \frac{\tilde{\alpha}}{2} + \frac{\tilde{\alpha}^2}{8}\right) \exp\left[-\frac{(\hat{t}-\tau)^2}{t_0^2}\right] - (\tilde{\beta} - i2\tilde{\gamma} - \tilde{\alpha}\tilde{\beta} + i2\tilde{\alpha}\tilde{\gamma}) \right. \\
&\quad \times I_{p0} \exp\left[-\frac{(\hat{t}-\tau)^2}{t_0^2}\right] \exp\left[-\frac{2\hat{t}^2}{t_0^2}\right] + (\tilde{\beta}^2 - 2\tilde{\gamma}^2 - i3\tilde{\beta}\tilde{\gamma}) \\
&\quad \left. \times I_{p0}^2 \exp\left[-\frac{(\hat{t}-\tau)^2}{t_0^2}\right] \exp\left[-\frac{4\hat{t}^2}{t_0^2}\right] + \dots \right\} \quad (2.36)
\end{aligned}$$

Using Fourier transform

$$\mathcal{F}\left[e^{-at^2}\right] = \frac{1}{\sqrt{2a}}e^{-\omega^2/(4a)} \quad (2.37)$$

We have

$$\begin{aligned}
\mathcal{F}[E_s(1, \hat{t})] &= E_{s0} \left\{ \frac{t_0}{\sqrt{2}} \left(1 - \frac{\tilde{\alpha}}{2} + \frac{\tilde{\alpha}^2}{8} \right) \exp[i\omega\tau] \exp\left[-\frac{\omega^2 t_0^2}{4}\right] \right. \\
&\quad - \frac{t_0}{\sqrt{6}} (\tilde{\beta} - i2\tilde{\gamma} - \tilde{\alpha}\tilde{\beta} + i2\tilde{\alpha}\tilde{\gamma}) I_{p0} \exp\left[i\frac{\omega\tau}{3}\right] \exp\left[-\frac{\omega^2 t_0^2}{12}\right] \exp\left[-\frac{2\tau^2}{3t_0^2}\right] \\
&\quad \left. + \frac{t_0}{\sqrt{10}} (\tilde{\beta}^2 - 2\tilde{\gamma}^2 - i3\tilde{\beta}\tilde{\gamma}) I_{p0}^2 \exp\left[i\frac{\omega\tau}{5}\right] \exp\left[-\frac{\omega^2 t_0^2}{20}\right] \exp\left[-\frac{4\tau^2}{5t_0^2}\right] + \dots \right\} \\
&= E_{s0} \frac{t_0}{\sqrt{2}} \exp[i\omega\tau] \exp\left[-\frac{\omega^2 t_0^2}{4}\right] \left\{ 1 - \left[\frac{\tilde{\alpha}}{2} + \frac{1}{\sqrt{3}} I_{p0} \right. \right. \\
&\quad \times \exp\left[-i\frac{2\omega\tau}{3}\right] \exp\left[\frac{\omega^2 t_0^2}{6}\right] \exp\left[-\frac{2\tau^2}{3t_0^2}\right] (\tilde{\beta} - i2\tilde{\gamma}) \right] + \left[\frac{\tilde{\alpha}^2}{8} \right. \\
&\quad \left. + \frac{1}{\sqrt{3}} I_{p0} \exp\left[-i\frac{2\omega\tau}{3}\right] \exp\left[\frac{\omega^2 t_0^2}{6}\right] \exp\left[-\frac{2\tau^2}{3t_0^2}\right] (\tilde{\alpha}\tilde{\beta} - i2\tilde{\alpha}\tilde{\gamma}) \right. \\
&\quad \left. + \frac{1}{\sqrt{5}} I_{p0}^2 \exp\left[-i\frac{4\omega\tau}{5}\right] \exp\left[\frac{\omega^2 t_0^2}{5}\right] \exp\left[-\frac{4\tau^2}{5t_0^2}\right] (\tilde{\beta}^2 - 2\tilde{\gamma}^2 - i3\tilde{\beta}\tilde{\gamma}) \right] \\
&\quad \left. + \dots \right\} \tag{2.38}
\end{aligned}$$

and

$$\begin{aligned}
|\mathcal{F}[E_s(1, \hat{t})]|^2 &= E_{s0}^2 \frac{t_0^2}{2} e^{-(\omega t_0)^2/2} \left\{ 1 - 2\text{Re} \left[\frac{\tilde{\alpha}}{2} + \frac{1}{\sqrt{3}} I_{p0} \right. \right. \\
&\quad \times \exp\left[-i\frac{2\omega\tau}{3}\right] \exp\left[\frac{\omega^2 t_0^2}{6}\right] \exp\left[-\frac{2\tau^2}{3t_0^2}\right] (\tilde{\beta} - i2\tilde{\gamma}) \right] \\
&\quad + 2\text{Re} \left[\frac{\tilde{\alpha}^2}{8} + \frac{1}{\sqrt{3}} I_{p0} \exp\left[-i\frac{2\omega\tau}{3}\right] \exp\left[\frac{\omega^2 t_0^2}{6}\right] \exp\left[-\frac{2\tau^2}{3t_0^2}\right] (\tilde{\alpha}\tilde{\beta} - i2\tilde{\alpha}\tilde{\gamma}) \right. \\
&\quad \left. + \frac{1}{\sqrt{5}} I_{p0}^2 \exp\left[-i\frac{4\omega\tau}{5}\right] \exp\left[\frac{\omega^2 t_0^2}{5}\right] \exp\left[-\frac{4\tau^2}{5t_0^2}\right] (\tilde{\beta}^2 - 2\tilde{\gamma}^2 - i3\tilde{\beta}\tilde{\gamma}) \right] \\
&\quad \left. + \left[\frac{\tilde{\alpha}}{2} + \frac{1}{\sqrt{3}} I_{p0} \exp\left[-i\frac{2\omega\tau}{3}\right] \exp\left[\frac{\omega^2 t_0^2}{6}\right] \exp\left[-\frac{2\tau^2}{3t_0^2}\right] (\tilde{\beta} - i2\tilde{\gamma}) \right] \right. \\
&\quad \left. \left[\frac{\tilde{\alpha}}{2} + \frac{1}{\sqrt{3}} I_{p0} \exp\left[i\frac{2\omega\tau}{3}\right] \exp\left[\frac{\omega^2 t_0^2}{6}\right] \exp\left[-\frac{2\tau^2}{3t_0^2}\right] (\tilde{\beta} + i2\tilde{\gamma}) \right] + \dots \right\} \\
&= E_{s0}^2 \frac{t_0^2}{2} e^{-(\omega t_0)^2/2} \left\{ 1 - \tilde{\alpha} + \frac{\tilde{\alpha}^2}{2} + \frac{2}{\sqrt{3}} I_{p0} \exp\left[\frac{\omega^2 t_0^2}{6}\right] \exp\left[-\frac{2\tau^2}{3t_0^2}\right] \right. \\
&\quad \times \left[2 \left(1 - \frac{3}{2} \tilde{\alpha} \right) \tilde{\gamma} \sin\left(\frac{2\omega\tau}{3}\right) - \left(1 - \frac{3}{2} \tilde{\alpha} \right) \tilde{\beta} \cos\left(\frac{2\omega\tau}{3}\right) \right] \\
&\quad + \frac{2}{\sqrt{5}} I_{p0}^2 \exp\left[\frac{\omega^2 t_0^2}{5}\right] \exp\left[-\frac{4\tau^2}{5t_0^2}\right] \left[(\tilde{\beta}^2 - 2\tilde{\gamma}^2) \cos\left(\frac{4\omega\tau}{5}\right) - 3\tilde{\beta}\tilde{\gamma} \sin\left(\frac{4\omega\tau}{5}\right) \right] \\
&\quad \left. + \frac{4}{3} I_{p0}^2 \exp\left[\frac{\omega^2 t_0^2}{3}\right] \exp\left[-\frac{4\tau^2}{3t_0^2}\right] \left(\frac{\tilde{\beta}^2}{4} + \tilde{\gamma}^2 \right) + \dots \right\} \tag{2.39}
\end{aligned}$$

Since

$$|\mathcal{F}[E_s(0, \hat{t})]|^2 = E_{s0}^2 \frac{t_0^2}{2} e^{-(\omega t_0)^2/2} \quad (2.40)$$

From Eqn. 2.26 we have

$$\begin{aligned} \frac{\Delta T}{T} = & \left\{ -\tilde{\alpha} + \frac{\tilde{\alpha}^2}{2} + \frac{2}{\sqrt{3}} I_{p0} \exp\left[\frac{\omega^2 t_0^2}{6}\right] \exp\left[-\frac{2\tau^2}{3t_0^2}\right] \right. \\ & \times \left[2\left(1 - \frac{3}{2}\tilde{\alpha}\right)\tilde{\gamma} \sin\left(\frac{2\omega\tau}{3}\right) - \left(1 - \frac{3}{2}\tilde{\alpha}\right)\tilde{\beta} \cos\left(\frac{2\omega\tau}{3}\right) \right] \\ & + \frac{2}{\sqrt{5}} I_{p0}^2 \exp\left[\frac{\omega^2 t_0^2}{5}\right] \exp\left[-\frac{4\tau^2}{5t_0^2}\right] \left[(\tilde{\beta}^2 - 2\tilde{\gamma}^2) \cos\left(\frac{4\omega\tau}{5}\right) - 3\tilde{\beta}\tilde{\gamma} \sin\left(\frac{4\omega\tau}{5}\right) \right] \\ & \left. + \frac{4}{3} I_{p0}^2 \exp\left[\frac{\omega^2 t_0^2}{3}\right] \exp\left[-\frac{4\tau^2}{3t_0^2}\right] \left(\frac{\tilde{\beta}^2}{4} + \tilde{\gamma}^2 \right) + \dots \right\} \quad (2.41) \end{aligned}$$

This expression reduces to Eqn. 2.7 when $\tilde{\alpha} = 0$ and only the lowest order terms of $\tilde{\beta}$ and $\tilde{\gamma}$ are kept. Note in the above derivation the center frequency has been shifted to 0 (we have taken out the carrier frequency) thus $\omega_0 = 0$ and $\omega = \delta$ is frequency detuning.

We have derived the general analytical expression for a SRTBC trace and an approximate algebraic expression for the SRTBC trace with Gaussian pulses up to second order of $\tilde{\alpha}$, $\tilde{\beta}$ and $\tilde{\gamma}$. In the next section, we will examine the intensity dependence (i.e. the dependence on I_{p0} of the SRTBC signal size.) We will also compare the approximate expression with the direct numerical calculation from Eqn. 2.11.

2.3 Comparison of linear approximation, second-order approximation and numerical simulation

While the approximate expressions derived in the last section are convenient and in general more transparent than the numerical simulation, as we will see very soon,

these expressions become invalid and introduce large errors as the nonlinear phase shift $\Delta\phi_{NL}$ becomes large. Under these conditions, numerical simulation must be used.

It is straightforward to simulate Eqn. 2.11. Fourth-order Runge-Kutta method is used to evaluate the propagation of the pulses. The Pulse intensity profile and phase function after propagation can be calculated and these can then be used to obtain the SRTBC signal trace. We have included the source code used in this work in the appendix (the source code is a generalized version including the higher-order nonlinearities, which will be discussed in the next chapter). For a given set of simulation parameters $\tilde{\alpha}$, $\tilde{\beta}$, and $\tilde{\gamma}$, a two-dimensional data matrix can be obtained. Fig. 2.4 and Fig. 2.5 show such a data matrix. One coordinate of the data matrix is the time delay between the pump- and probe-beam, the other coordinate is the frequency detuning. A SRTBC signal trace is obtained through spectrally selecting a specific frequency component and a typical bipolar signal trace is obtained. This is achieved using a monochromater in actual experiments.

Some important features of the SRTBC trace are evident in Fig. 2.4 and Fig. 2.5. In general, the larger the detuning, the larger the signal size. This characteristic is also evident in both the linear approximate expression and second-order approximate expression derived in the previous section. As in both expressions, factors such as $\exp(\delta^2 t_0^2/6)$ are present. Another interesting general property of the SRTBC signal trace is its invariance under the transformation:

$$\begin{aligned}\delta &\rightarrow -\delta \\ \tau &\rightarrow -\tau.\end{aligned}\tag{2.42}$$

Again, one can also see this from both approximate expressions derived in the last section. More generally, this is true for any initial pulse profile symmetric in time.

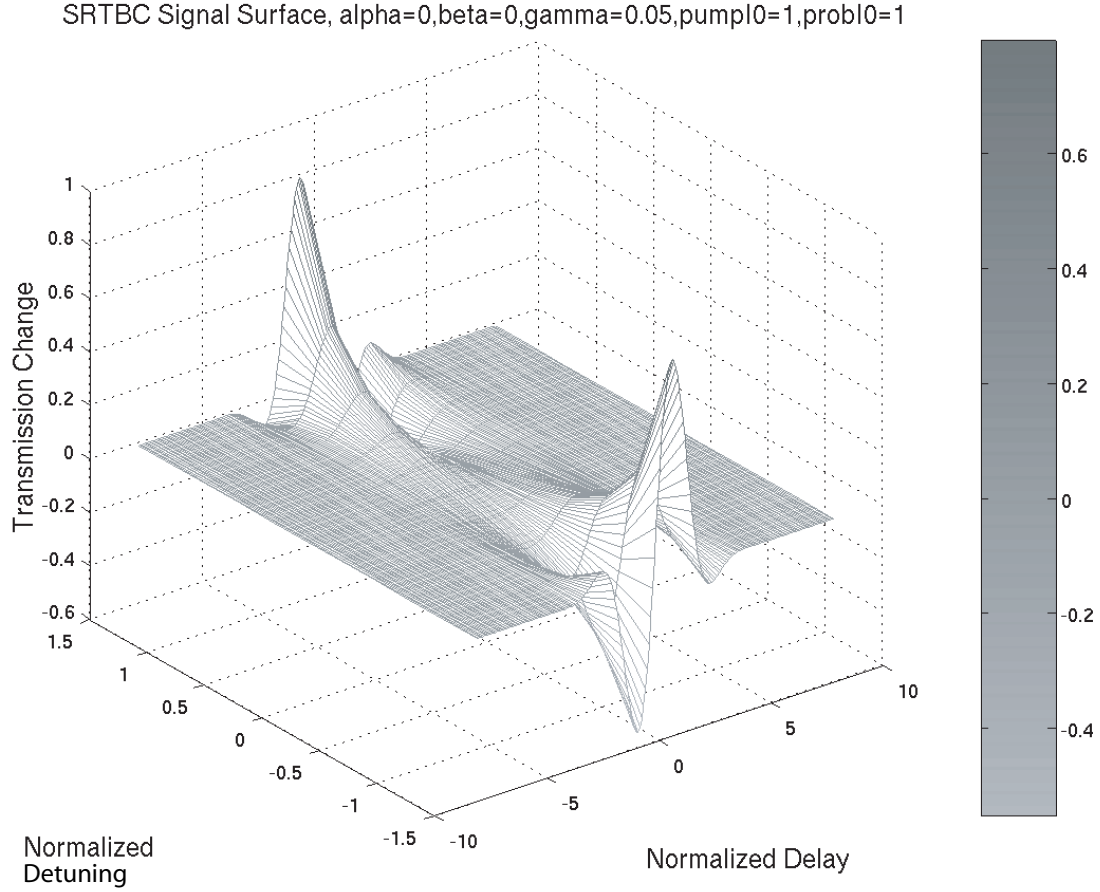


Figure 2.4: A two-dimensional data matrix of SRTBC. As indicated in the figure, the simulation parameters are $\tilde{\alpha} = 0$, $\tilde{\beta} = 0$, $\tilde{\gamma} = 0.05$, and $I_{p0} = 1$. This corresponds to a nonlinear phase shift $\Delta\phi_{NL} = 0.05$. The detuning is in the unit of FWHM PSD. The time delay is in the unit of half-width at $(1/e)$ -maximum of the intensity profile. A SRTBC signal trace can be obtained from sectioning the data matrix along a fixed detuning.

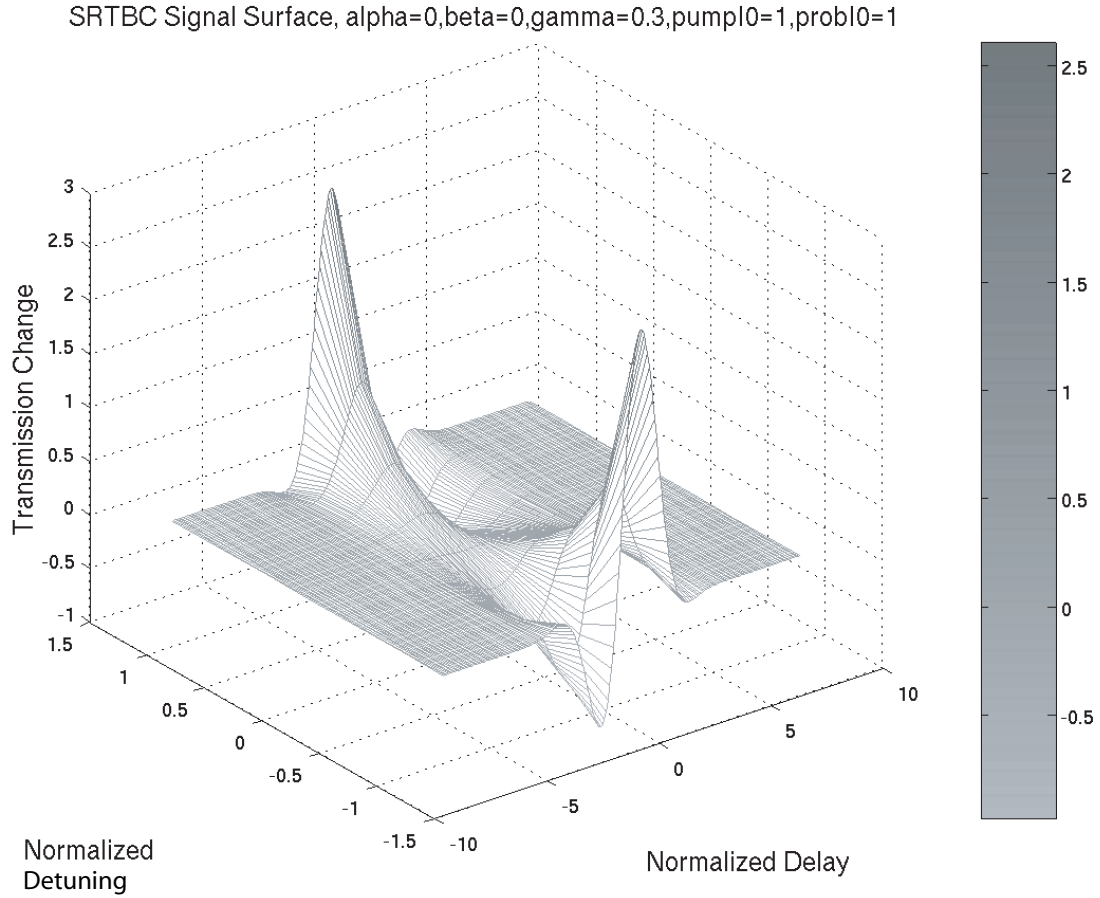


Figure 2.5: Another two-dimensional data matrix of SRTBC. Here, the simulation parameters are $\tilde{\alpha} = 0$, $\tilde{\beta} = 0$, $\tilde{\gamma} = 0.3$, and $I_{p0} = 1$. This corresponds to a nonlinear phase shift $\Delta\phi_{NL} = 0.3$. Similar to Fig. 2.4, the detuning is in the unit of FWHM PSD. The time delay is in the unit of half-width at $(1/e)$ -maximum of the intensity profile.

To prove this, assume that the probe beam electric field in time after propagation is $\Psi(\hat{t}, \tau)$, where \hat{t} and τ are time and delay respectively. The SRTBC signal trace is then related to the spectrum of the probe-beam, which is

$$\int \Psi(\hat{t}, \tau) e^{i\omega\hat{t}} d\hat{t}, \quad (2.43)$$

and this is invariant under the transformation Eqn. 2.42 if $\Psi(-\hat{t}, -\tau) = \Psi(\hat{t}, \tau)$. From the exact expression for the probe-beam field Eqn. 2.25 we can see that this condition can be satisfied as long as the initial pulse profile is symmetric in time, such as with an unchirped Gaussian pulse.

Both Fig. 2.4 and Fig. 2.5 show the typical two-dimensional data matrix of SRTBC. The difference between these two is the magnitude of the nonlinearity, the magnitude of the nonlinear phase shift the propagation generates. In Fig. 2.4, the nonlinear phase shift is 0.05, and in Fig. 2.5, it is 0.3. One can see from Fig. 2.5 that, as the nonlinear phase shift increases, the shape of the signal does not just scale up proportionally. Noticeable distortion is evident in Fig. 2.5. This is an indication that the linear approximate expression breaks down when the nonlinear phase shift exceeds a certain limit.

More detailed comparison can be done by restricting ourselves to a certain spectral component of the data, i.e. for a fixed detuning. This is illustrated in Fig. 2.6 (with nonlinear phase shift 0.05), and Fig 2.7 (with nonlinear phase shift 0.5). The detuning in both figures is 1 full-width at half-maximum (FWHM) of the power spectrum density (PSD). It is clear that in Fig. 2.6, both linear and second-order approximate expressions agree with the direct numerical simulation very well. On the other hand, as the nonlinear phase shift becomes larger (beyond ~ 0.1), the linear approximate expression quickly breaks down and the second-order approximate expression also starts to deviate from the numerical simulation,

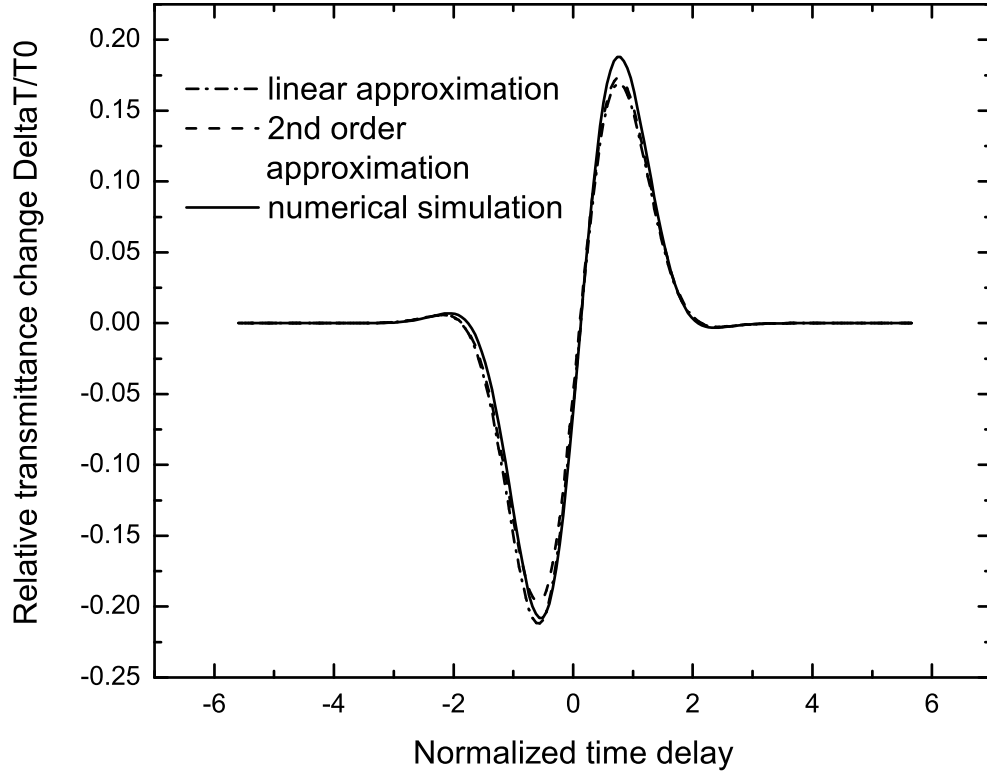


Figure 2.6: SRTBC signal traces produced by a linear approximate expression, a second-order approximate expression, and numerical simulation. The parameters used are $\tilde{\alpha} = 0$, $\tilde{\beta} = 0.02$, $\tilde{\gamma} = 0.05$, and $I_{p0} = 1$. The corresponding nonlinear phase shift $\Delta\phi_{NL} = 0.05$. The frequency detuning is 1 FWHM PSD, and the time delay is in the unit of half-width at $(1/e)$ -maximum of the field profile. The approximate expressions agree with numerical simulation well.

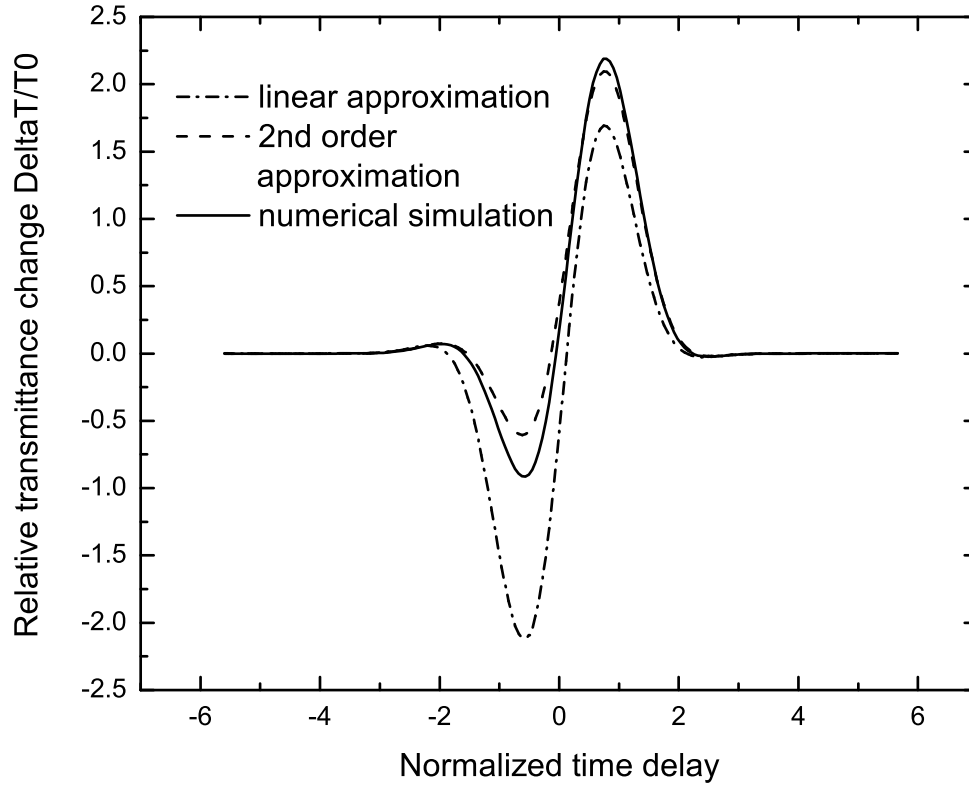


Figure 2.7: SRTBC signal traces produced by a linear approximate expression, a second-order approximate expression, and numerical simulation with parameters of 10 times the magnitude of those in Fig. 2.6. The parameters used are $\tilde{\alpha} = 0$, $\tilde{\beta} = 0.2$, $\tilde{\gamma} = 0.5$, and $I_{p0} = 1$. The corresponding nonlinear phase shift $\Delta\phi_{NL}$ is 0.5. The frequency detuning is 1 FWHM PSD, and the time delay is in the unit of half-width at $(1/e)$ -maximum of the field profile. It is clear that linear approximate expression breaks down. On the contrary, second-order approximate expression agrees with numerical simulation relatively well.

as shown in Fig. 2.7.

Although in general the second-order approximate expression holds up to larger nonlinear phase shifts (as is evident in Fig. 2.7), we expect this expression to break down as the nonlinear phase shift continues to increase. Figs. 2.8, 2.9, 2.10 and 2.11 show some systematic comparison of the SRTBC signal trace peak/valley magnitude and overall signal size (peak-valley) magnitude generated using the linear approximate expression, second-order approximate expression and direct numerical simulation. The frequency detuning in Fig. 2.8 and Fig. 2.9 is 1.5 FWHM PSD, and in Fig. 2.10 and Fig. 2.11 it is 0.5 FWHM PSD. From these figures, we can see that indeed the second-order approximate expression is applicable for a larger range of nonlinear phase shift than the linear approximate expression. However, both approximate expressions generate significant error for nonlinear phase shifts larger than ~ 0.3 . It is also interesting to note that for larger frequency detuning, the deviation is more significant. This is expected, since the sensitivity of the process is determined by factors such as $\exp(\delta^2 t_0^2/6)$.

Another significant implication from these observation is that in order to isolate the possible higher-order nonlinear effects (such as $\chi^{(5)}$, $\chi^{(7)}$), one can not rely on the linear or any approximate expression. Since the signal magnitude does not increase proportionally with the increase of the pulse intensity (thus the nonlinear phase shift), a measured signal intensity dependence deviating from a straight line itself is no guarantee that higher-order nonlinear effects are present. One will need to compare the measured result with the numerical simulated result to determine if higher-order nonlinear effects are observed. Moreover, if higher-order nonlinear effects are indeed present, in order to determine the magnitude of these effects, a more complicated model including higher-order nonlinearities will be needed. This

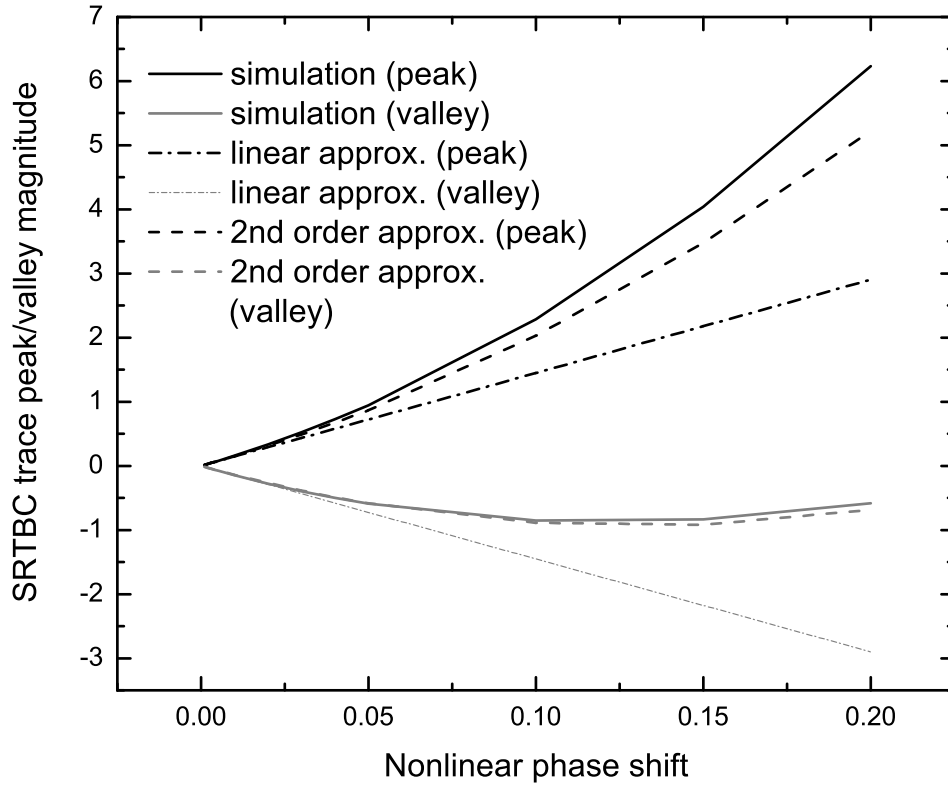


Figure 2.8: Nonlinear phase shift (and thus intensity) dependence of the SRTBC signal trace peak/valley magnitude predicted by a linear approximate expression, a second-order approximate expression, and numerical simulation. The frequency detuning is 1.5 FWHM PSD. While the second-order approximate expression agrees with the numerical simulation better than linear approximate simulation, at large nonlinear phase shift, the deviation of both approximate expressions is significant.

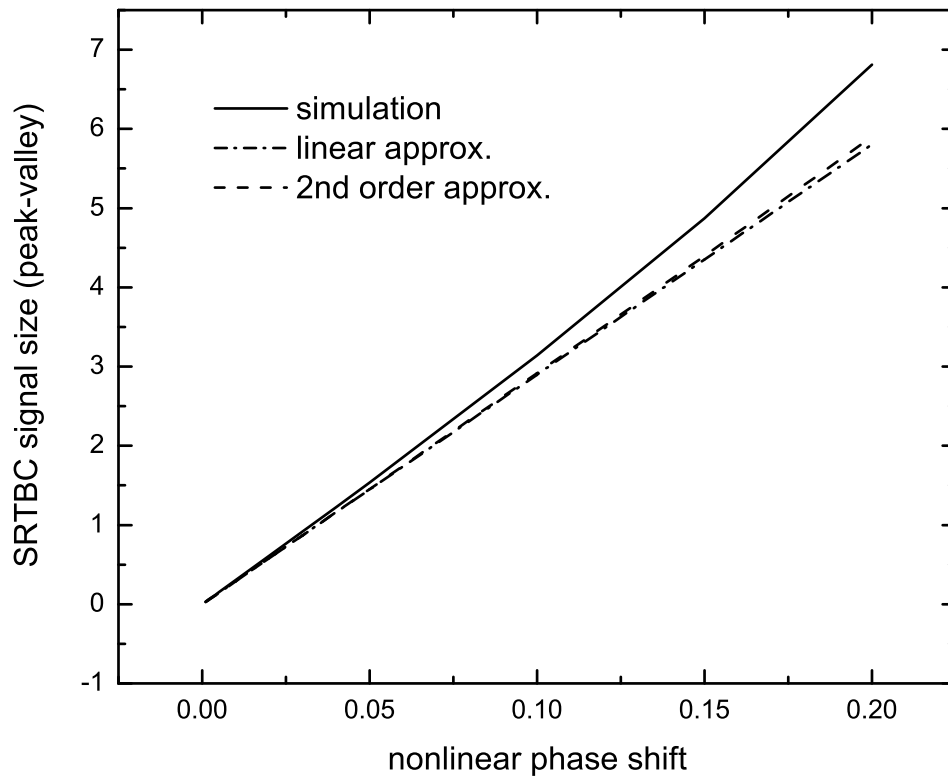


Figure 2.9: Nonlinear phase shift dependence of the SRTBC signal size (peak-valley). The frequency detuning is 1.5 FWHM PSD. The same data in Fig. 2.8 is presented here differently, with the SRTBC trace peak-valley amplitude plotted.

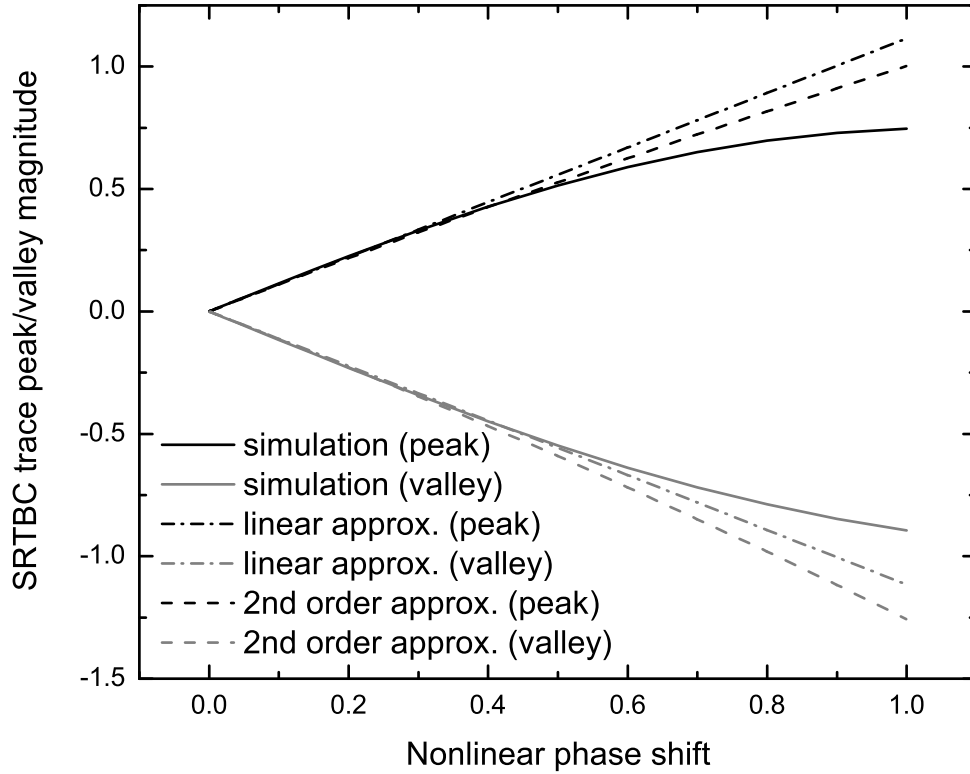


Figure 2.10: Nonlinear phase shift (and thus intensity) dependence of the SRTBC signal trace peak/valley magnitude predicted by a linear approximate expression, a second-order approximate expression, and numerical simulation. The frequency detuning is 0.5 FWHM PSD. While the second-order approximate expression agrees with the numerical simulation well up to a nonlinear phase shift ~ 0.5 , at large nonlinear phase shift, the deviation of both approximate expressions become significant.

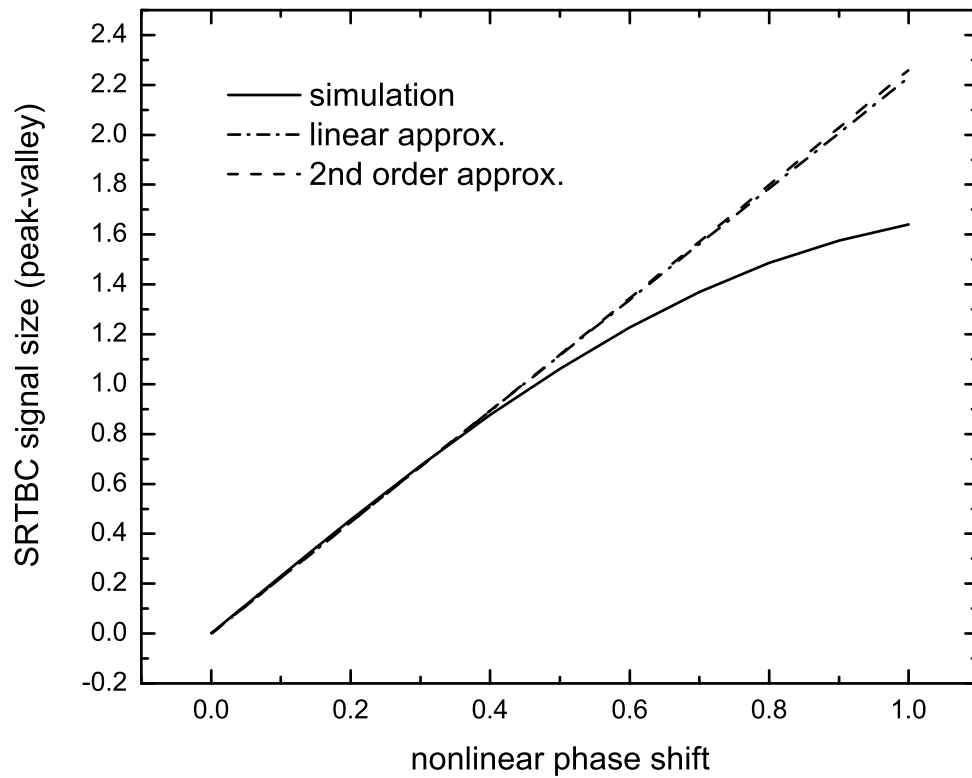


Figure 2.11: Nonlinear phase shift dependence of the SRTBC signal size (peak-valley). The frequency detuning is 0.5 FWHM PSD. The same data in Fig. 2.10 is presented here in differently, with the SRTBC trace peak-valley amplitude plotted.

is the main cause that motivates the work described in the next chapter.

2.4 Conclusions

We have derived the exact analytical expression for SRTBC signal traces with arbitrary initial pump-beam and probe-beam profile and phase in media with linear properties and instantaneous third-order nonlinearities ($\chi^{(3)}$). Approximative expressions are also derived from the exact analytical expression. Both linear and second-order approximate expressions are used to predict SRTBC signal traces. The comparison of these predictions with the numerical simulation shows that the linear approximate expression breaks down quickly as the nonlinear phase shift increases and becomes larger than ~ 0.1 . Although second-order approximate expression in general works over a larger range of nonlinear phase shift, it breaks down at a nonlinear phase shift ~ 0.5 . From these observations, we conclude that in order to isolate the existence of higher-order nonlinearities such as $\chi^{(5)}$ and $\chi^{(7)}$, one can not rely solely on the prediction from the approximate expressions, since the observation of higher-order nonlinearities in general requires measurements with high intensity, which results in large nonlinear-phase shifts and the approximate expressions break down. Numerical simulations will be required in these cases. Moreover, in order to determine the magnitude of higher-order nonlinearities, a more complicated analytical model which includes higher-order nonlinear effects is needed. In the next chapter, based on the same SRTBC technique, we will develop such a model and extend the technique into the regime of higher-order nonlinearities.

Chapter 3

Measurement of fifth- and seventh-order nonlinearities of glasses

We extend the spectrally-resolved two-beam coupling to the measurements of higher-order nonlinearities. The original theoretical model is generalized to include higher-order nonlinear effects. Based on the generalization, we perform the measurement of higher-order nonlinearities of several glasses and report the observation of saturation of the cubic optical nonlinearity. Fifth- and seventh-order nonlinearities are required to account for the measured nonlinear phase shifts. The observation of saturable nonlinear indices accompanied by only moderate nonlinear absorption will be relevant to some applications.

3.1 Introduction

The nonlinear optical properties of materials are of particular interest for telecommunications, high power lasers, and pulse-propagation applications. At high intensities, nonlinearities above the cubic one, $\chi^{(3)}$, become important and have to be included to describe the optical response. In some cases (*e.g.* ultrafast optical switching) higher-order nonlinear effects can cause problems. For other applications higher-order nonlinearities are desired: *e.g.* the formation of stable multi-dimensional optical solitons requires saturation of the instantaneous Kerr nonlinearity [13, 14]. A better understanding of higher-order nonlinearities in materials is then crucial.

The nonlinearities of glasses have received considerable attention, mainly in

the context of optical switching [15, 16]. In particular, the saturation of $\chi^{(3)}$ (equivalently, the presence of higher-order nonlinearities $\chi^{(5)}, \chi^{(7)}, \dots$) recently reported in chalcogenide glasses [17] also suggests that materials appropriate to applications requiring higher-order nonlinearities exist. However, the materials were investigated under the condition of large reduced-photon energy ($h\nu/E_g \sim 0.75$, where $h\nu$ is the laser photon energy and E_g is the linear absorption edge) and therefore exhibit large nonlinear absorption [17]. The absorption likely precludes the utility of these materials in applications. Nevertheless, it is possible that the saturation of $\chi^{(3)}$ could also occur at smaller reduced-photon energy, where the nonlinear absorption is moderate. This motivates the measurements of higher-order nonlinearities at other reduced-photon energies.

Here we report measurements of higher-order nonlinearities in materials with a range of reduced-photon energies ($h\nu/E_g = 0.25 - 0.76$). Significant saturation of $\chi^{(3)}$ is observed in materials with large reduced-photon energy (~ 0.76) as well as in materials with moderate reduced-photon energy (~ 0.5). The saturation is also observed to increase with the reduced-photon energy. In general, a negative $\chi^{(5)}$ is needed to account for the saturation of $\chi^{(3)}$, and when the saturation is very strong, a self-focusing $\chi^{(7)}$ is also needed.

The experimental technique we apply in this work is spectrally-resolved two-beam coupling (SRTBC) [11]. SRTBC uses a standard pump-probe setup with the addition of a monochromator to measure the pump-induced shift of the probe spectrum. The sample is kept at the intersection of the beams, and the energy transmitted through the monochromator at a fixed detuning from the center of the spectrum is monitored. The relative transmittance as a function of the delay between the pump beam and the probe beam is recorded [11]. In the absence

of nonlinear absorption, the signal has a bipolar shape, as shown in the inset of Fig. 3.1. For materials with nonlinear index n_2 and negligible higher-order nonlinearity, the analytical approximation shows that the signal magnitude is linearly proportional to the pump-beam intensity I_p if the nonlinear phase shift is small ($\Delta\phi \equiv (2\pi/\lambda)n_2I_pL < 0.1$, where L is the interaction length) [11]. To observe higher-order effects, we expose the materials to higher intensities and thus $\Delta\phi$ can exceed 0.1. Under these conditions the approximation is no longer valid and numerical evaluation is needed even for systems with only $\chi^{(3)}$. Indeed, as shown in Fig. 3.1 the numerical calculation shows significant deviation from the small-phase shift approximation for large $\Delta\phi$. Since higher-order nonlinearities manifest themselves as deviations from the cubic nonlinear response, a first step in extending the analysis of SRTBC to higher-order nonlinearities is to numerically generate the correct dependence of the signal on intensity for the cubic nonlinearity alone. The second step is to include the higher-order nonlinearities in the modelling of the SRTBC signal.

3.2 Spectrally-resolved two-beam coupling with high-order nonlinearities

In this section, we present the detailed derivation of the SRTBC governing equations with higher-order nonlinearities included. These equations are used to perform numerical simulations and obtain the theoretical SRTBC traces. The simulation results are then used to analyze the experimental measurements and determine the higher-order nonlinearities in the samples measured.

We start by considering the electric field for the pump- and the probe- beam

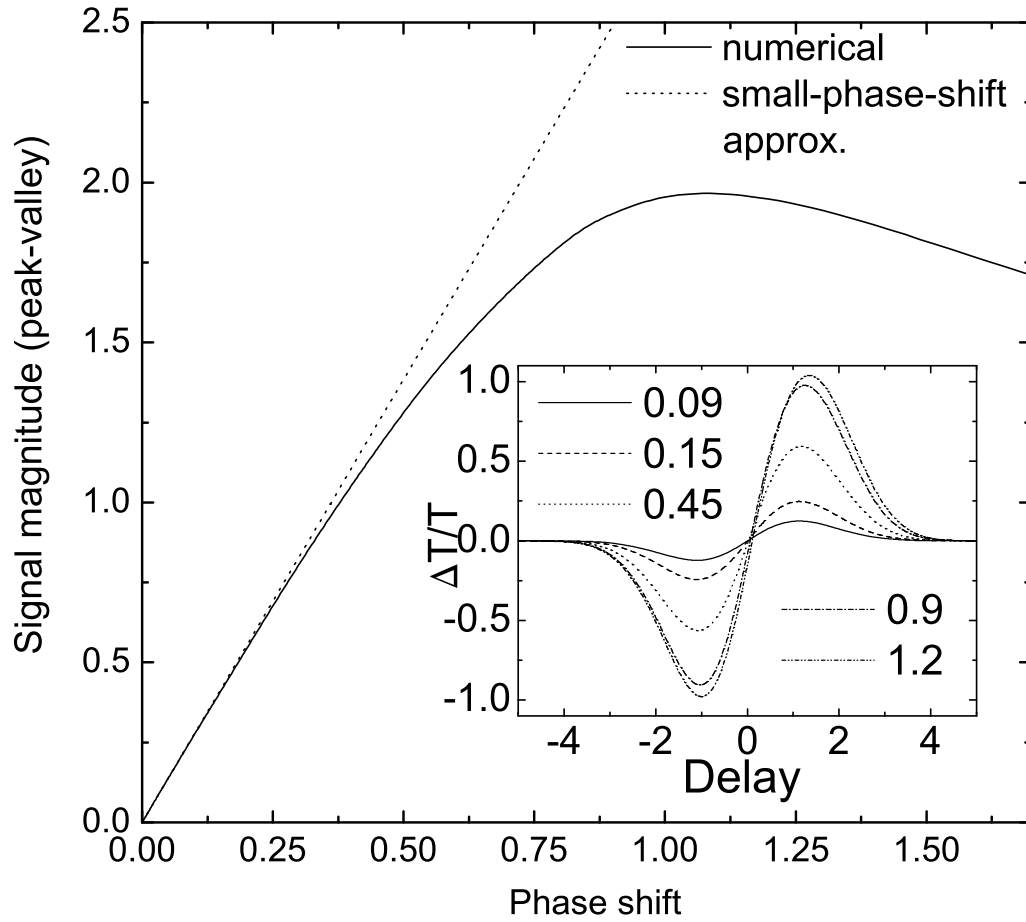


Figure 3.1: Numerical calculation is used to determine the dependence of the signal on pump-beam intensity in the presence of $\chi^{(3)}$ alone. Inset: SRTBC signals calculated for the indicated nonlinear phase shifts. The time delay is in the units of the pulse duration.

$E_p(z, t)$ and $E_s(z, t)$, these can be expressed as the following:

$$\begin{aligned} E_p(z, t) &= \frac{1}{2} \left\{ A_p(z, t) \exp[i(\beta_p z - \omega_p t)] + \text{c.c.} \right\} \\ E_s(z, t) &= \frac{1}{2} \left\{ A_s(z, t) \exp[i(\beta_s z - \omega_s t)] + \text{c.c.} \right\}, \end{aligned} \quad (3.1)$$

and

$$E(z, t) = E_p(z, t) + E_s(z, t). \quad (3.2)$$

Here ω_p and ω_s are the frequency for pump- and probe-beam respectively, and

$$\begin{aligned} \beta_p &= \frac{\omega_p n_{0R}(\omega_p)}{c} \\ \beta_s &= \frac{\omega_s n_{0R}(\omega_s)}{c}, \end{aligned} \quad (3.3)$$

where $n_{0R} = \text{Re}[n_0]$, the real part of the complex linear refractive index. Correspondingly, in frequency domain, we can express the field as:

$$\begin{aligned} \tilde{E}_p(z, \omega) &= \frac{1}{2} [a_p(z, \omega) + a_p^*(z, -\omega)] \\ \tilde{E}_s(z, \omega) &= \frac{1}{2} [a_s(z, \omega) + a_s^*(z, -\omega)] \end{aligned} \quad (3.4)$$

Where the Fourier transform has

$$\begin{aligned} a_p(z, \omega) &= F \left\{ A_p(z, t) \exp[i(\beta_p z - \omega_p t)] \right\} \\ a_s(z, \omega) &= F \left\{ A_s(z, t) \exp[i(\beta_s z - \omega_s t)] \right\}, \end{aligned} \quad (3.5)$$

with the Fourier transform defined as

$$F \{ h(t) \} \equiv \frac{1}{\sqrt{2\pi}} \int_{-\infty}^{\infty} h(t) e^{i\omega t} dt = \tilde{h}(\omega). \quad (3.6)$$

The corresponding inverse transform is

$$F^{-1} \{ \tilde{h}(\omega) \} \equiv \frac{1}{\sqrt{2\pi}} \int_{-\infty}^{\infty} \tilde{h}(\omega) e^{-i\omega t} d\omega = h(t). \quad (3.7)$$

From the above, we can express the linear polarization and nonlinear polarization in frequency domain as (assuming isotropic response):

$$\begin{aligned}\tilde{P}_L(z, \omega) &= \epsilon_0 \chi^{(1)}(\omega) \tilde{E}(z, \omega) \\ \tilde{P}_{NL}^{(n)}(z, \omega_1 + \omega_2 + \dots + \omega_n) &= \epsilon_0 \chi^{(n)}(\omega_1, \omega_2, \dots, \omega_n) \tilde{E}(z, \omega_1) \tilde{E}(z, \omega_2) \dots \tilde{E}(z, \omega_n)\end{aligned}\tag{3.8}$$

In the time domain, the corresponding polarization is

$$\begin{aligned}P_L(z, t) &= F^{-1} \{ \tilde{P}_L(z, \omega) \} \\ P_{NL}^{(n)}(z, t) &= F^{-1} \{ \tilde{P}_{NL}^{(n)}(z, \omega) \}\end{aligned}\tag{3.9}$$

Or more explicitly, it is

$$\begin{aligned}P_L(z, t) &= \frac{1}{\sqrt{2\pi}} \int_{-\infty}^{\infty} \epsilon_0 \chi^{(1)}(\omega) \tilde{E}(z, \omega) e^{-i\omega t} d\omega \\ &= \frac{1}{2} \frac{1}{\sqrt{2\pi}} \int_{-\infty}^{\infty} \epsilon_0 \chi^{(1)}(\omega) (a_p(z, \omega) + a_p^*(z, -\omega) \\ &\quad + a_s(z, \omega) + a_s^*(z, -\omega)) e^{-i\omega t} d\omega\end{aligned}\tag{3.10}$$

and

$$\begin{aligned}P_{NL}^{(n)}(z, t) &= \left(\frac{1}{\sqrt{2\pi}}\right)^n \int_{-\infty}^{\infty} \dots \int_{-\infty}^{\infty} \epsilon_0 \chi^{(n)}(\omega_1, \dots, \omega_n) \\ &\quad \times \tilde{E}(z, \omega_1) \dots \tilde{E}(z, \omega_n) \exp[-i(\omega_1 + \dots + \omega_n)t] d\omega_1 \dots d\omega_n \\ &= \left(\frac{1}{2}\right)^n \left(\frac{1}{\sqrt{2\pi}}\right)^n \int_{-\infty}^{\infty} \dots \int_{-\infty}^{\infty} \epsilon_0 \chi^{(n)}(\omega_1, \dots, \omega_n) \\ &\quad \times [a_p(z, \omega_1) + a_p^*(z, -\omega_1) + a_s(z, \omega_1) \\ &\quad + a_s^*(z, -\omega_1)] \dots [a_p(z, \omega_n) + a_p^*(z, -\omega_n) \\ &\quad + a_s(z, \omega_n) + a_s^*(z, -\omega_n)] \exp[-i(\omega_1 + \dots + \omega_n)t] \\ &\quad \times d\omega_1 \dots d\omega_n.\end{aligned}\tag{3.11}$$

Note that in the derivation above we have only assumed that the response is isotropic. To simplify the equations, here we introduce another assumption: the

spectral width compared with the range where the material has significant dispersion is small. More specifically, we assume that

$$\begin{aligned}
\chi^{(1)}(\omega_p - \Delta_p) &\cong \chi^{(1)}(\omega_p) \cong \chi^{(1)}(\omega_p + \Delta_p) \\
\chi^{(1)}(\omega_s - \Delta_s) &\cong \chi^{(1)}(\omega_s) \cong \chi^{(1)}(\omega_s + \Delta_s) \\
\chi^{(n)}(\omega_1, \omega_2, \dots, \omega_k = \omega_p - \Delta_p, \dots, \omega_n) &\cong \chi^{(n)}(\omega_1, \omega_2, \dots, \omega_k = \omega_p, \dots, \omega_n) \\
&\cong \chi^{(n)}(\omega_1, \omega_2, \dots, \omega_k = \omega_p + \Delta_p, \dots, \omega_n) \\
\chi^{(n)}(\omega_1, \omega_2, \dots, \omega_k = \omega_s - \Delta_s, \dots, \omega_n) &\cong \chi^{(n)}(\omega_1, \omega_2, \dots, \omega_k = \omega_s, \dots, \omega_n) \\
&\cong \chi^{(n)}(\omega_1, \omega_2, \dots, \omega_k = \omega_s + \Delta_s, \dots, \omega_n)
\end{aligned} \tag{3.12}$$

where ω_p and ω_s are the center frequency of the pump- and the probe-field respectively, as defined in Eqn. 3.1, and Δ_p and Δ_s are the bandwidth of the pump- and the probe-field respectively. Using Eqn. 3.12, we can simplify Eqn. 3.10 to get

$$\begin{aligned}
P_L(z, t) &\cong \frac{1}{2} \frac{1}{\sqrt{2\pi}} \epsilon_0 \chi^{(1)}(\omega_p) \int_{-\infty}^{\infty} a_p(z, \omega) e^{-i\omega t} d\omega \\
&\quad + \frac{1}{2} \frac{1}{\sqrt{2\pi}} \epsilon_0 \chi^{(1)}(-\omega_p) \int_{-\infty}^{\infty} a_p^*(z, -\omega) e^{-i\omega t} d\omega \\
&\quad + \frac{1}{2} \frac{1}{\sqrt{2\pi}} \epsilon_0 \chi^{(1)}(\omega_s) \int_{-\infty}^{\infty} a_s(z, \omega) e^{-i\omega t} d\omega \\
&\quad + \frac{1}{2} \frac{1}{\sqrt{2\pi}} \epsilon_0 \chi^{(1)}(-\omega_s) \int_{-\infty}^{\infty} a_s^*(z, -\omega) e^{-i\omega t} d\omega \\
&= \frac{1}{2} \epsilon_0 \chi^{(1)}(\omega_p) A_p(z, t) \exp[i(\beta_p z - \omega_p t)] \\
&\quad + \frac{1}{2} \epsilon_0 \chi^{(1)}(-\omega_p) A_p^*(z, t) \exp[-i(\beta_p z - \omega_p t)] \\
&\quad + \frac{1}{2} \epsilon_0 \chi^{(1)}(\omega_s) A_s(z, t) \exp[i(\beta_s z - \omega_s t)] \\
&\quad + \frac{1}{2} \epsilon_0 \chi^{(1)}(-\omega_s) A_s^*(z, t) \exp[-i(\beta_s z - \omega_s t)] \\
&= \frac{1}{2} \epsilon_0 \left\{ \chi^{(1)}(\omega_p) A_p(z, t) \exp[i(\beta_p z - \omega_p t)] \right. \\
&\quad \left. + \chi^{(1)}(\omega_s) A_s(z, t) \exp[i(\beta_s z - \omega_s t)] \right\} + \text{c.c.}
\end{aligned} \tag{3.13}$$

Note that we have used the relation $\chi^{(1)}(\omega) = \chi^{(1)*}(-\omega^*)$, and for real ω , it can be further simplified to $\chi^{(1)}(\omega) = \chi^{(1)*}(-\omega)$. For nonlinear polarization, we have

$$\begin{aligned}
P_{\text{NL}}^{(n)}(z, t) &\cong \left(\frac{1}{2}\right)^n \left(\frac{1}{\sqrt{2\pi}}\right)^n \sum_{\hat{\omega}_1; f_1} \dots \sum_{\hat{\omega}_n; f_n} \epsilon_0 \chi^{(n)}(\hat{\omega}_1, \dots, \hat{\omega}_n) \\
&\quad \times \int_{-\infty}^{\infty} \dots \int_{-\infty}^{\infty} f_1(z, \omega_1) \dots f_n(z, \omega_n) \exp[-i(\omega_1 + \dots + \omega_n)t] d\omega_1 \dots d\omega_n \\
&= \left(\frac{1}{2}\right)^n \sum_{\hat{\omega}_1; g_1} \dots \sum_{\hat{\omega}_n; g_n} \epsilon_0 \chi^{(n)}(\hat{\omega}_1, \dots, \hat{\omega}_n) g_1(z, t) \dots g_n(z, t) \\
&\quad \times \exp[-i(\hat{\omega}_1 + \dots + \hat{\omega}_n)t]
\end{aligned}$$

where

$$\begin{aligned}
\hat{\omega}_k &= \{\omega_p, -\omega_p, \omega_s, -\omega_s\} \\
f_k(z, \omega) &= \{a_p(z, \omega), a_p^*(z, -\omega), a_s(z, \omega), a_s^*(z, -\omega)\} \\
g_k(z, t) &= \left\{ A_p(z, t) \exp[i\beta_p z], A_p^*(z, t) \exp[-i\beta_p z] \right. \\
&\quad \left. , A_s(z, t) \exp[i\beta_s z], A_s^*(z, t) \exp[-i\beta_s z] \right\}
\end{aligned}$$

$$\text{for } k = 1, 2, \dots, n \quad (3.14)$$

Note that from the term $\exp[-i(\hat{\omega}_1 + \dots + \hat{\omega}_n)t]$ we can see that Eqn. 3.14 includes second harmonic generation ($\pm 2\omega_p$ or $\pm 2\omega_s$), difference frequency generation ($\pm(\omega_p - \omega_s)$), and high harmonic generation processes. Directly substituting Eqn. 3.14 into Maxwell's equations is difficult. Fortunately, there are more simplifications that can be made: (i) Consider only the case where the generation of wavelength components other than the original pump beam and prob beam ω_p and ω_s is negligible. In other words, we consider the case where in Eqn. 3.14,

only those $\chi^{(n)}(\hat{\omega}_1, \dots, \hat{\omega}_n)$ with $\hat{\omega}_1 + \dots + \hat{\omega}_n = \pm\omega_p$ or $\hat{\omega}_1 + \dots + \hat{\omega}_n = \pm\omega_s$ are significant. Physically, this means that the material is not phase-matched for any nonlinear generation processes. With this assumption, only nonlinear polarization with order $n = 2m + 1$ remain. This assumption helps to simplify the equation:

$$\begin{aligned}
P_{\text{NL}}^{(2m+1)}(z, t) &= \left(\frac{1}{2}\right)^{2m+1} \sum_{l=0}^m C_{l+1}^{2m+1} C_l^{2m-l} C_{m-l}^{2(m-l)} \\
&\times \left\{ \epsilon_0 \chi^{(2m+1)}(\underbrace{\omega_p, \dots, \omega_p}_{l+1}, \underbrace{-\omega_p, \dots, -\omega_p}_l, \underbrace{\omega_s, \dots, \omega_s}_{m-l}, \underbrace{-\omega_s, \dots, -\omega_s}_{m-l}) \right. \\
&\times A_p |A_p|^{2l} |A_s|^{2(m-l)} \exp[i(\beta_p z - \omega_p t)] \\
&+ \epsilon_0 \chi^{(2m+1)}(\underbrace{\omega_s, \dots, \omega_s}_{l+1}, \underbrace{-\omega_s, \dots, -\omega_s}_l, \underbrace{\omega_p, \dots, \omega_p}_{m-l}, \underbrace{-\omega_p, \dots, -\omega_p}_{m-l}) \\
&\times A_s |A_s|^{2l} |A_p|^{2(m-l)} \exp[i(\beta_s z - \omega_s t)] \left. \right\} \\
&+ \text{c.c.} \tag{3.15}
\end{aligned}$$

Note that intrinsic permutation symmetry has been used to arrive at the above expression. A simplification can also be made if we assume that the ratio of pump intensity to probe intensity is large, i.e. $A_p \gg A_s$, we could keep up to only the terms linear in A_s . Eqn. 3.14 is simplified to

$$\begin{aligned}
P_{\text{NL}}^{(2m+1)}(z, t) &= \left(\frac{1}{2}\right)^{2m+1} \left\{ C_{m+1}^{2m+1} C_m^m \epsilon_0 \chi^{(2m+1)}(\underbrace{\omega_p, \dots, \omega_p}_{m+1}, \underbrace{-\omega_p, \dots, -\omega_p}_m) \right. \\
&\times A_p |A_p|^{2m} \exp[i(\beta_p z - \omega_p t)] \\
&+ C_1^{2m+1} C_m^{2m} \epsilon_0 \chi^{(2m+1)}(\omega_s, \underbrace{\omega_p, \dots, \omega_p}_m, \underbrace{-\omega_p, \dots, -\omega_p}_m) \\
&\times A_s |A_p|^{2m} \exp[i(\beta_s z - \omega_s t)] \left. \right\} + \text{c.c.} \\
&= \left(\frac{1}{2}\right)^{2m+1} \left\{ \frac{(2m+1)!}{(m+1)!m!} \epsilon_0 \chi^{(2m+1)}(\underbrace{\omega_p, \dots, \omega_p}_{m+1}, \underbrace{-\omega_p, \dots, -\omega_p}_m) \right. \\
&\times A_p |A_p|^{2m} \exp[i(\beta_p z - \omega_p t)]
\end{aligned}$$

$$\begin{aligned}
& + \frac{(2m+1)!}{m!m!} \epsilon_0 \chi^{(2m+1)}(\omega_s, \underbrace{\omega_p, \dots, \omega_p}_m, \underbrace{-\omega_p, \dots, -\omega_p}_m) \\
& \times A_s |A_p|^{2m} \exp[i(\beta_s z - \omega_s t)] \Big\} + \text{c.c.} \tag{3.16}
\end{aligned}$$

Now we have the wave equation (for nonmagnetic system):

$$\frac{\partial^2}{\partial z^2} E(z, t) - \frac{1}{c^2} \frac{\partial^2}{\partial t^2} E(z, t) - \mu_0 \frac{\partial^2}{\partial t^2} P(z, t) = 0 \tag{3.17}$$

Where $P = P_L + P_{NL}$.

Using Eqn. 3.13 and Eqn. 3.16, we have

$$\begin{aligned}
& \frac{1}{2} \frac{\partial^2}{\partial z^2} \left\{ A_p \exp[i(\beta_p z - \omega_p t)] + A_s \exp[i(\beta_s z - \omega_s t)] \right\} \\
& - \frac{1}{2} \frac{1}{c^2} \frac{\partial^2}{\partial t^2} \left\{ A_p \exp[i(\beta_p z - \omega_p t)] + A_s \exp[i(\beta_s z - \omega_s t)] \right\} \\
& - \frac{1}{2} \epsilon_0 \mu_0 \frac{\partial^2}{\partial t^2} \left\{ \chi^{(1)}(\omega_p) A_p \exp[i(\beta_p z - \omega_p t)] + \chi^{(1)}(\omega_s) A_s \exp[i(\beta_s z - \omega_s t)] \right\} \\
& - \epsilon_0 \mu_0 \frac{\partial^2}{\partial t^2} \sum_{m=1}^{\infty} \left(\frac{1}{2} \right)^{2m+1} \left\{ \frac{(2m+1)!}{(m+1)!m!} \chi^{(2m+1)}(\underbrace{\omega_p, \dots, \omega_p}_{m+1}, \underbrace{-\omega_p, \dots, -\omega_p}_m) \right. \\
& \times A_p |A_p|^{2m} \exp[i(\beta_p z - \omega_p t)] \\
& + \frac{(2m+1)!}{m!m!} \chi^{(2m+1)}(\omega_s, \underbrace{\omega_p, \dots, \omega_p}_m, \underbrace{-\omega_p, \dots, -\omega_p}_m) \\
& \left. \times A_s |A_p|^{2m} \exp[i(\beta_s z - \omega_s t)] \right\} + \text{c.c.} = 0 \tag{3.18}
\end{aligned}$$

The above equation can be decomposed into two equations by separating different time dependence ω_p and ω_s

$$\begin{aligned}
& \frac{1}{2} \frac{\partial^2}{\partial z^2} \left\{ A_p \exp[i(\beta_p z - \omega_p t)] \right\} - \frac{1}{2} \frac{1}{c^2} \frac{\partial^2}{\partial t^2} \left\{ A_p \exp[i(\beta_p z - \omega_p t)] \right\} \\
& - \frac{1}{2} \epsilon_0 \mu_0 \frac{\partial^2}{\partial t^2} \left\{ \chi^{(1)}(\omega_p) A_p \exp[i(\beta_p z - \omega_p t)] \right\} \\
& - \epsilon_0 \mu_0 \frac{\partial^2}{\partial t^2} \sum_{m=1}^{\infty} \left(\frac{1}{2} \right)^{2m+1} \left\{ \frac{(2m+1)!}{(m+1)!m!} \chi^{(2m+1)}(\underbrace{\omega_p, \dots, \omega_p}_{m+1}, \underbrace{-\omega_p, \dots, -\omega_p}_m) \right. \\
& \left. \times A_p |A_p|^{2m} \exp[i(\beta_p z - \omega_p t)] \right\} = 0 \tag{3.19}
\end{aligned}$$

and

$$\begin{aligned}
& \frac{1}{2} \frac{\partial^2}{\partial z^2} \left\{ A_s \exp[i(\beta_s z - \omega_s t)] \right\} - \frac{1}{2} \frac{1}{c^2} \frac{\partial^2}{\partial t^2} \left\{ A_s \exp[i(\beta_s z - \omega_s t)] \right\} \\
& - \frac{1}{2} \epsilon_0 \mu_0 \frac{\partial^2}{\partial t^2} \left\{ \chi^{(1)}(\omega_s) A_s \exp[i(\beta_s z - \omega_s t)] \right\} \\
& - \epsilon_0 \mu_0 \frac{\partial^2}{\partial t^2} \sum_{m=1}^{\infty} \left(\frac{1}{2} \right)^{2m+1} \left\{ \frac{(2m+1)!}{m!m!} \chi^{(2m+1)}(\omega_s \underbrace{\omega_p, \dots, \omega_p}_m, \underbrace{-\omega_p, \dots, -\omega_p}_m) \right. \\
& \left. \times A_s |A_p|^{2m} \exp[i(\beta_s z - \omega_s t)] \right\} = 0 \tag{3.20}
\end{aligned}$$

We now introduce the slowly varying envelope approximation (SVEA). More specifically, this approximation allows us to neglect the higher order differential terms on the “envelop function”, such as $(\partial^2 A_p / \partial z^2)$, $(\partial^2 A_p / \partial t^2)$, $(\partial^2 A_s / \partial z^2)$, $(\partial^2 A_s / \partial t^2)$, $(\partial A_p / \partial z)^2$, $(\partial A_p / \partial t)^2$, $(\partial A_s / \partial z)^2$, $(\partial A_s / \partial t)^2$, $(\partial A_p / \partial z)(\partial A_s / \partial z)$ etc. I.e., we keep only up to the order of $(\partial \cdot / \partial z)$ and $(\partial \cdot / \partial t)$, where \cdot is any of the A_p , A_s , A_p^* and A_s^* . With this approximation, and after some straightforward manipulations, we have:

$$\begin{aligned}
& -\frac{1}{2} \beta_p^2 A_p + i\beta_p \frac{\partial A_p}{\partial z} + \frac{1}{2} \frac{\omega_p^2}{c^2} A_p + \frac{i\omega_p}{c^2} \frac{\partial A_p}{\partial t} + \frac{1}{2} \frac{\omega_p^2}{c^2} \chi^{(1)}(\omega_p) A_p + \frac{i\omega_p}{c^2} \chi^{(1)}(\omega_p) \frac{\partial A_p}{\partial t} \\
& + \left(\frac{\omega_p^2}{c^2} + 2 \frac{i\omega_p}{c^2} \frac{\partial}{\partial t} \right) \sum_{m=1}^{\infty} \left(\frac{1}{2} \right)^{2m+1} \left[\frac{(2m+1)!}{(m+1)!m!} \chi^{(2m+1)}(\omega_p \underbrace{\omega_p, \dots, \omega_p}_{m+1}, \underbrace{-\omega_p, \dots, -\omega_p}_m) \right. \\
& \left. \times A_p |A_p|^{2m} \right] = 0 \tag{3.21}
\end{aligned}$$

and

$$\begin{aligned}
& -\frac{1}{2} \beta_s^2 A_s + i\beta_s \frac{\partial A_s}{\partial z} + \frac{1}{2} \frac{\omega_s^2}{c^2} A_s + \frac{i\omega_s}{c^2} \frac{\partial A_s}{\partial t} + \frac{1}{2} \frac{\omega_s^2}{c^2} \chi^{(1)}(\omega_s) A_s + \frac{i\omega_s}{c^2} \chi^{(1)}(\omega_s) \frac{\partial A_s}{\partial t} \\
& + \left(\frac{\omega_s^2}{c^2} + 2 \frac{i\omega_s}{c^2} \frac{\partial}{\partial t} \right) \sum_{m=1}^{\infty} \left(\frac{1}{2} \right)^{2m+1} \left[\frac{(2m+1)!}{m!m!} \chi^{(2m+1)}(\omega_s \underbrace{\omega_p, \dots, \omega_p}_m, \underbrace{-\omega_p, \dots, -\omega_p}_m) \right. \\
& \left. \times A_s |A_p|^{2m} \right] = 0 \tag{3.22}
\end{aligned}$$

Further rearrange the equations:

$$i\beta_p \frac{\partial A_p}{\partial z} =$$

$$\begin{aligned}
& \frac{1}{2} \left\{ \beta_p^2 - \frac{\omega_p^2}{c^2} \left[1 + \chi^{(1)}(\omega_p) + \sum_{m=1}^{\infty} \left(\frac{1}{2} \right)^{2m} \frac{(2m+1)!}{(m+1)!m!} \chi^{(2m+1)}(\omega_p) |A_p|^{2m} \right] \right\} A_p \\
& - \frac{i\omega_p}{c^2} \frac{\partial}{\partial t} \left\{ \left[1 + \chi^{(1)}(\omega_p) + \sum_{m=1}^{\infty} \left(\frac{1}{2} \right)^{2m} \frac{(2m+1)!}{(m+1)!m!} \chi^{(2m+1)}(\omega_p) |A_p|^{2m} \right] A_p \right\}
\end{aligned} \tag{3.23}$$

and

$$\begin{aligned}
& i\beta_s \frac{\partial A_s}{\partial z} = \\
& \frac{1}{2} \left\{ \beta_s^2 - \frac{\omega_s^2}{c^2} \left[1 + \chi^{(1)}(\omega_s) + \sum_{m=1}^{\infty} \left(\frac{1}{2} \right)^{2m} \frac{(2m+1)!}{m!m!} \chi^{(2m+1)}(\omega_s) |A_p|^{2m} \right] \right\} A_s \\
& - \frac{i\omega_s}{c^2} \frac{\partial}{\partial t} \left\{ \left[1 + \chi^{(1)}(\omega_s) + \sum_{m=1}^{\infty} \left(\frac{1}{2} \right)^{2m} \frac{(2m+1)!}{m!m!} \chi^{(2m+1)}(\omega_s) |A_p|^{2m} \right] A_s \right\}
\end{aligned} \tag{3.24}$$

Note that we have used the shorthand

$$\begin{aligned}
\chi^{(2m+1)}(\omega_p) & \equiv \chi^{(2m+1)}(\underbrace{\omega_p, \dots, \omega_p}_{m+1}, \underbrace{-\omega_p, \dots, -\omega_p}_m) \\
\chi^{(2m+1)}(\omega_s) & \equiv \chi^{(2m+1)}(\omega_s, \underbrace{\omega_p, \dots, \omega_p}_m, \underbrace{-\omega_p, \dots, -\omega_p}_m)
\end{aligned} \tag{3.25}$$

Using Eqn. 3.3 to express the above equations in terms of linear refractive index

n_0 :

$$\begin{aligned}
& i \frac{\partial A_p}{\partial z} - \frac{1}{2} \frac{\omega_p (n_{0I}(\omega_p))^2}{c n_{0R}(\omega_p)} A_p + i \frac{(n_0(\omega_p))^2}{c n_{0R}(\omega_p)} \frac{\partial A_p}{\partial t} = \\
& - \frac{1}{2} \left[i \frac{2\omega_p n_{0I}(\omega_p)}{c} + \sum_{m=1}^{\infty} \left(\frac{1}{2} \right)^{2m} \frac{(2m+1)!}{(m+1)!m!} \frac{\omega_p}{c n_{0R}(\omega_p)} \right. \\
& \times \chi^{(2m+1)}(\omega_p) |A_p|^{2m} \Big] A_p - i \frac{\partial}{\partial t} \left[\sum_{m=1}^{\infty} \left(\frac{1}{2} \right)^{2m} \frac{(2m+1)!}{(m+1)!m!} \right. \\
& \times \left. \frac{\chi^{(2m+1)}(\omega_p)}{c n_{0R}(\omega_p)} |A_p|^{2m} A_p \right]
\end{aligned} \tag{3.26}$$

and

$$i \frac{\partial A_s}{\partial z} - \frac{1}{2} \frac{\omega_s (n_{0I}(\omega_s))^2}{c n_{0R}(\omega_s)} A_s + i \frac{(n_0(\omega_s))^2}{c n_{0R}(\omega_s)} \frac{\partial A_s}{\partial t} =$$

$$\begin{aligned}
& -\frac{1}{2} \left[i \frac{2\omega_s n_{0I}(\omega_s)}{c} + \sum_{m=1}^{\infty} \left(\frac{1}{2}\right)^{2m} \frac{(2m+1)!}{m!m!} \frac{\omega_s}{cn_{0R}(\omega_s)} \right. \\
& \times \chi^{(2m+1)}(\omega_s) |A_p|^{2m} \left. \right] A_s - i \frac{\partial}{\partial t} \left[\sum_{m=1}^{\infty} \left(\frac{1}{2}\right)^{2m} \frac{(2m+1)!}{m!m!} \right. \\
& \times \left. \frac{\chi^{(2m+1)}(\omega_s)}{cn_{0R}(\omega_s)} |A_p|^{2m} A_s \right] \tag{3.27}
\end{aligned}$$

Where $n_0 = n_{0R} + in_{0I} = \sqrt{1 + \chi^{(1)}}$ is in general complex. We now further restrict ourselves to the case where the effect of nonlinear responses is smaller than the linear response, as is true in most situations. This means in general the terms such as $\chi^{(2m+1)}(\omega_p) |A_p|^{2m} (\partial A_p / \partial t)$ and $\chi^{(2m+1)}(\omega_s) |A_s|^{2m} (\partial A_s / \partial t)$ can be neglected when compared with other terms, due to the simultaneous smallness of $\chi^{(2m+1)}(\omega_p)$ (or $\chi^{(2m+1)}(\omega_s)$) and $\partial A_p / \partial t$ (or $\partial A_s / \partial t$). This allows us to rewrite the equations:

$$\begin{aligned}
& i \frac{\partial A_p}{\partial z} - \frac{1}{2} \frac{\omega_p (n_{0I}(\omega_p))^2}{cn_{0R}(\omega_p)} A_p + i \frac{(n_0(\omega_p))^2}{cn_{0R}(\omega_p)} \frac{\partial A_p}{\partial t} = \\
& -\frac{1}{2} \left[i \frac{2\omega_p n_{0I}(\omega_p)}{c} + \sum_{m=1}^{\infty} \left(\frac{1}{2}\right)^{2m} \frac{(2m+1)!}{(m+1)!m!} \frac{\omega_p}{cn_{0R}(\omega_p)} \right. \\
& \times \left. \chi^{(2m+1)}(\omega_p) |A_p|^{2m} \right] A_p \tag{3.28}
\end{aligned}$$

and

$$\begin{aligned}
& i \frac{\partial A_s}{\partial z} - \frac{1}{2} \frac{\omega_s (n_{0I}(\omega_s))^2}{cn_{0R}(\omega_s)} A_s + i \frac{(n_0(\omega_s))^2}{cn_{0R}(\omega_s)} \frac{\partial A_s}{\partial t} = \\
& -\frac{1}{2} \left[i \frac{2\omega_s n_{0I}(\omega_s)}{c} + \sum_{m=1}^{\infty} \left(\frac{1}{2}\right)^{2m} \frac{(2m+1)!}{m!m!} \frac{\omega_s}{cn_{0R}(\omega_s)} \right. \\
& \times \left. \chi^{(2m+1)}(\omega_s) |A_p|^{2m} \right] A_s \tag{3.29}
\end{aligned}$$

Further simplification can be obtained by introducing a transform:

$$\begin{aligned}
A_p &= \exp[-i\theta_p z] \hat{A}_p \\
\theta_p &= \frac{\omega_p (n_{0I}(\omega_p))^2}{2cn_{0R}(\omega_p)} \\
A_s &= \exp[-i\theta_s z] \hat{A}_s \\
\theta_s &= \frac{\omega_s (n_{0I}(\omega_s))^2}{2cn_{0R}(\omega_s)} \tag{3.30}
\end{aligned}$$

The new equations are now:

$$\begin{aligned}
& i \frac{\partial \hat{A}_p}{\partial z} + i \frac{(n_0(\omega_p))^2}{cn_{0R}(\omega_p)} \frac{\partial \hat{A}_p}{\partial t} = \\
& -\frac{1}{2} \left[i \frac{2\omega_p n_{0I}(\omega_p)}{c} + \sum_{m=1}^{\infty} \left(\frac{1}{2}\right)^{2m} \frac{(2m+1)!}{(m+1)!m!} \frac{\omega_p}{cn_{0R}(\omega_p)} \right. \\
& \left. \times \chi^{(2m+1)}(\omega_p) |\hat{A}_p|^{2m} \right] \hat{A}_p
\end{aligned} \tag{3.31}$$

and

$$\begin{aligned}
& i \frac{\partial \hat{A}_s}{\partial z} + i \frac{(n_0(\omega_s))^2}{cn_{0R}(\omega_s)} \frac{\partial \hat{A}_s}{\partial t} = \\
& -\frac{1}{2} \left[i \frac{2\omega_s n_{0I}(\omega_s)}{c} + \sum_{m=1}^{\infty} \left(\frac{1}{2}\right)^{2m} \frac{(2m+1)!}{m!m!} \frac{\omega_s}{cn_{0R}(\omega_s)} \right. \\
& \left. \times \chi^{(2m+1)}(\omega_s) |\hat{A}_p|^{2m} \right] \hat{A}_s
\end{aligned} \tag{3.32}$$

We can further assume that $n_{0R} \gg n_{0I}$, as is true for transparent material. The approximation $(n_0)^2/cn_{0R} \cong n_{0R}/c$ then can be justified. Further with the definition $(1/v) \equiv (n_{0R}/c)$ (If the first order dispersion effect is taken into account, we have $(1/v) \equiv (n_{0R}/c) + (\omega/c)(dn_{0R}/d\omega)$). This effect and the dispersion effects of the nonlinearities can be accounted for during the derivation. It can be done by expanding the susceptibility functions around ω_s and ω_p when evaluating Eqn. 3.10 and Eqn. 3.11.), we have:

$$\begin{aligned}
& i \frac{\partial \hat{A}_p}{\partial z} + i \frac{1}{v(\omega_p)} \frac{\partial \hat{A}_p}{\partial t} = -\frac{1}{2} \left[i \frac{2\omega_p n_{0I}(\omega_p)}{c} \right. \\
& \left. + \sum_{m=1}^{\infty} \left(\frac{1}{2}\right)^{2m} \frac{(2m+1)!}{(m+1)!m!} \frac{\omega_p}{cn_{0R}(\omega_p)} \chi^{(2m+1)}(\omega_p) |\hat{A}_p|^{2m} \right] \hat{A}_p
\end{aligned} \tag{3.33}$$

and

$$\begin{aligned}
& i \frac{\partial \hat{A}_s}{\partial z} + i \frac{1}{v(\omega_s)} \frac{\partial \hat{A}_s}{\partial t} = -\frac{1}{2} \left[i \frac{2\omega_s n_{0I}(\omega_s)}{c} \right. \\
& \left. + \sum_{m=1}^{\infty} \left(\frac{1}{2}\right)^{2m} \frac{(2m+1)!}{m!m!} \frac{\omega_s}{cn_{0R}(\omega_s)} \chi^{(2m+1)}(\omega_s) |\hat{A}_p|^{2m} \right] \hat{A}_s
\end{aligned} \tag{3.34}$$

Using the notations:

$$\begin{aligned}
\alpha_0 &\equiv \frac{2\omega n_{0I}}{c} \\
\hat{n}_{2m} &\equiv \frac{1}{n_{0R}} \frac{(2m+1)!}{2^{2m+1}(m+1)!m!} \text{Re}[\chi^{(2m+1)}] \\
\hat{\alpha}_{2m} &\equiv \frac{\omega}{cn_{0R}} \frac{(2m+1)!}{2^{2m}(m+1)!m!} \text{Im}[\chi^{(2m+1)}] \\
m &\geq 1
\end{aligned} \tag{3.35}$$

the equations become:

$$\begin{aligned}
i \frac{\partial \hat{A}_p}{\partial z} + i \frac{1}{v(\omega_p)} \frac{\partial \hat{A}_p}{\partial t} &= -i \left[\frac{1}{2} \alpha_0(\omega_p) + \sum_{m=1}^{\infty} \frac{1}{2} \hat{\alpha}_{2m}(\omega_p) |\hat{A}_p|^{2m} \right] \hat{A}_p \\
- \sum_{m=1}^{\infty} \frac{\omega_p}{c} \hat{n}_{2m}(\omega_p) |\hat{A}_p|^{2m} \hat{A}_p &
\end{aligned} \tag{3.36}$$

and

$$\begin{aligned}
i \frac{\partial \hat{A}_s}{\partial z} + i \frac{1}{v(\omega_s)} \frac{\partial \hat{A}_s}{\partial t} &= -i \left[\frac{1}{2} \alpha_0(\omega_s) + \sum_{m=1}^{\infty} \frac{1}{2} (m+1) \hat{\alpha}_{2m}(\omega_s) |\hat{A}_p|^{2m} \right] \hat{A}_s \\
- \sum_{m=1}^{\infty} \frac{\omega_s}{c} (m+1) \hat{n}_{2m}(\omega_s) |\hat{A}_p|^{2m} \hat{A}_s &
\end{aligned} \tag{3.37}$$

The above equations could be decoupled into equations describing phase evolution and amplitude evolution if we use the following transforms:

$$\begin{aligned}
\hat{A}_p &\equiv \Psi_p \exp[i\phi_p] \\
\hat{A}_s &\equiv \Psi_s \exp[i\phi_s]
\end{aligned} \tag{3.38}$$

The new equations become:

$$\begin{aligned}
&i \left[\left(\frac{\partial}{\partial z} + i \frac{\partial \phi_p}{\partial z} \right) \Psi_p + \frac{1}{v(\omega_p)} \left(\frac{\partial}{\partial t} + i \frac{\partial \phi_p}{\partial t} \right) \Psi_p \right] \\
&+ i \left[\frac{1}{2} \alpha_0(\omega_p) + \sum_{m=1}^{\infty} \frac{1}{2} \hat{\alpha}_{2m}(\omega_p) |\Psi_p|^{2m} \right] \Psi_p \\
&+ \sum_{m=1}^{\infty} \frac{\omega_p}{c} \hat{n}_{2m}(\omega_p) |\Psi_p|^{2m} \Psi_p = 0
\end{aligned} \tag{3.39}$$

and

$$\begin{aligned}
& i \left[\left(\frac{\partial}{\partial z} + i \frac{\partial \phi_s}{\partial z} \right) \Psi_s + \frac{1}{v(\omega_s)} \left(\frac{\partial}{\partial t} + i \frac{\partial \phi_s}{\partial t} \right) \Psi_s \right] \\
& + i \left[\frac{1}{2} \alpha_0(\omega_s) + \sum_{m=1}^{\infty} \frac{1}{2} (m+1) \hat{\alpha}_{2m}(\omega_s) |\Psi_p|^{2m} \right] \Psi_s \\
& + \sum_{m=1}^{\infty} \frac{\omega_s}{c} (m+1) \hat{n}_{2m}(\omega_s) |\Psi_p|^{2m} \Psi_s = 0
\end{aligned} \tag{3.40}$$

Separate the real part and imaginary part, we get the equations:

$$\begin{aligned}
\frac{\partial \Psi_p}{\partial z} + \frac{1}{v(\omega_p)} \frac{\partial \Psi_p}{\partial t} &= \\
& - \left[\frac{1}{2} \alpha_0(\omega_p) + \sum_{m=1}^{\infty} \frac{1}{2} \hat{\alpha}_{2m}(\omega_p) |\Psi_p|^{2m} \right] \Psi_p \\
\frac{\partial \phi_p}{\partial z} + \frac{1}{v(\omega_p)} \frac{\partial \phi_p}{\partial t} &= \sum_{m=1}^{\infty} \frac{\omega_p}{c} \hat{n}_{2m}(\omega_p) |\Psi_p|^{2m} \\
\frac{\partial \Psi_s}{\partial z} + \frac{1}{v(\omega_s)} \frac{\partial \Psi_s}{\partial t} &= \\
& - \left[\frac{1}{2} \alpha_0(\omega_s) + \sum_{m=1}^{\infty} \frac{1}{2} (m+1) \hat{\alpha}_{2m}(\omega_s) |\Psi_p|^{2m} \right] \Psi_s \\
\frac{\partial \phi_s}{\partial z} + \frac{1}{v(\omega_s)} \frac{\partial \phi_s}{\partial t} &= \sum_{m=1}^{\infty} \frac{\omega_s}{c} (m+1) \hat{n}_{2m}(\omega_s) |\Psi_p|^{2m}
\end{aligned} \tag{3.41}$$

Since the intensity is proportional to the square of the field amplitude, i.e. $I_p = (1/2)n_{0R}\sqrt{\epsilon_0/\mu_0}|\Psi_p|^2$ and $I_s = (1/2)n_{0R}\sqrt{\epsilon_0/\mu_0}|\Psi_s|^2$, it is straightforward to rewrite above equation as

$$\begin{aligned}
\frac{\partial I_p}{\partial z} + \frac{1}{v(\omega_p)} \frac{\partial I_p}{\partial t} &= -(\alpha_0(\omega_p) + \sum_{m=1}^{\infty} \alpha_{2m}(\omega_p) I_p^m) I_p, \\
\frac{\partial \phi_p}{\partial z} + \frac{1}{v(\omega_p)} \frac{\partial \phi_p}{\partial t} &= \frac{\omega_p}{c} \sum_{m=1}^{\infty} n_{2m}(\omega_p) I_p^m, \\
\frac{\partial I_s}{\partial z} + \frac{1}{v(\omega_s)} \frac{\partial I_s}{\partial t} &= -(\alpha_0(\omega_s) + \sum_{m=1}^{\infty} (m+1) \alpha_{2m}(\omega_s) I_p^m) I_s, \\
\frac{\partial \phi_s}{\partial z} + \frac{1}{v(\omega_s)} \frac{\partial \phi_s}{\partial t} &= \frac{\omega_s}{c} \sum_{m=1}^{\infty} (m+1) n_{2m}(\omega_s) I_p^m,
\end{aligned} \tag{3.42}$$

Note that:

$$\alpha_{2m}(\omega_p) \equiv \frac{2^m \hat{\alpha}_{2m}(\omega_p)}{n_{0R}^m(\omega_p)} \left(\frac{\mu_0}{\epsilon_0} \right)^{m/2}$$

$$\begin{aligned}
n_{2m}(\omega_p) &\equiv \frac{2^m \hat{n}_{2m}(\omega_p)}{n_{0R}^m(\omega_p)} \left(\frac{\mu_0}{\epsilon_0}\right)^{m/2} \\
\alpha_{2m}(\omega_s) &\equiv \frac{2^m \hat{\alpha}_{2m}(\omega_s)}{n_{0R}^m(\omega_p)} \left(\frac{\mu_0}{\epsilon_0}\right)^{m/2} \\
n_{2m}(\omega_s) &\equiv \frac{2^m \hat{n}_{2m}(\omega_s)}{n_{0R}^m(\omega_p)} \left(\frac{\mu_0}{\epsilon_0}\right)^{m/2}
\end{aligned} \tag{3.43}$$

We have derived the SRTBC governing equations with higher-order nonlinearities present. In the derivation we have employed the slowly-varying envelope approximation and neglected group-velocity dispersion (GVD). These equations are used to calculate the signals produced by higher-order nonlinear processes (Fig. 3.2 and Fig. 3.3) and as well as to extract the values of n_{2m} and α_{2m} by fitting experimental data.

3.3 Experimental results

In the case where the pump-beam frequency is the same as the probe-beam frequency, i.e., $\omega_p = \omega_s$, the equations become

$$\begin{aligned}
\frac{\partial I_p}{\partial z} + \frac{1}{v} \frac{\partial I_p}{\partial t} &= -(\alpha_0 + \sum_{m=1}^{\infty} \alpha_{2m} I_p^m) I_p, \\
\frac{\partial \phi_p}{\partial z} + \frac{1}{v} \frac{\partial \phi_p}{\partial t} &= \frac{\omega_0}{c} \sum_{m=1}^{\infty} n_{2m} I_p^m, \\
\frac{\partial I_s}{\partial z} + \frac{1}{v} \frac{\partial I_s}{\partial t} &= -(\alpha_0 + \sum_{m=1}^{\infty} (m+1) \alpha_{2m} I_p^m) I_s, \\
\frac{\partial \phi_s}{\partial z} + \frac{1}{v} \frac{\partial \phi_s}{\partial t} &= \frac{\omega_0}{c} \sum_{m=1}^{\infty} (m+1) n_{2m} I_p^m,
\end{aligned} \tag{3.44}$$

where $I_{p(s)}$ and $\phi_{p(s)}$ are the intensity and the phase of the temporal envelope of the pump (probe) beam. We have adopted the notations $v \equiv v(\omega_p) = v(\omega_s)$, $\alpha_{2m} \equiv \alpha_{2m}(\omega_p) = \alpha_{2m}(\omega_s)$, $n_{2m} \equiv n_{2m}(\omega_p) = n_{2m}(\omega_s)$, and $\omega_0 \equiv \omega_p = \omega_s$

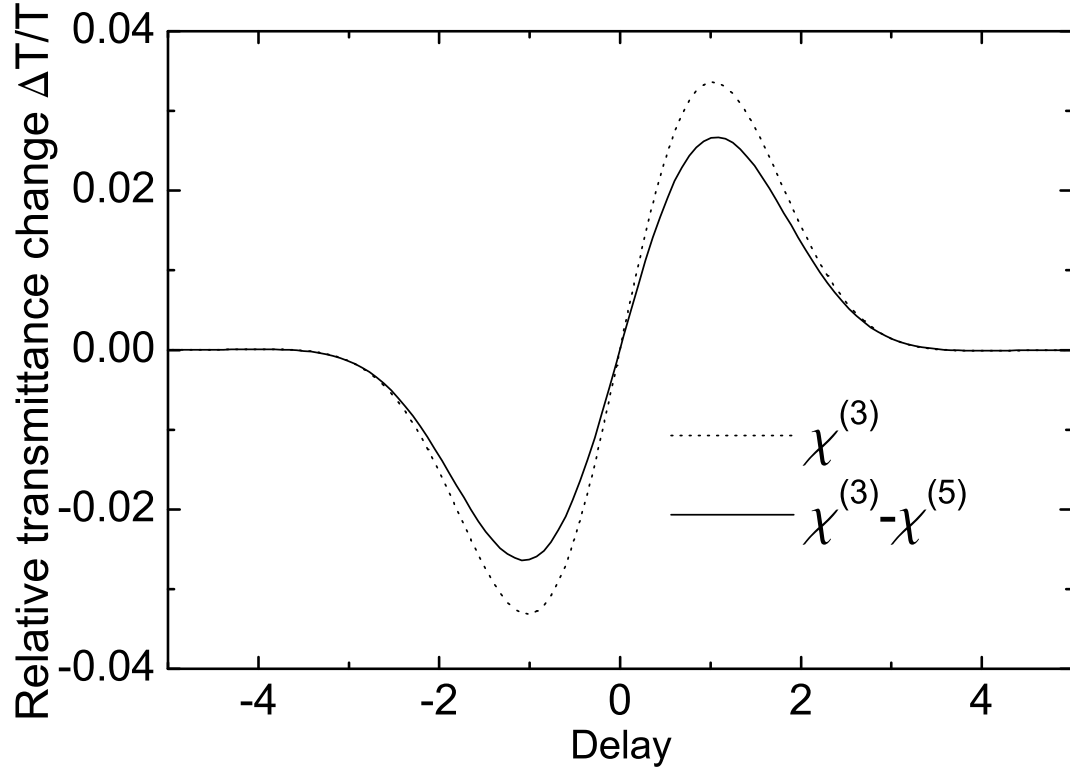


Figure 3.2: Extension of SRTBC to higher-order nonlinearities: The model including higher-order nonlinear effects is used to predict the SRTBC signal. Shown here is the effect of a self-defocusing $\chi^{(5)}$ on a self-focusing $\chi^{(3)}$. The time delay is in the units of the pulse duration.

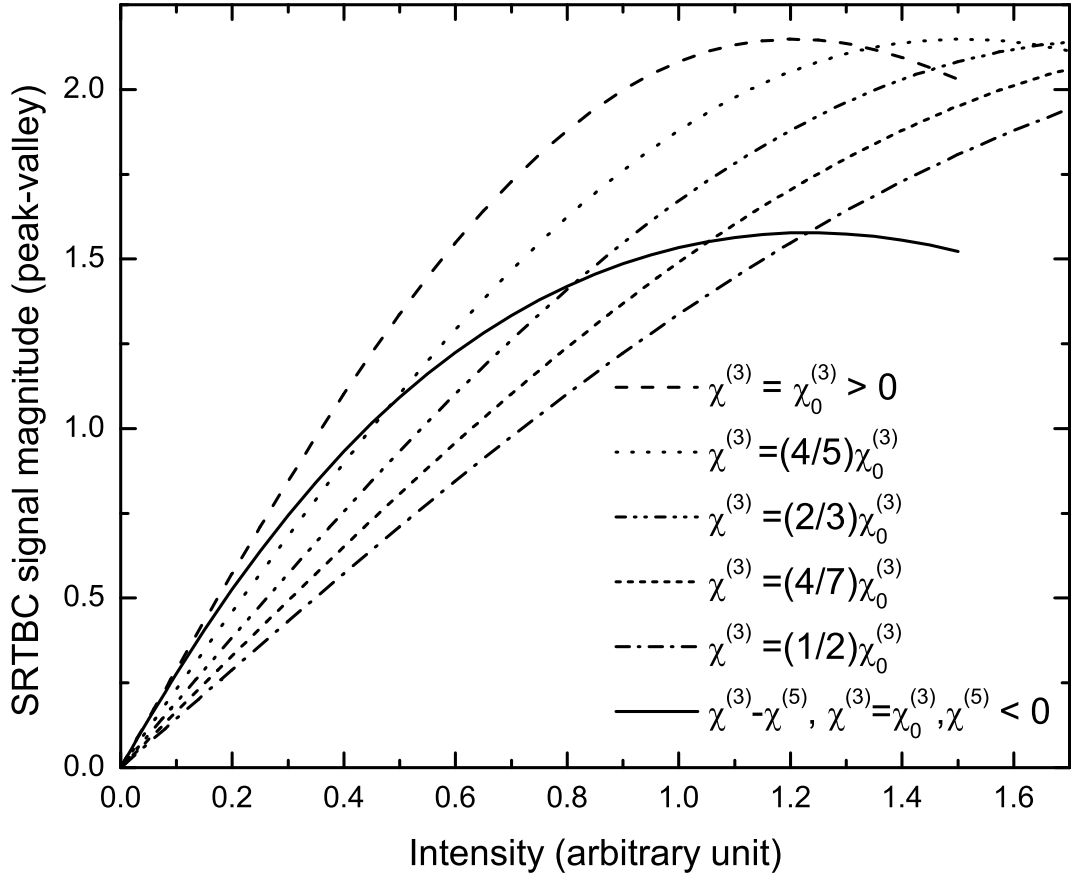


Figure 3.3: Intensity dependence of the SRTBC signal magnitude (peak-valley) for various values of self-focusing $\chi^{(3)}$ and for a self-focusing $\chi^{(3)}$ with a self-defocusing $\chi^{(5)}$.

In deriving Eqns. 3.44, we have made the slowly-varying envelope approximation and neglected group-velocity dispersion (GVD). It can also be verified that these equations reduce to the more familiar conventional SRTBC governing equations when nonlinearities above third-order are neglected [11]. These equations are used to calculate the signal traces produced by higher-order nonlinear processes (as shown in Fig. 3.2). The intensity dependence of the signal magnitude (Fig. 3.3) is then used to extract the values of n_{2m} and α_{2m} by fitting experimental data.

The SRTBC signal traces produced by higher-order processes in general do not differ qualitatively from those produced solely by the third-order process (as is evident in Fig. 3.2). It is thus difficult to identify the presence of higher-order processes from a single signal trace. This difficulty is resolved by observing the intensity dependence of the signal magnitude. In Fig. 3.3 we illustrate the theoretical prediction of the signal magnitude intensity dependence produced by self-focusing $\chi^{(3)}$ processes with various values of $\chi^{(3)}$ and by a $\chi^{(3)} - \chi^{(5)}$ process with a self-focusing $\chi^{(3)}$ and a self-defocusing $\chi^{(5)}$. It is clear that from the signal magnitude intensity dependence the presence of higher-order processes can be identified unambiguously.

Measurements are performed with a Ti:sapphire regenerative amplifier centered at 790 nm with a repetition rate of 1 kHz. The pulse duration is 100 fs. The pump and probe beams are non-collinear, and their polarizations are linear and parallel. Their intensities are in the ratio $I_p : I_s = 15 : 1$ and the typical interaction length of two beams is < 1 mm, so GVD is indeed negligible. Several materials with various linear absorption edges are measured: sapphire (~ 200 nm), SF-59 (~ 400 nm), La-Ga-S glass (~ 500 nm), and As₂S₃ glass (~ 600 nm), with corresponding reduced-photon energies of $h\nu/E_g = 0.25, 0.51, 0.63,$ and 0.76 respectively. (The crystalline

sapphire sample was measured with the electric field perpendicular to the c-axis and the propagation vector parallel to the a-axis.)

As I_p increases, we expect the nonlinearity to saturate in a way qualitatively similar to that of a simple two-level system:

$$\Delta n(I) = \frac{n_2 I}{(1 + I/I_{\text{sat}})}, \quad (3.45)$$

where $\Delta n(I)$ is the nonlinear refractive index and I_{sat} is the saturation intensity.

On the other hand, by expanding $\Delta n(I)$ in the perturbative form:

$$\begin{aligned} \Delta n(I) &= n_2 I - \frac{n_2}{I_{\text{sat}}} I^2 + \frac{n_2}{(I_{\text{sat}})^2} I^3 - \dots \\ &\equiv n_2 I + n_4 I^2 + n_6 I^3 + \dots, \end{aligned} \quad (3.46)$$

it can be seen that as the I approaches I_{sat} , the higher-order processes become important, and for materials with lower I_{sat} (usually with larger $h\nu/E_g$), the higher-order nonlinearities can be probed more easily.

Fifth-order nonlinearities are observed in all materials except sapphire, and seventh-order nonlinearities are observed in As_2S_3 . As an example, here we focus on the results from As_2S_3 . The measured SRTBC signal magnitude vs. I_p and nonlinear absorption signal magnitude vs. I_p are shown in Fig. 3.4. The deviation from the theoretical prediction based on $\chi^{(3)}$ alone is evident at high intensities. The inclusion of $\chi^{(5)}$ alone cannot account for the data, while introduction of a $\chi^{(7)}$ terms produces good agreement. From the numerical fitting, higher-order nonlinearities are estimated: $n_2 = 2.7 \times 10^{-13} \text{cm}^2/\text{W}$, $n_4 = -7.8 \times 10^{-23} \text{cm}^4/\text{W}^2$ and $n_6 = 7.2 \times 10^{-33} \text{cm}^6/\text{W}^3$; and $\alpha_2 = 2.1 \times 10^{-8} \text{cm}/\text{W}$, $\alpha_4 = 4.9 \times 10^{-18} \text{cm}^3/\text{W}^2$, and $\alpha_6 = 4.6 \times 10^{-28} \text{cm}^5/\text{W}^3$. Here $\chi^{(3)}$ and $\chi^{(7)}$ are self-focusing, and $\chi^{(5)}$ is self-defocusing. The alternating signs of $\chi^{(2m+1)}$ are consistent with Eqn. (3.46). The saturation intensity for As_2S_3 is $\sim 3 \text{ GW}/\text{cm}^2$, in reasonable agreement with

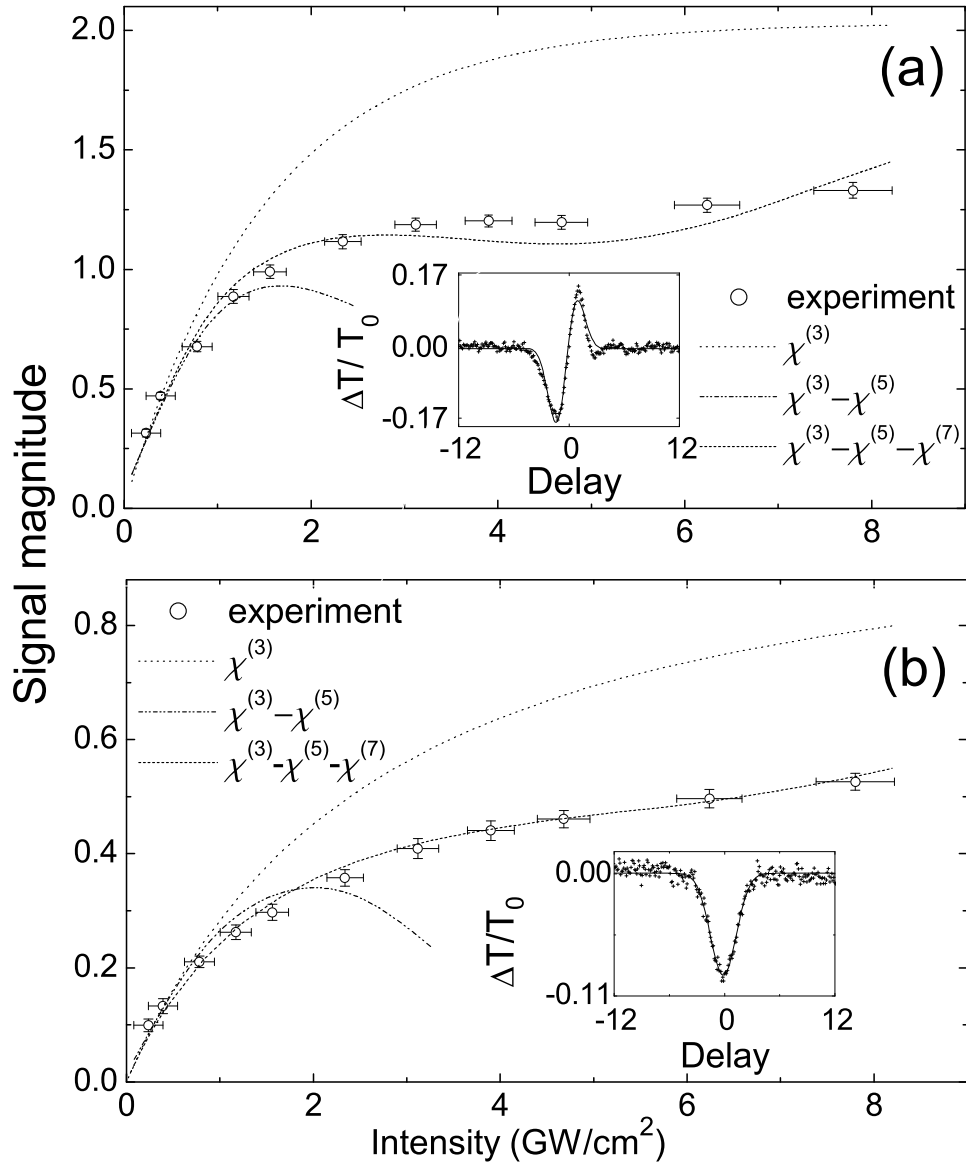


Figure 3.4: Intensity dependence of the (a) SRTBC signal magnitude (normalized peak-valley transmission difference) and (b) nonlinear absorption signal of As_2S_3 . Insets show examples of SRTBC and nonlinear absorption traces (symbols) along with the best fit theoretical curves. The time delay is given in units of the pulse duration.

Table 3.1: Measured n_2 , $|n_4/n_2|$, and α_2 . For sapphire, both n_4 and α_2 are under the detection limit and upper-limits are given. For all samples, a self-defocusing $n_4(< 0)$ is observed.

sample	$h\nu/E_g$	n_2 (10^{-15} cm ² /W)	$ n_4/n_2 $ (10^{-12} cm ² /W)	α_2 (10^{-10} cm/W)
sapphire	0.25	2	< 1	< 0.001
SF-59	0.51	26	48	0.2
La-Ga-S	0.63	36	67	3
As ₂ S ₃	0.76	270	290	210

previously reported value [17].

Results similar to those shown in Fig. 3.4 are obtained for the other materials, with the difference in the strength of saturation of the cubic nonlinearity. For sapphire (with smallest $h\nu/E_g$), no saturation of n_2 is detectable, nor is any nonlinear absorption. Saturation of the nonlinear index is observed in SF-59 and La-Ga-S glass. A self-defocusing $n_4 < 0$ is inferred for these two samples, while n_6 is observed in neither. Two-photon absorption is also observed for both SF-59 and La-Ga-S glass, however, no detectable α_4 is observed.

The measurements are summarized in Table 3.1. The measured values of n_2 are consistent with previously-reported values [15, 17, 18]. It is important to note that the saturation strength $|n_4/n_2|$ increases with reduced-photon energy. In other words, the higher-order nonlinearities become more important as the laser frequency gets closer to the linear absorption edge. Strong saturation of the instantaneous Kerr nonlinearity then is possible when the light frequency is close

to the resonance. However, this large saturation is accompanied by strong nonlinear absorption, which is problematic for applications. Nevertheless, for a given application an optimal range of reduced-photon energy could exist, in which the combination of nonlinearity saturation and nonlinear loss would be acceptable for applications. Table 3.1 shows that, although both α_2 and $|n_4/n_2|$ decrease as $h\nu/E_g$ decreases, α_2 decreases much faster than $|n_4/n_2|$ does. As a result, when $h\nu/E_g$ decreases, the nonlinear absorption can be acceptably small while the saturation is still significant. Both SF-59 and La-Ga-S glass exhibit reasonably low saturation intensities ($I_{\text{sat}} \sim 20 \text{ GW/cm}^2$ for SF-59 and $I_{\text{sat}} \sim 15 \text{ GW/cm}^2$ for La-Ga-S glass) with moderate nonlinear absorption. Chen *et al.* employed similar reasoning [19] to assess nonlinear glasses as media that can support multidimensional optical solitons [13, 14].

3.4 Conclusions

SRTBC is extended to include higher-order nonlinear effects. We have used this technique to measure the higher-order nonlinearities of several glasses. Fifth-order nonlinearities are observed, and seventh-order nonlinearities are also required to account for the nonlinear response when the excitation is well above the two-photon absorption edge. Near the two-photon edge, saturation of the cubic nonlinearity is observed with moderate nonlinear absorption. We believe that these observations will have important implications for the formation of multi-dimensional optical solutions in instantaneous Kerr media [13, 14, 19].

3.5 Acknowledgements

This work was supported by the National Science Foundation under grant PHY-0099564.

Chapter 4

Criteria for the experimental observation of multi-dimensional optical solitons in saturable media*

Criteria for experimental observation of multi-dimensional optical solitons in media with saturable refractive nonlinearities are developed. The criteria are applied to actual material parameters (characterizing the cubic self-focusing and quintic self-defocusing nonlinearities, two-photon loss, and optical-damage threshold) for various glasses. This way, we identify operation windows for soliton formation in these glasses. It is found that two-photon absorption sets stringent limits on the windows. We conclude that, while a well-defined window of parameters exists for two-dimensional solitons (spatial or spatiotemporal), for their three-dimensional spatiotemporal counterparts such a window *does not* exist, due to the nonlinear loss in glasses.

4.1 Introduction

Solitons are localized wave packets and/or beams that result from the balance of the linear and nonlinear responses of a physical system. Depending on the physical properties of the underlying system, solitons take different forms. They can be hydrodynamic wave packets, such as solitary waves in the ocean [20] and atmosphere [21]. They can also be spin-wave packets, such as magnetic solitons [22, 23]. Bose-Einstein condensates provide a medium to produce matter-wave solitons

*Most of the results presented in this chapter have been published in [19].

[24]. Other examples of soliton dynamics can be found in a wide variety of fields, including astrophysics, plasma physics, nuclear physics, and even metabolic biology [25, 26, 27, 28], among others. Very accurate experiments have been performed with topological solitons (fluxons) in long Josephson junctions, including a recent direct observation of their macroscopic quantum properties [29].

Solitons in optics, which are known in their temporal, spatial, and spatiotemporal varieties (the latter ones being frequently called “light bullets”), constitute, perhaps, the most versatile and well-studied (both theoretically and experimentally) class of solitons in physics. In particular, temporal solitons in optical fibers [30] have recently made a commercial debut in high-speed telecommunications links [30, 31]. It has been pointed out that multi-dimensional (multi-D) spatiotemporal optical solitons can be used in the design of high-speed all-optical logic gates and, eventually, in all-optical computation and communications systems [2].

The balance of linear and nonlinear dynamical features is only the first step in the soliton formation. Securing the stability of this balance is the second, equally important step. A well-known difficulty is that the most common optical nonlinearity – the instantaneous Kerr effect in dielectrics – gives rise to soliton solutions which are unstable in more than one dimension against the wave collapse, as discussed (in particular) in original papers [32, 33, 34] and in the review [35]. Several mechanisms that can suppress the collapse have been investigated. These include saturation of the instantaneous Kerr nonlinearity [4], higher-order dispersion or diffraction (also referred to as “non-paraxiality”) [36], multiphoton ionization [37], and stimulated Raman scattering (SRS) [38, 39]. In particular, importance of the multi-photon absorption and SRS for the spatiotemporal self-focusing of light in the instantaneous Kerr medium was inferred from experimental data in Ref. [40].

However, these mechanisms eventually reduce the intensity and cause the pulse to expand in time and space, precluding the achievement of multi-dimensional solitons [41].

Different versions of the saturable nonlinearity (which implies saturation of the cubic nonlinear susceptibility, $\chi^{(3)}$, with high-intensity fields) have been studied theoretically in detail. It was shown that both rational [13, 42, 43, 44, 45] and cubic-quintic (CQ) [14, 46, 47] variants of the saturation readily support stable two-dimensional (2D) and three-dimensional (3D) solitons. A difference between them is that the former cannot stabilize “spinning” solitons with an intrinsic vorticity, but the CQ nonlinearity makes it possible, in the 2D [48, 49, 50] and even 3D [51] cases.

The first observation of a self-trapped beam in an instantaneous Kerr medium was reported by Bjorkholm and Ashkin in 1974 [52]. The experiment was done in sodium vapor around the D_2 transition line, and self-focusing arose from strong saturation of the transition (i.e. saturation of the linear susceptibility, $\chi^{(1)}$). Studies of 2D solitons have made rapid progress since the mid-1990’s in the study of two new nonlinearities featuring saturation. Segev *et al.* predicted that the photorefractive (PR) effect in electro-optic materials could be exploited to create an effective saturable nonlinear index of refraction that would support solitons [53]. PR solitons were observed experimentally soon afterward [54]. In parallel to this, there was a resurgence of interest in the so-called cascading nonlinearity, which is produced by the interaction of two or three waves in media with quadratic ($\chi^{(2)}$) nonlinear susceptibility. Both 1D and multi-D solitons in the quadratic media had been studied theoretically in numerous works (see reviews [3] and [55]). Stationary 2D spatial solitons (in the form of self-supporting cylindrical beams) were

first generated in quadratic media by Torruellas *et al.* [56]. Later, Di Trapani *et al.* observed temporal $\chi^{(2)}$ solitons [57], and, finally, spatiotemporal solitons were produced by Liu *et al.* [10, 58]. Under appropriate conditions, both the PR and cascading nonlinearities may be modeled as saturable generalizations of the instantaneous Kerr nonlinearity (despite the fact that the PR media are, strictly speaking, non-instantaneous, nonlocal, and anisotropic). However, to date, multi-D solitons in true saturable instantaneous Kerr media have not been observed.

In this work, we examine the possibility of stabilizing solitons (arresting the collapse) in saturable instantaneous Kerr media [4], from the perspective of experimental implementation. Existing theories provide for parameter regions where formation of stable solitons is possible, but neglect linear and nonlinear losses, as well as other limitations, such as optical damage in high-intensity fields. First, we propose a criterion for acceptable losses, and determine the consequences of the loss for the observation of soliton-like beams and/or pulses. Then, as benchmark saturable instantaneous Kerr media, we consider nonlinear glasses. Direct experimental measurements of the higher-order nonlinearities and nonlinear (two-photon) loss in a series of glasses allow us to link the theoretical predictions to experimentally relevant values of the parameters. As a result, we produce “maps” of the experimental-parameter space where 2D and 3D solitons can be produced. To our knowledge, this is the first systematic analysis of the effects of nonlinear absorption on soliton formation in saturable instantaneous Kerr media. We conclude that it should be possible, although challenging, to experimentally produce 2D spatial and 2D spatiotemporal solitons in homogeneous saturable media. Spatiotemporal solitons require anomalous group-velocity dispersion (GVD). Under conditions relevant to saturation of the instantaneous Kerr nonlinearity, material

dispersion is likely to be normal. In that case, anomalous GVD might be obtained by pulse-tilting, e.g. On the contrary, the prospects for stabilizing 3D solitons seem poor, even ignoring the need for anomalous GVD. This conclusion suggests that qualitatively different nonlinearities, such as $\chi^{(2)}$, may be more relevant to making light bullets.

We focus on Gaussian beam profiles, which are the prototypical localized solutions. Very recent work has shown that nonlinear loss can induce a transition from Gaussian to conical waves, which can be stationary and localized [59, 60]. The conical waves are very interesting, but represent a different regime of wave propagation from that considered here. An interesting feature of such waves is that their shape effectively induces anomalous dispersion, in a manner similar to pulse-tilting [61].

The rest of the Chapter is organized as follows. The theoretical analysis of the necessary conditions for the formation of the 2D and 3D solitons is presented in Section 2. In Section 3, we revisit the experimental results of the nonlinear parameters briefly. Final results, in the form of windows in the space of physical parameters where the solitons may be experimentally generated, are displayed in Section 4, and this Chapter is concluded in Section 5.

4.2 Theoretical analysis of the necessary conditions for the existence of two- and three-dimensional solitons

Evolution of the amplitude E of the electromagnetic wave in a lossless instantaneous Kerr-like medium with anomalous GVD obeys the well-known scaled equa-

tion [13, 43, 44, 45]

$$iE_z + \frac{1}{2}(E_{xx} + E_{yy} + E_{tt}) + f(I)E = 0, \quad (4.1)$$

where z and (x, y) are the propagation and transverse coordinates respectively, and t is the reduced temporal variable, and $f(I)$ is proportional to the nonlinear correction to the refractive index $\Delta n(I)$. In the instantaneous Kerr medium proper, the refractive index is $n(I) \equiv n_0 + \Delta n(I) = n_0 + n_2 I$, which, as was mentioned above, gives rise to unstable multi-dimensional solitons, including the weakly unstable *Townes soliton* in the 2D case [35]. Upon the propagation, the unstable solitons will either spread out or collapse towards a singularity, depending on small perturbations added to the exact soliton solution.

Conditions for the soliton formation are usually expressed in terms of the normalized energy content, but from an experimental point of view it is more relevant to express the conditions in terms of intensity and size (temporal duration and/or transverse width) of the pulse/beam. They can also be converted into the dispersion and diffraction lengths, which are characteristics of the linear propagation. We transform the results of Ref. [34] to estimate the parameters of the 2D and 3D solitons in physical units. The transformation is based on the fact that the solutions are scalable with the beam size. Without losing generality, the estimation also assumes a Gaussian profile for the solutions. The relations between the critical peak intensity necessary for the formation of the soliton and diffraction length, in SI units are:

$$I_{\text{critical}} \approx \begin{cases} 0.52 \left(\frac{n_0^2}{n_2}\right) \left(\frac{\lambda_0}{L_{\text{diffr}}}\right) & \text{for 2D,} \\ 0.79 \left(\frac{n_0^2}{n_2}\right) \left(\frac{\lambda_0}{L_{\text{diffr}}}\right) & \text{for 3D,} \end{cases} \quad (4.2)$$

where $L_{\text{diff}} = 2\pi n_0 w_0^2 / \lambda_0$ is the diffraction length of the beam with the waist width w_0 . Eqn.4.2 is easy to understand for the 2D spatial case. For the 2D spatiotemporal and the 3D case, we have assumed that the light bullet experiences anomalous GVD, and has a dispersion length equal to the diffraction length, i.e. we have assumed spatiotemporal symmetry for the system, as is evident in Eqn. (4.1). Further examination of Eqn. (4.2) shows that the beam's power is independent of its size for 2D solitons, which is a well-known property of the Townes solitons, and the light-bullet's energy decreases as its size decreases in the 3D case [34].

As said above, two different forms of the saturation of the instantaneous Kerr nonlinearity were previously considered in detail theoretically, with $\Delta n(I)$ in rational form [13, 43, 44, 45],

$$\Delta n(I) = \frac{n_2 I}{(1 + I/I_{\text{sat}})} , \quad (4.3)$$

and CQ (cubic-quintic) [14, 46, 47, 48, 49, 50],

$$\Delta n(I) = n_2 I - n_4 I^2 , \quad (4.4)$$

with both n_2 and n_4 positive. Although these two models are usually treated separately (and, as mentioned above, they produce qualitatively different results for vortex solitons), they are two approximate forms of the nonlinear index for real materials. When the light frequency is close to a resonance, Eqn. (4.3) describes the system well; if the frequency is far away from resonance, Eqn. (4.4) is a better approximation. When $I \ll I_{\text{sat}}$, Eqn. (4.3) can be expanded, becoming equivalent to the CQ model,

$$\Delta n(I) \approx n_2 I - (n_2/I_{\text{sat}}) I^2 \equiv n_2 I - n_4 I^2 . \quad (4.5)$$

with $n_4 \equiv n_2/I_{\text{sat}}$. The two models produce essentially different results when the expansion is not valid.

Critical conditions for the formation of 2D solitons in these systems were found numerically by Quiroga-Teixeiro *et al.* [14] (2D), and by Edmundson *et al.* [44] and McLeod *et al.* [45] for the 3D solitons. From those results, we can estimate the necessary experimental parameters for both the 2D and 3D case by the transformation to physical units. The transformation is based on scaling properties of the governing equation (4.1). The estimate again assumes a Gaussian profile, which yields

$$I \geq I_{\text{stable}} \approx \begin{cases} 0.16 (n_2/n_4) & \text{for 2D,} \\ 1.25 (n_2/n_4) & \text{for 3D,} \end{cases} \quad (4.6)$$

for the minimum peak intensity needed to launch a stable soliton, and

$$w_0 \geq w_{\text{stable}} \approx \begin{cases} 0.77\lambda_0\sqrt{n_0n_4}/n_2 & \text{for 2D,} \\ 0.3\lambda_0\sqrt{n_0n_4}/n_2 & \text{for 3D,} \end{cases} \quad (4.7)$$

for the minimum size of the beam. The latter translates into the minimum diffraction length,

$$L_{\text{diffr}} \geq \begin{cases} 3.68\lambda_0n_4 (n_0/n_2)^2 & \text{for 2D,} \\ 0.56\lambda_0n_4 (n_0/n_2)^2 & \text{for 3D.} \end{cases} \quad (4.8)$$

In general, these results show that the required intensity decreases with (n_2/n_4) . This means that a larger self-defocusing coefficient n_4 makes it easier to arrest collapse, as expected. On the other hand, a larger n_4 also makes the beam size larger. This is also understandable, since stronger self-defocusing reduces the overall focusing effect and makes the beam balanced at a larger size.

Up to this point, the medium was assumed lossless. In real materials, saturable nonlinear refraction is accounted for by proximity to a certain resonance, which

implies inevitable presence of considerable loss. Strictly speaking, solitons cannot exist with the loss. Of course, dissipation is present in any experiment. The challenge is to build a real physical medium which is reasonably close to the theoretical models predicting stable solitons. In particular, this implies, as a goal, the identification of materials that exhibit the required saturable nonlinear refraction, with accompanying losses low enough to allow the observation of the essential features of the solitons. Under these conditions, only soliton-like beams (“quasi-solitons”), rather than true solitons, can be produced. Nevertheless, in cases where losses are low enough for such quasi-solitons to exist (the conditions will be described below), we refer to the objects as “solitons”.

As candidate optical materials for the soliton generation, we focus on glasses, as they offer a number of attractive properties [15, 62, 63]. Their $\chi^{(3)}$ susceptibility is generally well-known, varying from the value of fused silica ($n_2 \sim 3 \times 10^{-16} \text{cm}^2/\text{W}$) up to 1000 times that value. The linear and nonlinear susceptibilities of glasses exhibit an almost universal behavior that depends largely on the reduced photon energy ($\hbar\omega/E_g$, where $\hbar\omega$ is the photon energy, and E_g is the absorption edge, as defined in Refs. [15, 62, 63]). This results in simple and clear trends that can be easily understood. The wide variety of available glasses offers flexibility in the design of experiments. Glasses are solid, with uniform isotropic properties that make them easy to handle and use. There are recent experimental reports of saturable nonlinearities in some chalcogenide glasses [17]. The saturable nonlinearity was actually measured with the photon energy above the two-photon absorption edge, hence this case is not relevant to the pulse propagation, as the loss would be unacceptably high. However, these measurements encourage the search for the situation where the nonlinearity saturation is appreciable while the loss is reasonably

low.

It is possible to crudely estimate the conditions that will be relevant to soliton formation based on the general features of the nonlinearities of glasses. The nonlinearity of the $(2n - 1)$ th order will become significant and increase rapidly when the photon energy crosses the n -photon resonance. Just as the nonlinear index increases rapidly (and is accompanied by two-photon absorption, 2PA) when $\hbar\omega/E_g \sim 0.5$, we expect n_4 to become significant (and be accompanied by three-photon absorption, 3PA) when $\hbar\omega/E_g \sim 0.33$. The requirement that n_4 be appreciable without excessive 2PA or 3PA implies that, within the window $0.33 < \hbar\omega/E_g < 0.5$, the solitons may be possible.

To formulate these conditions in a more accurate form, it is necessary to identify a maximum loss level beyond which the dynamics deviate significantly from that of a lossless system. This issue can be addressed by theoretical consideration of quasi-solitons in (weakly) dissipative systems. First of all, we fix, as a *tolerance limit*, an apparently reasonable value of $\ell_{\text{tolerance}} \equiv 10\%$ peak-intensity loss per characteristic (diffraction) length, L_{diffr} . From what follows below, it will be clear how altering this definition may impact the predicted parameter window for soliton formation.

If the loss is produced by 2PA, the corresponding evolution equation for the peak intensity $I(z)$ is

$$\frac{dI}{dz} = -\beta_{2\text{PA}}I^2, \quad (4.9)$$

where $\beta_{2\text{PA}}$ is the 2PA coefficient. It follows that the loss per L_{diffr} (provided that it is small enough) is $\Delta I \approx -\beta_{2\text{PA}}I^2L_{\text{diffr}}$. The substitution of the above definition of the tolerance threshold, $|\Delta I|/I < \ell_{\text{tolerance}}$, into the latter result leads

to an upper bound on the intensity:

$$I < I_{2\text{PA tolerance}} \equiv \frac{\ell_{\text{tolerance}}}{\beta_{2\text{PA}} L_{\text{diff}}} . \quad (4.10)$$

Notice that the condition (4.7) implies that the diffraction length cannot be too short, hence the upper limit in Eqn. (4.10) cannot be extremely high.

An analogous result for 3PA is

$$I^2 < I_{3\text{PA tolerance}}^2 \equiv \frac{\ell_{\text{tolerance}}}{\beta_{3\text{PA}} L_{\text{diff}}} ,$$

which follows from the evolution equation [cf. Eqn. (4.9)] $dI/dz = -\beta_{3\text{PA}} I^3$. However, as will be discussed later, in the case relevant to the soliton formation, 2PA dominates over 3PA.

However, within the distance necessary for the observation of the soliton, its peak intensity must remain above the threshold value (4.6), to prevent disintegration of the soliton. Solving Eqn. (4.9), this sets another constraint on the intensity:

$$\frac{I_0}{1 + N\beta_{2\text{PA}} I_0 L_{\text{diff}}} > I_{\text{stable}} , \quad (4.11)$$

where I_0 is the initial peak intensity, and N is the number of diffraction lengths required for the experiment. In this work, we assume $N = 5$, which is sufficient for the reliable identification of the soliton [10, 58]. Note that the condition (4.11) can never be met if the necessary value I_{stable} is too high,

$$I_{\text{stable}} > I_{\text{max}} \equiv (N\beta_{2\text{PA}} L_{\text{diff}})^{-1} . \quad (4.12)$$

In the case of $I_0 \geq I_{\text{max}}$, the overall peak-intensity loss with the propagation will be $\geq 50\%$. We will refer to the situation in which $I_{\text{stable}} > I_{\text{max}}$ as a “loss dominating” one, and the opposite as “saturation dominating”, since $1/I_{\text{stable}}$ and $1/I_{\text{max}}$ can be viewed, respectively, as measures of saturation and loss in the system.

When saturation dominates over the 2PA loss, and hence creation of the soliton is possible, Eqn. (4.11) can cast into the form of a necessary condition for the initial peak power,

$$I_0 > I_{\min} \equiv \frac{I_{\text{stable}}}{1 - I_{\text{stable}}/I_{\text{max}}} . \quad (4.13)$$

The material-damage threshold, I_{damage} , also limits the highest possible peak intensity that can be used experimentally. Although this threshold depends on both the material and pulse duration, we will assume $I_{\text{damage}} \simeq 100 \text{ GW/cm}^2$, which is typical for nonlinear glasses and pulses with the duration $\sim 100 \text{ fs}$. Thus, all the above results can be summarized in the form

$$I_{\min} < I_0 < \min \{ I_{2\text{PA tolerance}}, I_{\text{damage}} \} . \quad (4.14)$$

In a material with known nonlinearity and loss, experimental observation of the solitons is feasible if the corresponding window (4.14) exists.

A somewhat simplified but convenient way to assess this is to define a figure of merit (FOM). In the case when $I_{\text{damage}} > I_{2\text{PA tolerance}}$,

$$\begin{aligned} \text{FOM} &\equiv \log \left(\frac{I_{2\text{PA tolerance}}}{I_{\min}} \right) \\ &= \begin{cases} \log \left[\ell_{\text{tolerance}} \left(1.74 \frac{n_2}{n_0^2 \lambda_0 \beta_{2\text{PA}}} - N \right) \right] , & \text{for 2D,} \\ \log \left[\ell_{\text{tolerance}} \left(1.42 \frac{n_2}{n_0^2 \lambda_0 \beta_{2\text{PA}}} - N \right) \right] , & \text{for 3D.} \end{cases} \end{aligned} \quad (4.15)$$

If I_{damage} is smaller than $I_{2\text{PA tolerance}}$, the definition becomes

$$\text{FOM} \equiv \log\left(\frac{I_{\text{damage}}}{I_{\text{min}}}\right) = \begin{cases} \log\left[I_{\text{damage}}\frac{n_4}{n_2}\left(6.4 - 3.68N\beta_{2\text{PA}}\frac{\lambda_0 n_0^2}{n_2}\right)\right], & \text{for 2D,} \\ \log\left[I_{\text{damage}}\frac{n_4}{n_2}\left(0.8 - 0.56N\beta_{2\text{PA}}\frac{\lambda_0 n_0^2}{n_2}\right)\right], & \text{for 3D.} \end{cases} \quad (4.16)$$

The FOM is a measure of the range between the minimum required and maximum allowed values of the peak intensity. Of course, it must be positive, and the larger the FOM, the better the chance to observe solitons.

It seems to be commonly accepted that a larger quintic self-defocusing coefficient n_4 is always desirable, but the above results show that this is not always true. From the FOM we can see that a larger n_4 is better in the sense that it reduces the lower threshold I_{min} , helping to secure the positiveness of the FOM (4.16). However, as soon as I_{min} is low enough that the damage threshold no longer poses a problem, Eqn. (4.15) shows that larger n_4 does not help, and the loss factor $\beta_{2\text{PA}}$ dominates. One can understand this, noticing that, although larger n_4 reduces I_{min} , at the same time it increases the beam's width and makes the needed experimental propagation length longer, as is clearly shown by Eqn. (4.8). In turn, more loss accumulates due to a longer propagation length, which offsets the benefit of a

lower I_{\min} .

4.3 Measurements of nonlinear parameters of glasses

The eventual objective is to answer the following question: for a given category of materials (such as glasses), with known nonlinear, loss, and damage characteristics, does there exist a combination of material and wavelength such that solitons can be observed? To this end, we have measured the nonlinearity in a series of glasses with 100-fs pulses from a Ti:sapphire regenerative amplifier with center wavelength at 790 nm. Sapphire is used (it has $\hbar\omega/E_g \cong 0.25$ in this case) as a reference material with minimum nonlinearity. Although fused silica can also be used for this purpose, sapphire's higher damage threshold allows us to measure at higher intensities.

We measured several glasses, including: SF59 (with $\hbar\omega/E_g \simeq 0.5$), La-Ga-S (with $\hbar\omega/E_g \simeq 0.56$), and As_2S_3 (with $\hbar\omega/E_g \simeq 0.75$). To determine the effective $\chi^{(3)}$ and $\chi^{(5)}$ susceptibilities, spectrally resolved two-beam coupling (SRTBC) was used [11]. The extended application of this method taking into account both higher-order nonlinearities and strong signals is used. In general, 2PA is observable even for $\hbar\omega/E_g < 0.5$ owing to the absorption-edge broadening present in all glasses.

As has been discussed in the previous chapter, typical experimental traces obtained from As_2S_3 are shown in the insets of Fig. 3.4, along with the theoretical fits. The intensity dependence of the SRTBC signal magnitude and normalized nonlinear absorption signal magnitude are shown in Fig. 3.4. The dotted curves in both panels are predictions for the pure $\chi^{(3)}$ nonlinearity. The deviation of the experimental points from these curves is evidence of the saturation of the nonlinearity. Postulating the presence of the $\chi^{(5)}$ self-defocusing nonlinearity provides

for good agreement with the experiments. Similar results were produced by all four samples used in the measurements; in particular, in all the cases the sign of the real part of $\chi^{(5)}$ turns out to be opposite to that of $\chi^{(3)}$, i.e., the quintic nonlinearity is self-defocusing indeed. The measured $\chi^{(3)}$ coefficients are consistent with previously reported values [15, 17, 18].

From these results, we also observe that higher-order nonlinearities become more important as the optical frequency approaches a resonance, as expected on physical grounds. The $\chi^{(5)}$ part of the nonlinearity is most significant for As_2S_3 , while for sapphire it is below the detection threshold.

4.4 Stability windows for the two- and three-dimensional solitons

The measurements provide the information needed to construct the window for the soliton formation. The results for 2D case are shown graphically in Fig. 4.1. The intensity limitations are plotted on the diagram against the reduced photon energy. The parameter space can be divided into two regions which were defined above, viz., the saturation-dominating and absorption-dominating ones, with the boundary between them determined by Eqn. (4.12). To demonstrate the dramatic effect of the loss, we also plot the window for the (unrealistic) case when loss is completely neglected (the hatched area). In the absence of loss, the window is very large and the FOM increases monotonically with the reduced photon energy. The shaded area is the window remaining after inclusion of the loss. It is greatly reduced compared to the lossless case, and the best FOM is obtained near $\hbar\omega/E_g \simeq 0.35$. From this diagram, we conclude that, while the saturation of the nonlinearity is

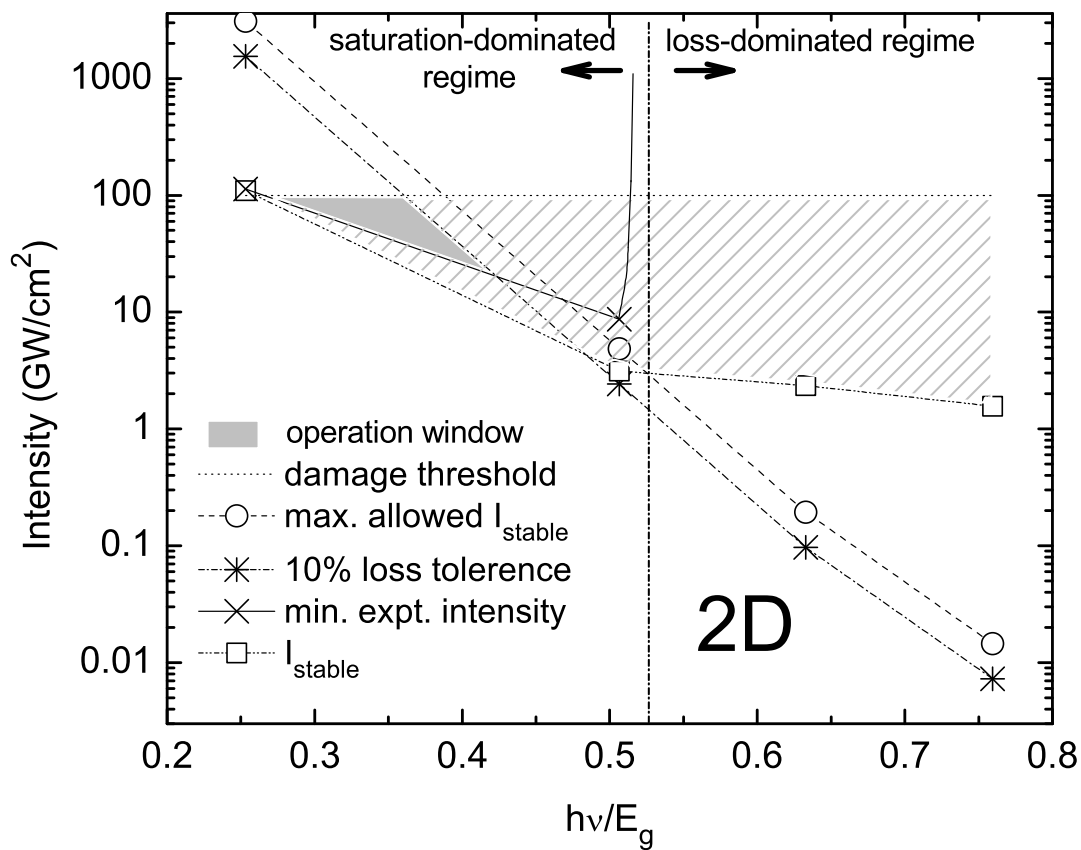


Figure 4.1: The operation window for the 2D solitons, as predicted on the basis of the experimentally-measured characteristics of the glass. The hatched area is the window neglecting loss. The shaded area is the dramatically reduced (but definitely existing) window found with loss taken into account.

definitely necessary to stabilize the soliton, major restrictions on the window are imposed by the loss.

From the above rough estimation that were based on the band-edge arguments, one might expect that 3PA would further curtail the window, when the 2PA effects are weak (which is the case exactly inside the predicted window). However, n_2 and 2PA have been observed in glasses for the reduced photon energy as low as ~ 0.35 [62], due to the fact that the band edge in glasses extends well below the nominal value. Since significant 2PA remains in this region, 3PA may be neglected indeed. Hence, 2PA presents the fundamental limitation to observing solitons in these media [as quantified by the FOM in Eqns. (4.15) and (4.16)].

The results of the analysis for the 3D solitons are summarized in Fig. 4.2. Note that another major issue in this case is the requirement of anomalous GVD. This requirement is neglected here (addition of it will only further constrain the window, which does not really exist even without that, see below). From Fig. 4.2, we observe that, even in the lossless case, the window (hatched area) is significantly smaller than in the 2D case. This is expected, because collapse is stronger in 3D than 2D [35]. As in the 2D case, the loss again is a major concern for performing experiments. The most important inference is that the window closes up completely when loss is taken into account. Thus, it appears that loss will preclude the creation of 3D solitons in glasses, while leaving room for the 2D solitons.

Our overall conclusion is that it is a challenge to perform experimental studies of 2D solitons in saturable instantaneous Kerr media. Both spatial and spatiotemporal solitons are possible to be produced experimentally. Among these two, the 2D spatiotemporal case is more complicated since it requires anomalous GVD. In general, this will naturally constrain the window further. In this case tilted-pulse

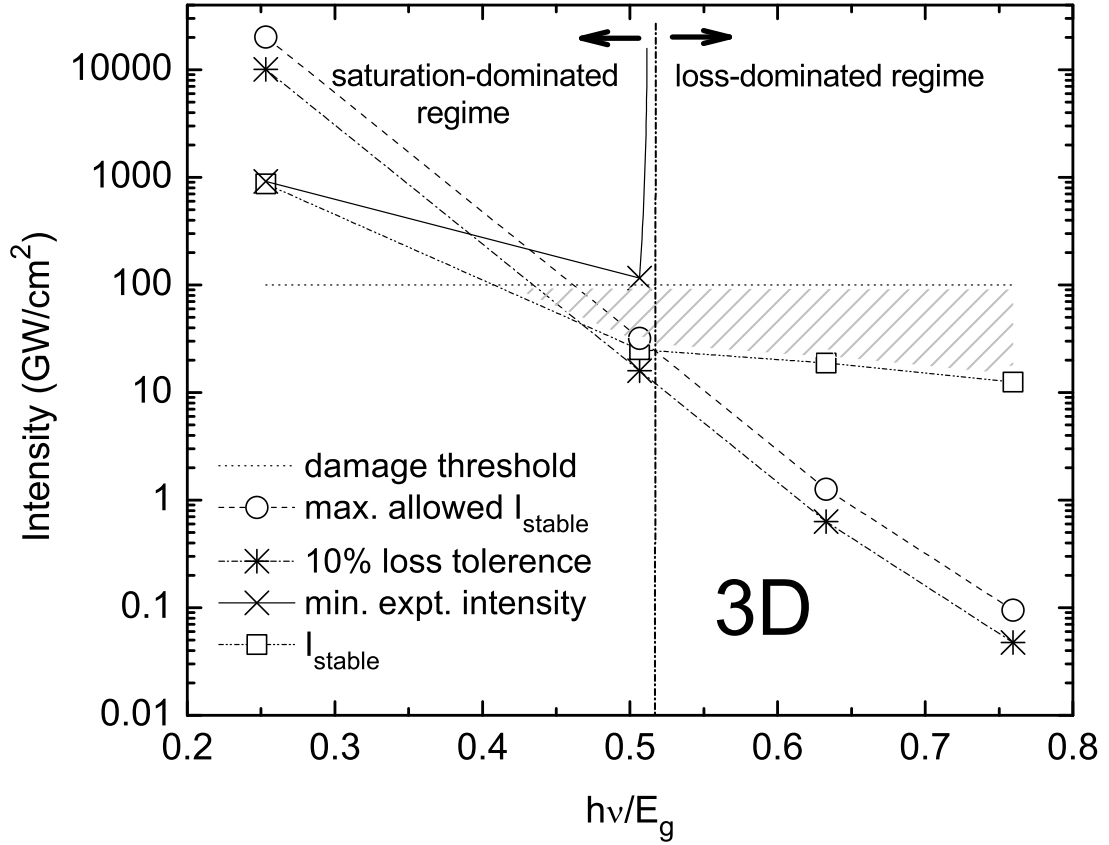


Figure 4.2: The operation window for 3D solitons. The meaning of the hatched area is the same as in the 2D case, i.e., it shows the window obtained neglecting loss. When loss is taken into account, the window vanishes completely.

techniques could be used to obtain anomalous GVD. It is also possible to use a planar waveguide to perform 2D spatiotemporal soliton experiments.

Of course, the predicted window depends on the assumed parameters (such as the damage threshold) and criteria (such as the 10% loss per diffraction length). Variations in these parameters will naturally impact the window, and our analysis provides the guidelines for searching for the most favorable materials and wavelength. A next natural step is to perform numerical simulations of the pulse propagation with the parameters selected in the present work. It is conceivable that the window for 3D solitons would finally open through variations of material parameters. In that case, one would still have to find an overlap of the resulting window with the condition that the GVD must be anomalous. More generally, non-glass materials may be tried to improve the possibilities for the experiment.

4.5 Conclusions

We have developed criteria for experimental observation of multi-dimensional solitons – spatial and spatiotemporal 2D solitons and spatiotemporal 3D ones. Using these criteria and measured properties of nonlinear glasses within a range of reduced photon energies, we have shown that the loss that accompanies higher-order nonlinearities (which are tantamount to saturation of the cubic nonlinearity) will set very stringent limits on the material parameters appropriate for the experiment. While loss was thus far neglected in theoretical treatments of multi-dimensional solitons, this work motivates more systematic studies of the soliton-like propagation in lossy media.

The criteria developed in this paper can also be applied, as an assessment tool, to materials other than glasses. More generally, the same rationale used for ob-

taining the relevant boundaries in this paper can also be used in systems other than optical ones. In these cases the specific mathematical forms of the boundaries will be different. In any case, the analysis presented here suggests that there is a small but apparently usable window of parameters in which 2D solitons can be generated. On the contrary, the prospects for generating 3D solitons in glasses are quite poor.

4.6 Acknowledgements

This work was supported by the National Science Foundation under grant PHY-0099564, and the U.S.-Israel Binational Science Foundation (Contract No.1999459). We thank Jeffrey Harbold for valuable discussions.

Chapter 5

Future directions

The usable window of parameters for producing 2D solitons is small but nonzero. The candidate materials should have the reduced-photon energy in the range of $0.3 \sim 0.4$. For pulse center wavelength at 790 nm there are many commercially available glasses in this reduced-photon energy range. Some examples are Schott glass PK1 (reduced-photon energy $h\nu/E_g \sim 0.36$), PK2 ($h\nu/E_g \sim 0.38$), PK3 ($h\nu/E_g \sim 0.38$), PSK2 ($h\nu/E_g \sim 0.38$), PSK3 ($h\nu/E_g \sim 0.38$), BK1 ($h\nu/E_g \sim 0.38$), BK3 ($h\nu/E_g \sim 0.38$), BK7 ($h\nu/E_g \sim 0.38$), UBK7 ($h\nu/E_g \sim 0.37$), BK8 ($h\nu/E_g \sim 0.38$), and BK10 ($h\nu/E_g \sim 0.37$). In fact, attempts have been made very recently to produce stable propagation of a 2D beam in BK7. Some encouraging initial results which could eventually lead to the production of stable 2D solitons were obtained [64].

However, it seems difficult to achieve the ultimate goal of observation of 3D solitons in a saturable instantaneous Kerr-type nonlinear media. Since the predicted window of parameters for 3D solitons is essentially zero, it is expected to be a major challenge to find materials which have strong enough higher-order nonlinearities without too much absorption, if they exist. Even if such a material does exist, another challenge is the requirement of anomalous group velocity dispersion (GVD). Generally, in passive materials, anomalous GVD occurs at longer wavelengths (e.g. for BBO, anomalous GVD occurs at wavelengths larger than $1.4\mu\text{m}$). To reach this wavelength region, significant investment in the development of a suitable light source has to be made and it remains a question that if the higher-order nonlinear properties are “appropriate” for stabilizing the 3D solitons at these

frequency ranges.

There is a potential alternative, however. Assuming that the efforts to produce stable 2D optical solitons in saturable instantaneous Kerr-like media turn out to be successful and materials supporting stable 2D optical solitons are identified, for the same materials to be able to support stable 3D solitons, two obstacles have to be overcome. The problem with these materials is that they do not have the correct sign of GVD in the frequency range where the higher-order nonlinear properties are large enough. They would also be too lossy for producing 3D solitons since in general the loss tolerance for 3D solitons is smaller.

An interesting idea is to “borrow” the properties of an inverted Lorentz oscillator. The dispersion properties (for both phase velocity dispersion and GVD) for an inverted Lorentz oscillator exhibits opposite sign to that of the noninverted oscillator. More specifically, since GVD is

$$\frac{d^2k}{d\omega^2} = \frac{2}{c} \frac{dn}{d\omega} + \frac{\omega}{c} \frac{d^2n}{d\omega^2}, \quad (5.1)$$

, when an Lorentz oscillator is inverted, all the derivatives of the refractive index will change sign. This is illustrated in Fig. 5.1, both the slope of the curve (corresponding to the phase velocity dispersion) and the concavity of the curve (which usually dominantly determines GVD) is inverted. It is then possible to combine this anomalous GVD from the inverted oscillator (presumably a gain medium) with the nonlinear properties from the materials supporting 2D solitons. Both the loss and normal dispersion from the 2D-soliton-supporting material can then be compensated by the inverted Lorentz oscillator and this changes the prospects of producing 3D optical solitons in a instantaneous Kerr-type saturable nonlinear medium.

One possible way to achieve this is immersing a porous substrate made from

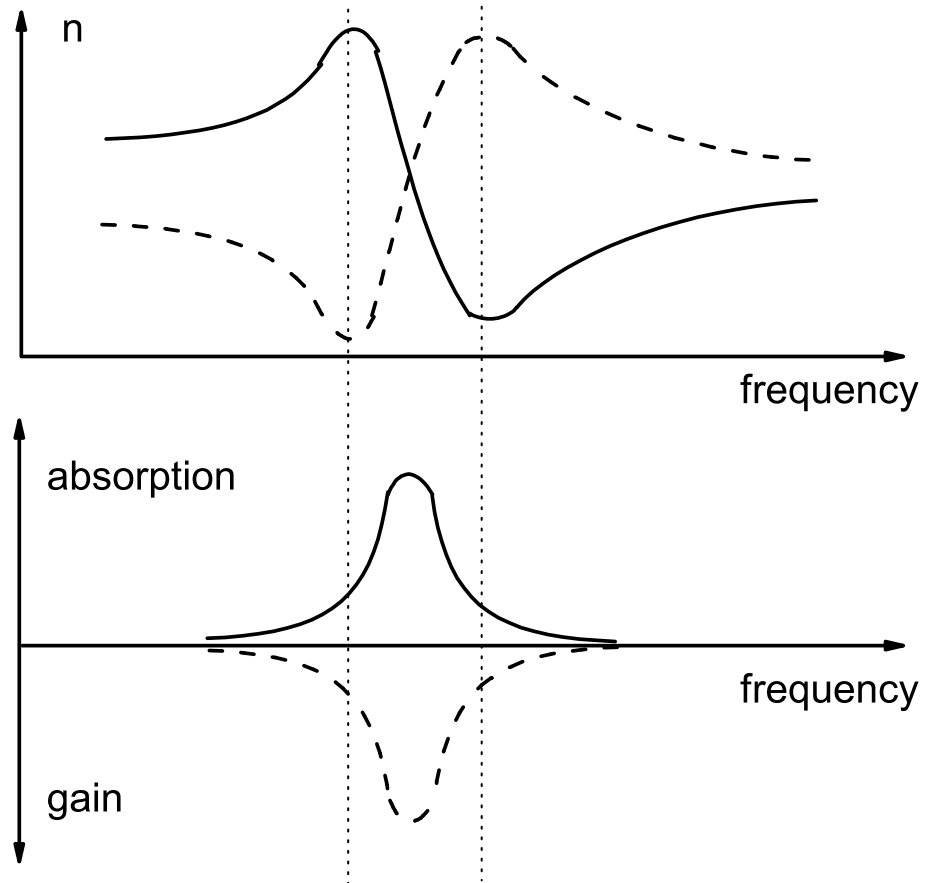


Figure 5.1: The refractive index and absorption/gain for a noninverted Lorentz oscillator (solid line) and an inverted Lorentz oscillator (dashed line). For a give frequency, the sign of the dispersion properties for an inverted Lorentz oscillator will be opposite to that of an noninverted oscillator.

2D soliton supporting glasses in a gaseous or liquid gain medium which provides the desirable dispersion properties. The pore size should be small enough (smaller than tenth of wavelength) that the substrate can still be viewed as homogeneous, but also large enough that the mixing with the external gain medium can occur.

We can even extend the same concept to quadratic nonlinear systems. In fact, as mentioned before, cascading quadratic process generates large and saturable nonlinearity and 2D stable spatial optical solitons have been demonstrated in these systems (KTP crystal, for example) [3]. It is then intriguing to think about the possibility of combining the dispersion property of an inverted Lorentz oscillator and the nonlinear property of a quadratic crystal. One can imagine a piece of porous KTP or BBO crystal immersed in a gain medium.

Of course it remains an open question if such an approach can be realized. There are many questions that have to be answered. Some of them are: Where can we find or how can we produce such a system with the desired frequency response and dispersion properties? How do the nonlinear and linear properties change when a bulk nonlinear material is made porous? What is the role of quantum effects? How small is the pore size when simple scaling can no longer be used to estimate these properties? Will the mixture of the gain medium and the porous substrate give rise to new effects? How does one produce such a porous substrate? It is not a trivial task to resolve these questions.

On the contrary, a more promising possible route of achieving stable 3D optical solitons is through the cascading quadratic nonlinearities. As mentioned before, the cascading process produces large and saturable nonlinearities. It has been used in demonstrating many types of solitons, including 2D spatial and 2D spatiotemporal solitons (see, for example, the review article [3]). Initial theoretical

investigations and the search of available materials for experimentally demonstrating 3D stable optical solitons in a quadratic system have shown promising signs [65]. Although one still faces the same dispersion problem and would need to work at a different wavelength regime such as $3 - 4 \mu\text{m}$, to obtain the needed anomalous dispersion, using quadratic nonlinearity has a major advantage: the $\chi^{(2)}$ nonlinearities are much better documented and can be measured more easily in a wider range of wavelengths (compared with higher-order nonlinearities such as $\chi^{(5)}$) and its magnitude is in general much larger than $\chi^{(3)}$. In addition, there is also a wide variety of commercial available $\chi^{(2)}$ crystals on the market. All these help reduce the search of 3D stable optical soliton to a single engineering problem: How does one build a high-quality light-source which produce stable, transform-limited pulses with good beam profile and enough intensity? In fact, recent developments in this direction shows some encouraging signs [66] and it might not be too difficult to develop the required source in the very near future. We believe this direction is currently the most promising option and deserves more research investment and attention.

Appendix A

Simulation code

In the following pages we include the simulation code used in this work. The simulation basically calculates the evolution of Eqn. 3.42 using Runge-Kutta algorithm. The code is in C and includes the following files: “runsrtdc. c”, “srtbc. c”, “propagate. c”, “initpulse. c”, “rk. c”, “F1. c”, “F2. c”, “F3. c”, “F4. c”, “srtbc. h”, and “srtbcset. h”. The display and visualization of the simulation result is handled using MATLAB and two visualization application files “cut. m” and “fulldisplayc. m” are also included.

“main()” function is defined in file “runsrtdc. c”, this is also where the output file name and path are defined. When executed, “main()” calls function “srtbc()”, which is defined in file “srtbc. c”, and starts a loop handling the time-delay. In this loop, “srtbc()” calls function “propagate()” defined in file “propagate. c”. This function will then initiate a loop handling the spatial propagation of the pulses. To do this, “propagate()” calls “initpulse()” (defined in “initpulse. c” for the first propagation step and then calls “rungekutta()” (defined in “rk. c”) to calculate the pulse evolution along the propagation. The main components of “rungekutta()” are four functions “function1()”, “function2()”, “function3()”, and “function4()”, which represent the four governing equations respectively. They are defined in files “F1. c”, “F2. c”, “F3. c”, and “F4.c” and the highest order nonlinearity included is $\chi^{(7)}$. The extension to including even higher order terms can be done straight-forwardly by changing these four files and other parameters accordingly.

file name: runsrtbc.c

```

#include "srtbc.h"
#include "srtbcset.h"
#include "mat.h"

int main(void)
{

    double inpowd[TRES];

    double refpowd[TRES];

    double signal[DELAYRES][TRES];

    double pumppowd[DELAYRES][TRES];

    double probpowd[DELAYRES][TRES];

    int res[2]={TRES,ZRES};

    double
pulse_param[6]={PUMPR,PROBR,PUMPDELAY,PROBDELAY,PUMPWID,P
ROBWID};

    double parameter[3]={ALPHA,BETA,GAMMA};

    double delayparam[2]={MAXDELAY,DELAYRES};

    double FWHM=(double)(0.265010363*TRES/PROBWID);

    double pulsep[4]={PUMPR,PROBR,PUMPWID,PROBWID};

    MATFile *mfout;
    mxArray *inp,*ref,*sig,*prb;
    mxArray *dims,*norm,*para,*psp;
    int numelem = DELAYRES*TRES;
    int dd[1]={2};
    int dp[1]={3};
    int dsp[1]={4};
    int dt[1]={TRES};
    double dimen[2]={TRES,DELAYRES};
    int dimenf[2]={TRES,DELAYRES};
    double normal[2]={FWHM,MAXDELAY};

```

```

int t;

srtbc(inpowd,refpowd,signal,pumpowd,probpowd,res,pulse_param,parameter
,delayparam);

//for (t=0;t<=TRES-1;t++)
// printf("\nref2 %f t= %d",refpowd[t],t);

if((mfout = matOpen("test.mat","w"))== NULL)
{
    fprintf(stderr,"\nERROR:cannot creat matlab output file");
    return 0;
}

// for (t=0;t<=TRES-1;t++)
// printf("\nref2 %f t= %d",refpowd[t],t);

dims = mxCreateNumericArray(1,dd,mxDOUBLE_CLASS,mxREAL);
mxSetName(dims,"dimensions");
memcpy((void*)(mxGetPr(dims)),(void*)dimen,sizeof(dimen));
matPutArray(mfout,dims);
mxDestroyArray(dims);

norm = mxCreateNumericArray(1,dd,mxDOUBLE_CLASS,mxREAL);
mxSetName(norm,"normalization");
memcpy((void*)(mxGetPr(norm)),(void*)normal,sizeof(normal));
matPutArray(mfout,norm);
mxDestroyArray(norm);

para = mxCreateNumericArray(1,dp,mxDOUBLE_CLASS,mxREAL);
mxSetName(para,"parameters");
memcpy((void*)(mxGetPr(para)),(void*)parameter,sizeof(parameter));
matPutArray(mfout,para);
mxDestroyArray(para);

psp = mxCreateNumericArray(1,dpsp,mxDOUBLE_CLASS,mxREAL);
mxSetName(psp,"pulseparameters");
memcpy((void*)(mxGetPr(psp)),(void*)pulsep,sizeof(pulsep));
matPutArray(mfout,psp);
mxDestroyArray(psp);

```

```
inp = mxCreateNumericArray(1,dt,mxDOUBLE_CLASS,mxREAL);
mxSetName(inp,"inputprobpsd");
memcpy((void*)(mxGetPr(inp)),(void*)inpowd,sizeof(inpowd));
matPutArray(mfout,inp);
mxDestroyArray(inp);
```

```
ref = mxCreateNumericArray(1,dt,mxDOUBLE_CLASS,mxREAL);
mxSetName(ref,"referencepsd");
memcpy((void*)(mxGetPr(ref)),(void*)refpowd,sizeof(refpowd));
matPutArray(mfout,ref);
mxDestroyArray(ref);
```

```
sig = mxCreateNumericArray(2,dimenf,mxDOUBLE_CLASS,mxREAL);
mxSetName(sig,"signal");
memcpy((void*)(mxGetPr(sig)),(void*)signal ,numelem*sizeof(double));
matPutArray(mfout,sig);
mxDestroyArray(sig);
```

```
prb = mxCreateNumericArray(2,dimenf,mxDOUBLE_CLASS,mxREAL);
mxSetName(prb,"probpsd");
memcpy((void*)(mxGetPr(prb)),(void*)probpowd ,numelem*sizeof(double));
matPutArray(mfout,prb);
mxDestroyArray(prb);
```

```
matClose(mfout);
```

```
}
```

file name: srtbc.c

```
#include "srtbc.h"
```

```
void srtbc(double *inpowd, double *refpowd, double signal[][TRES], double
pumpowd[][TRES], double probpowd[][TRES], int *res, double *pulse_param
double *parameter, double *delayparam)
```

```
{
    double delay_inc,delay_center;
    double *lpu,*Phipu,*lpr,*Phipr;
    double pulse_param0[6];
    fftw_complex *temp,*pusp0,*prsp0,*pump_spect,*prob_spect;
    fftw_plan fplan;
    int fcenter,delay,init,t,dt;
```

```
    fplan =
    fftw_create_plan(res[0],FFTW_BACKWARD,FFTW_MEASURE|FFTW_USE_
WISDOM);
```

```
    printf("\n pass1");
```

```
    lpu=(double *)malloc(res[0]*sizeof(double));
```

```
    if(!(lpu == NULL)) printf("\n pass2");
```

```
    Phipu=(double *)malloc(res[0]*sizeof(double));
```

```
    if(!(Phipu == NULL)) printf("\n pass3");
```

```
    lpr=(double *)malloc(res[0]*sizeof(double));
```

```
    if(!(lpr == NULL)) printf("\n pass4");
```

```
    Phipr=(double *)malloc(res[0]*sizeof(double));
```

```
    if(!(Phipr == NULL)) printf("\n pass5");
```

```
    temp=(fftw_complex *)malloc(res[0]*sizeof(fftw_complex));
```

```
    if (!(temp== NULL)) printf("\n pass6");
```

```
    pusp0=(fftw_complex *)malloc(res[0]*sizeof(fftw_complex));
```

```
    if (!(pusp0== NULL)) printf("\n pass7");
```

```

prsp0=(fftw_complex *)malloc(res[0]*sizeof(fftw_complex));

if (!(prsp0==NULL)) printf("\n pass8");

pump_spect=(fftw_complex *)malloc(res[0]*sizeof(fftw_complex));

if (!(pump_spect==NULL)) printf("\n pass9");

prob_spect=(fftw_complex *)malloc(res[0]*sizeof(fftw_complex));

if (!(prob_spect== NULL)) printf("\n pass10");

printf("\n");

fcenter=(int)ceil(((double)res[0]-1.)/2.);
delay_inc = (double)(2.*delayparam[0]/delayparam[1]);
delay_center=(double)((delayparam[1]-1.)/2.);
dt=(int)ceil(fcenter-(((double)res[0]-1.)/2.));

printf("\n test  dt = %e, halfc= %e, fcenter = %e,
delaycenter= %e", (double)dt, (double)(res[0]-1)/2, (double)fcenter,
delay_center);
pulse_param0[0]=0;
pulse_param0[1]=pulse_param[1];
pulse_param0[2]=pulse_param[2];
pulse_param0[3]=pulse_param[3];
pulse_param0[4]=pulse_param[4];
pulse_param0[5]=pulse_param[5];

propagate(fplan,temp,puasp0,prsp0,pump_spect,prob_spect,lpu,Phipu,lpr,Phipr
,res,pulse_param0,parameter,0);

for (t=0;t<=(fcenter-1); t++)
{

    refpowd[t]=pow((double)(pow((double)(prob_spect[t+fcenter-
dt+1].re),2)+pow((double)(prob_spect[t+fcenter-dt+1].im),2)),1);

    // printf("\nref= %f, t= %d",refpowd[t],t);
}
for (t=fcenter;t<=(res[0]-1); t++)
{

```

```

        refpowd[t]=pow((double)(pow((double)(prob_spect[t-
fcenter].re),2)+pow((double)(prob_spect[t-fcenter].im),2)),1);

        // printf("\nref= %f, t= %d",refpowd[t],t);

    }

for(delay=0; delay<=((int)delayparam[1]-1); delay++)
{

    pulse_param[2]=(double)delay_inc*(double)(delay-delay_center);

    if(delay==0)
        init=1;
    else
        init=0;

    propogate(fplan,temp,pusp0,prsp0,pump_spect,prob_spect,lpu,Phipu,l
pr,Phipr,res,pulse_param,parameter,init);

    for (t=0;t<=(fcenter-1); t++)
    {
        if(init==1)
        {
            inpowd[t]=pow((double)(pow((double)(prsp0[t+fcenter-
dt+1].re),2)+pow((double)(prsp0[t+fcenter-dt+1].im),2)),1);
            // printf("\ninp= %f, t= %d",inpowd[t],t);
            // printf("\nref3= %f, t= %d",refpowd[t],t);
        }

        probpowd[delay][t]=pow((double)(pow((double)(prob_spect[t+fcenter-
dt+1].re),2)+pow((double)(prob_spect[t+fcenter-dt+1].im),2)),1);
        signal[delay][t]=((double)probpowd[delay][t]-
(double)refpowd[t])/(double)refpowd[t];
        // printf("\nsignal= %e, ref %e
prob %e",signal[delay][t],refpowd[t],probpowd[t]);
    }
    for (t=fcenter;t<=(res[0]-1); t++)
    {
        if(init==1)
        {

```

```

        inpowd[t]=pow((double)(pow((double)(prsp0[t-
fcenter].re),2)+pow((double)(prsp0[t-fcenter].im),2)),1);
        // printf("\ninp= %f, t= %d",inpowd[t],t);
        // printf("\nref3= %f, t= %d",refpowd[t],t);
    }

        probpowd[delay][t]=pow((double)(pow((double)(prob_spect[t-
fcenter].re),2)+pow((double)(prob_spect[t-fcenter].im),2)),1);
        signal[delay][t]=((double)probpowd[delay][t]-
(double)refpowd[t])/(double)refpowd[t];

    }

        printf("\nDelay Step %d / %d complete !!",
delay+1,(int)delayparam[1]);

    }

printf("\n");

    fftw_destroy_plan(fplan);

    free((void *)lpu);
    free((void *)Phipu);
    free((void *)lpr);
    free((void *)Phipr);
    free((void *)temp);
    free((void *)pusp0);
    free((void *)prsp0);
    free((void *)pump_spect);
    free((void *)prob_spect);

}
//
spect=propogate(t_res,z_res,pu_ratio,pr_ratio,pu_delay,pr_delay,pu_wid,pr_w
id,alpha,beta,gamma);

//
spect_0=propogate(t_res,z_res,0,pr_ratio,pu_delay,pr_delay,pu_wid,pr_wid,al
pha,beta,gamma);

//    fcenter=ceil((t_res+1)/2);

```

```

// PumpS=spect(:,1)';
// ProbS=spect(:,2)';

// ProbS_0=spect_0(:,2)';

// trans =(abs(ProbS(floor(fcenter+detune))+
(ProbS(ceil(fcenter+detune))-ProbS(floor(fcenter+detune))))*(detune-
floor(detune))))^2;

// trans_0 =(abs( ProbS_0(floor(fcenter+detune))+
(ProbS_0(ceil(fcenter+detune))-ProbS_0(floor(fcenter+detune))))*(detune-
floor(detune))))^2;

//%tt=1:t_res;

//%subplot(2,1,1)

//%plot(tt,abs(PumpS(tt)),'--b')
//%hold on
//%plot(tt,angle(PumpS(tt)),'--g')
//%hold off

//%subplot(2,1,2)

//%plot(tt,abs(ProbS(tt)),'--b')
//%hold on
//%plot(tt,angle(ProbS(tt)),'--g')
//%hold off

//signal=[trans,trans_0,(trans/trans_0-1)];

```

file name: propagate.c

```

#include "srtbc.h"

void propogate(fftw_plan fplan,fftw_complex *temp,fftw_complex *pusp0,
fftw_complex *prsp0, fftw_complex *pump_spect, fftw_complex
*prob_spect,double *lpu,double *Phipu, double *lpr, double *Phipr, int *res,
double *pulse_param, double *parameter,int init)

{

double landPhi[4];
double inc_z;
int z,t;

inc_z=(1./(double)res[1]);

initpulse(lpu,Phipu,lpr,Phipr,pulse_param,res);

if(init == 1)
{
for (t=0; t<= (res[0]-1); t++)
{
temp[t].re=pow(lpu[t],0.5)*cos(Phipu[t]);
temp[t].im=pow(lpu[t],0.5)*sin(Phipu[t]);
}
fftw_one(fplan,temp,pusp0);

for (t=0; t<= (res[0]-1); t++)
{
temp[t].re=pow(lpr[t],0.5)*cos(Phipr[t]);
temp[t].im=pow(lpr[t],0.5)*sin(Phipr[t]);
}
fftw_one(fplan,temp,prsp0);
}

for (z=0; z <= (res[1]-1); z++)
{
for (t=0; t<= (res[0]-1); t++)
{
landPhi[0]=lpu[t];

```

```

landPhi[1]=Phipu[t];
landPhi[2]=lpr[t];
landPhi[3]=Phipr[t];

// printf("\nlpu before %e ,z=%d, t= %d",lpu[t],z,t);
// printf("\n increment is %f",inc_z);
rungekutta(inc_z,landPhi,parameter);

lpu[t]=landPhi[0];

// printf("\nlpu after %e,z= %d, t= %d", lpu[t],z,t);

Phipu[t]=landPhi[1];
lpr[t]=landPhi[2];
Phipr[t]=landPhi[3];
}
}

for (t=0; t<= (res[0]-1); t++)
{
temp[t].re=pow(lpu[t],0.5)*cos(Phipu[t]);
temp[t].im=pow(lpu[t],0.5)*sin(Phipu[t]);
}
fftw_one(fplan,temp,pump_spect);

for (t=0; t<= (res[0]-1); t++)
{
temp[t].re=pow(lpr[t],0.5)*cos(Phipr[t]);
temp[t].im=pow(lpr[t],0.5)*sin(Phipr[t]);
}
fftw_one(fplan,temp,prob_spect);
}

// lpump(z_res+1,t_res)=0;
// Phipump(z_res+1,t_res)=0;
// lprob(z_res+1,t_res)=0;
// Phiprob(z_res+1,t_res)=0;

// lpump(1,:)=initpulse_l(pu_delay,pu_ratio,t_res,pu_wid);

// Phipump(1,:)=initpulse_Phi(pu_delay,pu_ratio,t_res,pu_wid);

```

```

// lprob(1,:)=initpulse_l(pr_delay,pr_ratio,t_res,pr_wid);

// Phiprob(1,:)=initpulse_Phi(pr_delay,pr_ratio,t_res,pr_wid);

// %test output
// if(0)
// tt=1:t_res
// plot(tt,lpump(1,tt),'--b')
// hold on
// plot(tt,lprob(1,tt),'--g')
// plot(tt,Phipump(1,tt),'--b')
// hold on
// plot(tt,Phiprob(1,tt),'--g')
// hold off
// end

// z_inc=1/z_res;

// for zstep=1:z_res;
// for tt=1:t_res;
//
temp=rk(z_inc,lpump(zstep,tt),Phipump(zstep,tt),lprob(zstep,tt),Phiprob(zstep,
tt),alpha,beta,gamma);

// lpump(zstep+1,tt)= temp(1);
// Phipump(zstep+1,tt)= temp(2);
// lprob(zstep+1,tt)= temp(3);
// Phiprob(zstep+1,tt)= temp(4);

// end
// end

// %test output
// if(0)
// tt=1:t_res;

// subplot(2,1,1)

// plot(tt,lpump(z_res+1,tt),'--b')
// hold on
// plot(tt,lprob(z_res+1,tt),'--g')
// hold off

```

```

// subplot(2,1,2)

// plot(tt,Phipump(z_res+1,tt),'--b')
// hold on
// plot(tt,Phiprob(z_res+1,tt),'--g')
// hold off

// end

// for t=1:t_res;

// Apump(t)=(lpump(z_res+1,t)^0.5)*exp(i*Phipump(z_res+1,t));
// Aprob(t)=(lprob(z_res+1,t)^0.5)*exp(i*Phiprob(z_res+1,t));

// end

// PumpSpect_0=fft(Apump);
// ProbSpect_0=fft(Aprob);

// fcenter=ceil((t_res+1)/2);
// dt=ceil(fcenter-(t_res+1)/2);
// for t=fcenter:t_res;

// PumpSpect(t)=PumpSpect_0(t-fcenter+1);
//ProbSpect(t)=ProbSpect_0(t-fcenter+1);

//end

//for t=1:fcenter-1;

//PumpSpect(t)=PumpSpect_0(t+fcenter-dt);
//ProbSpect(t)=ProbSpect_0(t+fcenter-dt);

//end

//%test output
//if (0)

```

```
//tt=1:t_res;  
  
//subplot(2,1,1)  
  
//plot(tt,abs(PumpSpect(tt)),'--b')  
//hold on  
//plot(tt,angle(PumpSpect(tt)),'--g')  
//hold off  
  
//subplot(2,1,2)  
  
//plot(tt,abs(ProbSpect(tt)),'--b')  
//hold on  
//plot(tt,angle(ProbSpect(tt)),'--g')  
//hold off  
//end  
//endspect=[PumpSpect',ProbSpect'];
```

file name: initpulse.c

```

#include "srtbc.h"

void initpulse(double *lpu0, double *Phipu0, double *lpr0, double *Phipr0,
double *pulse_param, int *res)
{
    %% this generates a 1D array with element number = resolution. width=width
    %% centered at (resolution+1)/2, delayed by delayXwidth, amplitude= ratio
    double incpu,incpr;
    double center;
    int t;
    //inc=1/width;
    incpu=(double)(1/pulse_param[4]);
    incpr=(double)(1/pulse_param[5]);
    //center=(resolution+1)/2;
    center=(double)((res[0]-1)/2);
    //for t=1:resolution;

    // printf("\n pumpwid %f probwid %f incpu %f
    incpr %f",pulse_param[4],pulse_param[5],incpu,incpr);
    for (t = 0; t <= res[0]-1; t++)
    {

        //pulse(t)=ratio*exp(-((t-center)*inc-delay)^2);

        lpu0[t]=pulse_param[0]*exp(-pow(((double)(((double)t-center)*incpu-
pulse_param[2])),2));/*pow((((double)t-center)*incpu-
pulse_param[2]),2.)*exp(t/10);*/
        Phipu0[t]=0;

        lpr0[t]=pulse_param[1]*exp(-pow(((double)(((double)t-center)*incpr-
pulse_param[3])),2));

        Phipr0[t]=0;

        //printf("\n test %d",t);
        //printf("\nlpu %e t %d",lpu0[t],t);
    }
    //end;
}

```

file name: rk.c

```

#include "srtbc.h"
void rungekutta(double h, double *landPhi, double *parameter)
{
    double F11,F12,F13,F14,
           F21,F22,F23,F24,
           F31,F32,F33,F34,
           F41,F42,F43,F44;
    double lpu,Phipu,lpr,Phipr;

    lpu=landPhi[0];
    Phipu=landPhi[1];
    lpr=landPhi[2];
    Phipr=landPhi[3];

    F11=function1(lpu,Phipu,lpr,Phipr, parameter);
    F21=function2(lpu,Phipu,lpr,Phipr, parameter);
    F31=function3(lpu,Phipu,lpr,Phipr, parameter);
    F41=function4(lpu,Phipu,lpr,Phipr, parameter);

    F12=function1(lpu+(h/2)*F11,Phipu+(h/2)*F21,lpr+(h/2)*F31,Phipr+(h/2)*F41,
parameter);

    F22=function2(lpu+(h/2)*F11,Phipu+(h/2)*F21,lpr+(h/2)*F31,Phipr+(h/2)*F41,
parameter);

    F32=function3(lpu+(h/2)*F11,Phipu+(h/2)*F21,lpr+(h/2)*F31,Phipr+(h/2)*F41,
parameter);

    F42=function4(lpu+(h/2)*F11,Phipu+(h/2)*F21,lpr+(h/2)*F31,Phipr+(h/2)*F41,
parameter);

    F13=function1(lpu+(h/2)*F12,Phipu+(h/2)*F22,lpr+(h/2)*F32,Phipr+(h/2)*F42,
parameter);

    F23=function2(lpu+(h/2)*F12,Phipu+(h/2)*F22,lpr+(h/2)*F32,Phipr+(h/2)*F42,
parameter);

```

```

F33=function3(lpu+(h/2)*F12,Phipu+(h/2)*F22,lpr+(h/2)*F32,Phipr+(h/2)*F42,
parameter);

F43=function4(lpu+(h/2)*F12,Phipu+(h/2)*F22,lpr+(h/2)*F32,Phipr+(h/2)*F42,
parameter);

F14=function1(lpu+h*F13,Phipu+h*F23,lpr+h*F33,Phipr+h*F43,parameter);
F24=function2(lpu+h*F13,Phipu+h*F23,lpr+h*F33,Phipr+h*F43,parameter);
F34=function3(lpu+h*F13,Phipu+h*F23,lpr+h*F33,Phipr+h*F43,parameter);
F44=function4(lpu+h*F13,Phipu+h*F23,lpr+h*F33,Phipr+h*F43,parameter);

//lpunext=lpu+(h/6)*(F11+2*F12+2*F13+F14);
landPhi[0]=lpu+(h/6)*(F11+2*F12+2*F13+F14);

//Phipunext=Phipu+(h/6)*(F21+2*F22+2*F23+F24);
landPhi[1]=Phipu+(h/6)*(F21+2*F22+2*F23+F24);

//lprnext=lpr+(h/6)*(F31+2*F32+2*F33+F34);
landPhi[2]=lpr+(h/6)*(F31+2*F32+2*F33+F34);

//Phiprnext=Phipr+(h/6)*(F41+2*F42+2*F43+F44);
landPhi[3]=Phipr+(h/6)*(F41+2*F42+2*F43+F44);

}

```

file name: F1.c

```
#include "srtbc.h"
double function1(double lpu, double Phipu, double lpr, double Phipr, double
*parameter)
{

double F1;
//F1=-(alpha+(beta*lpu))*lpu;
F1=-
(parameter[0]+(parameter[1]*lpu)+(ALPHA4*lpu*lpu)+(ALPHA6*lpu*lpu*lpu))*l
pu;
return F1;

}
```

file name: F2.c

```
#include "srtbc.h"
double function2(double lpu, double Phipu, double lpr, double Phipr, double
*parameter)

{
    double F2;

    // F2= gamma*lpu;
    F2=(parameter[2]+(GAMMA4*lpu)+(GAMMA6*lpu*lpu))*lpu;
    return F2;
}
```

file name: F3.c

```
#include "srtbc.h"
double function3(double lpu, double Phipu, double lpr, double Phipr, double
*parameter)
{
    double F3;
    //F3=-(alpha+(2*beta*lpu))*lpr;
    F3=-
(parameter[0]+(2*parameter[1]*lpu)+(3*ALPHA4*lpu*lpu)+(4*ALPHA6*lpu*lpu
*lpu))*lpr;
    return F3;
}
```

file name: F4.c

```
#include "srtbc.h"
double function4(double lpu, double Phipu, double lpr, double Phipr, double
*parameter)
{
    double F4;

    //F4= 2*gamma*lpu;
    F4=((2*parameter[2])+(3*GAMMA4*lpu)+(4*GAMMA6*lpu*lpu))*lpu;
    return F4;
}
```

File name: srtbc.h

```
#include "srtbcset.h"
#include <stdio.h>
#include <math.h>
#include <stdlib.h>
#include <fftw.h>
#include <rfftw.h>

extern void srtbc(double *inpowd,double *refpowd,double signal[][TRES],
double pumppowd[][TRES], double probpowd[][TRES],int *res, double
*pulse_param, double *parameter, double *delayparam);

extern void propogate(fftw_plan fplan,fftw_complex *temp,fftw_complex
*pusp0, fftw_complex *prsp0, fftw_complex *pump_spect, fftw_complex
*prob_spect,double *lpu,double *Phipu, double *lpr, double *Phipr, int *res,
double *pulse_param, double *parameter,int init);

extern void initpulse(double *lpu0, double *Phipu0, double *lpr0, double
*Phipr0, double *pulse_param, int *res);

extern void rungekutta(double h, double *landPhi, double *parameter);

extern double function1(double lpu, double Phipu,double lpr, double Phipr,
double *parameter);

extern double function2(double lpu, double Phipu, double lpr, double Phipr,
double *parameter);

extern double function3(double lpu, double Phipu, double lpr, double Phipr,
double *parameter);

extern double function4(double lpu, double Phipu, double lpr, double Phipr,
double *parameter);
```

file name: srtbcset.h

```

#define TRES 256 //number of bin in time

#define ZRES 128 //number of bin in z

#define PUMPR 11 //initial pump peak intensity normalized by prob
#define PROBR 1 // set to 1
#define PUMPDELAY 0 // not used explicitly, set to 0
#define PROBDELAY 0 // not used explicitly, set to 0
#define PUMPWID 20 //number of bin from center when intensity drop to 1/e
#define PROBWID 20

#define ALPHA 0.01*0
#define BETA 0.*1*0.3*0.05780467//0*(-0.01377/11) //((0.018856/15)*0.6)
#define GAMMA 1*0.05780467//((0.28*0.05)*20*0.7*0.85*0.9*1.2
//((0.020076/15)*0.6)
#define ALPHA4 -0.001//(-0.026*0.05*0.05*20*20)*1.2*1.2
#define GAMMA4 1.945618*0.1*0.1*0//(-
0.018*0.05*0.05*20*20)*0.7*0.92*0.9*1.2*1.2
#define ALPHA6 0//((0.00135*0.05*0.05*0.05*20*20*20)*1.2*1.2*1.2
#define GAMMA6 0

#define MAXDELAY 8 //max delay of each side normalized by pumpwidth as
defined above
#define DELAYRES 200 // number of bin for delay

```

file name: cut.m

```

function []=cut(file,griddetune)

load(file,'dimensions','normalization','parameters','pulseparameters','inputprob
psd','referencepsd','signal','probpsd')

delay_res=dimensions(2)
maxdelay=normalization(2)
t_res=dimensions(1)
FWHM=normalization(1)
ALPHA=parameters(1)
BETA=parameters(2)
GAMMA=parameters(3)
PUMPI=pulseparameters(1)
PROBI=pulseparameters(2)
PUMPWID=pulseparameters(3)
PROBWID=pulseparameters(4)

delay_center=(delay_res+1)/2

delay_inc=(2*maxdelay)/delay_res

grid_unitdelay = 1/delay_inc

f_center=ceil((t_res+1)/2)

delay=1:delay_res;

%sig=signal(f_center+griddetune,:)

sig=signal(f_center+floor(griddetune),:)+(signal(f_center+ceil(griddetune),:)-
signal(f_center+floor(griddetune),:))*(griddetune-floor(griddetune));
sigmax=max(sig)
sigmin=min(sig)
figure
plot(sig(delay)),grid on,whitebg('white');

%detune=1:t_res;

```

```

%detune=(f_center-
floor(FWHM*detunerange)):(f_center+floor(FWHM*detunerange))
%  signal(detune,delay);

if(0)
figure
    mesh(((delay-delay_center)*delay_inc),((detune-
f_center)/FWHM),signal(detune,delay)),ylabel('Normalized
Detune','FontSize',12),xlabel('Normalized
Delay','FontSize',12),zlabel('Transmission Change','FontSize',12),shading
interp,colormap(cool(512)),colorbar,whitebg('black'),title(['SRTBC Signal
Surface, alpha=',num2str(ALPHA),',beta=',num2str(BETA),',gamma=',
num2str(GAMMA),',pumpI0=',num2str(PUMPI),',probi0=',num2str(PROBI)],'Fo
ntSize',12),grid on
end
    if(0)
figure
        meshc(((delay-delay_center)*delay_inc),((detune-
f_center)/FWHM),probpsd(detune,delay)),ylabel('Normalized
Detune','FontSize',12),xlabel('Normalized
Delay','FontSize',12),zlabel('PSD','FontSize',12),shading
interp,colormap(cool(512)),colorbar,whitebg('black'),title(['SRTBC Prob PSD,
alpha=',num2str(ALPHA),',beta=',num2str(BETA),',gamma=',
num2str(GAMMA),',pumpI0=',num2str(PUMPI),',probi0=',num2str(PROBI)],'Fo
ntSize',12),grid on
end
        if(0)
figure
            f=1:t_res;
            whitebg('white'), grid on
            plot(f,inputprobpsd(f),'--g');
end
            if(0)
figure
                plot(f,referencepsd(f),'-b');
end
            %  surf(((delay-delay_center)*delay_inc),((detune-
f_center)/FWHM),probpsd(detune,delay)),ylabel('Normalized
Detune','FontSize',12),xlabel('Normalized
Delay','FontSize',12),zlabel('Transmission Change','FontSize',12),ylim([-
detunerange detunerange]),xlim([ -(delay_inc*delay_res/2)
(delay_inc*delay_res/2)]),shading
interp,colormap(cool(512)),colorbar,whitebg('black'),title('SRTBC Signal
Surface','FontSize',15),grid on

```

```

% surf1(((delay-delay_center)*delay_inc),((detune-
f_center)/FWHM),signal(detune,delay)),ylabel('Normalized
Detune','FontSize',12),xlabel('Normalized
Delay','FontSize',12),zlabel('Transmission Change','FontSize',12),ylim([-
detunerange detunerange]),xlim([- (delay_inc*delay_res/2)
(delay_inc*delay_res/2)]),shading
interp,colormap(cool(512)),colorbar,whitebg('black'),title('SRTBC Signal
Surface','FontSize',15),grid on

%hold on
%surf1(((detune-f_center)/FWHM),((delay-
delay_center)*delay_inc),trace_pt_f(delay,detune)+2),xlabel('Normalized
Detune','FontSize',12),ylabel('Normalized
Delay','FontSize',12),zlabel('Transmission Change','FontSize',12),xlim([-
detunerange detunerange]),ylim([- (delay_inc*delay_res/2)
(delay_inc*delay_res/2)]),shading
interp,colormap(cool(512)),colorbar,whitebg('black'),title('SRTBC Signal
Surface','FontSize',15),grid on

sigt=sigt;

f=strrep(file,'.mat','_')

space=999999999;

save(['/home/yc245/csrtbchiorder/',f,'cut_',num2str(griddetune),'.txt'],'dimensio
ns','normalization','parameters','pulseparameters','griddetune','sigmax','sigmin',
'sigt','-ASCII','-DOUBLE')

clear

```

file name: fulldisplayc.m

```

function []=full_display(file,detunerange)

load(file,'dimensions','normalization','parameters','pulseparameters','inputprob
psd','referencepsd','signal','probpsd')

delay_res=dimensions(2)
maxdelay=normalization(2)
t_res=dimensions(1)
FWHM=normalization(1)
ALPHA=parameters(1)
BETA=parameters(2)
GAMMA=parameters(3)
PUMPI=pulseparameters(1)
PROBI=pulseparameters(2)
PUMPWID=pulseparameters(3)
PROBWID=pulseparameters(4)

delay_center=(delay_res+1)/2

delay_inc=(2*maxdelay)/delay_res

grid_unitdelay = 1/delay_inc

f_center=ceil((t_res+1)/2)

delay=1:delay_res;
%detune=1:t_res;
detune=(f_center-
floor(FWHM*detunerange)):(f_center+floor(FWHM*detunerange))
    signal(detune,delay);

figure
    mesh(((delay-delay_center)*delay_inc),((detune-
f_center)/FWHM),signal(detune,delay)),ylabel('Normalized
Detune','FontSize',12),xlabel('Normalized
Delay','FontSize',12),zlabel('Transmission Change','FontSize',12),shading
interp,colormap(cool(512)),colorbar,whitebg('black'),title(['SRTBC Signal
Surface, alpha=',num2str(ALPHA),',beta=',num2str(BETA),',gamma='

```

```
num2str(GAMMA),' ,pumpI0=',num2str(PUMPI),' ,probi0=',num2str(PROBI)],'Fo
ntSize',12),grid on
```

```
figure
```

```
meshc(((delay-delay_center)*delay_inc),((detune-
f_center)/FWHM),probpsd(detune,delay)),ylabel('Normalized
Detune','FontSize',12),xlabel('Normalized
Delay','FontSize',12),zlabel('PSD','FontSize',12),shading
interp,colormap(cool(512)),colorbar,whitebg('black'),title(['SRTBC Prob PSD,
alpha=',num2str(ALPHA),' ,beta=',num2str(BETA),' ,gamma=',
num2str(GAMMA),' ,pumpI0=',num2str(PUMPI),' ,probi0=',num2str(PROBI)],'Fo
ntSize',12),grid on
```

```
if(0)
```

```
figure
```

```
f=1:t_res;
whitebg('white'), grid on
plot(f,inputprobpsd(f),'--g');
```

```
end
```

```
if(0)
```

```
figure
```

```
plot(f,referencepsd(f),'-b');
end
```

```
% surf(((delay-delay_center)*delay_inc),((detune-
f_center)/FWHM),probpsd(detune,delay)),ylabel('Normalized
Detune','FontSize',12),xlabel('Normalized
Delay','FontSize',12),zlabel('Transmission Change','FontSize',12),ylim([-
detunerange detunerange]),xlim([- (delay_inc*delay_res/2)
(delay_inc*delay_res/2)]),shading
interp,colormap(cool(512)),colorbar,whitebg('black'),title('SRTBC Signal
Surface','FontSize',15),grid on
```

```
% surf(((delay-delay_center)*delay_inc),((detune-
f_center)/FWHM),signal(detune,delay)),ylabel('Normalized
Detune','FontSize',12),xlabel('Normalized
Delay','FontSize',12),zlabel('Transmission Change','FontSize',12),ylim([-
detunerange detunerange]),xlim([- (delay_inc*delay_res/2)
(delay_inc*delay_res/2)]),shading
interp,colormap(cool(512)),colorbar,whitebg('black'),title('SRTBC Signal
Surface','FontSize',15),grid on
```

```
%hold on
```

```
%surf(((detune-f_center)/FWHM),((delay-  
delay_center)*delay_inc),trace_pt_f(delay,detune)+2),xlabel('Normalized  
Detune','FontSize',12),ylabel('Normalized  
Delay','FontSize',12),zlabel('Transmission Change','Fontsize',12),xlim([-  
detunerange detunerange]),ylim([- (delay_inc*delay_res/2)  
(delay_inc*delay_res/2)]),shading  
interp,colormap(cool(512)),colorbar,whitebg('black'),title('SRTBC Signal  
Surface','FontSize',15),grid on  
  
clear
```

BIBLIOGRAPHY

- [1] A. T. Filippov, *The Versatile Soliton* (Birkhäuser, Boston, 2000).
- [2] T. E. Bell, *IEEE Spectr.* **27**, 56 (1990).
- [3] A. V. Buryak, P. Di Trapani, D. V. Skryabin, and S. Trillo, *Phys. Rep.* **370**, 63 (2002).
- [4] J. H. Marburger and E. Dawes, *Phys. Rev. Lett.* **21**, 556 (1968).
- [5] M. Remoissenet, *Waves Called Solitons* (Springer, New York, 1999).
- [6] F. Gesztesy and H. Holden, *Soliton Equations and Their Algebro-Geometric Solutions* (Cambridge, New York, 2003).
- [7] J. S. Russell, *Report on Waves* (Rep. 14th Meet. British Assoc. Adv. Sci. 1844).
- [8] Loosely define, a system is said to be integrable (sometimes it's also called completely integrable or completely separable) if the Hamilton-Jacobi equation describing the system is separable into N independent equations, one for each degree of freedom.
- [9] G. I. Stegeman, M. Sheik-Bhae, E. Van Stryland, and G. Assanto, *Opt. Lett.* **18**, 13 (1993).
- [10] X. Liu, L. Qian, and F. W. Wise, *Phys. Rev. Lett.* **82**, 4631 (1999).
- [11] I. Kang, T. Krauss, and F. W. Wise, *Opt. Lett.* **22**, 1077 (1997).
- [12] P. S. Spencer and K. A. Shore, *J. Opt. Soc. Am. B* **12**, 67 (1997).
- [13] R. H. Enns, S. S. Rangnekar, and A. E. Kaplan, *Phys. Rev. A* **35**, 466 (1987).
- [14] M. L. Quiroga-Teixeiro, A. Berntson, and H. Michinel, *J. Opt. Soc. Am. B* **16**, 1697 (1999).
- [15] I. Kang, T. D. Krauss, F. W. Wise, B. G. Aitken, and N. F. Borrelli, *J. Opt. Soc. Am. B* **12**, 2053 (1995).
- [16] J. M. Harbold, F. Ö. Ilday, F. W. Wise, J. S. Sanghera, V. O. Nguyen, L. B. Shaw, and I. D. Aggarwal, *Opt. Lett.* **27**, 119 (2002).
- [17] F. Smektala, C. Quemard, V. Couderc and A. Barthélémy, *J. Non-Cryst. Sol.* **274**, 232 (2000).
- [18] D. W. Hall, M. A. Newhouse, N. F. Borrelli, W. H. Dumbaugh, and D. L. Weidman, *Appl. Phys. Lett.* **54**, 1293 (1989).

- [19] Y.-F. Chen, K. Beckwitt, F. W. Wise, and B. A. Malomed, Phys. Rev. E. **70**, 046610 (2004).
- [20] T. P. Stanton and L. A. Ostrovsky, Geophys. Res. Lett. **25**, 2695 (1998).
- [21] S. Zhao, X. Xiong, F. Hu, and J. Zhu, Phys. Rev. E **64**, 056621 (2001).
- [22] J. Schefer, M. Boehm, B. Roessli, G. A. Petrákovskii, B. Ouladdiaf, and U. Staub, Appl. Phys. A **74**, s1740 (2002).
- [23] M. Hiraoka, H. Sakamoto, K. Mizoguchi, and R. Kato, Synth. Met. **133-134**, 417 (2003).
- [24] L. Khaykovich, F. Schreck, G. Ferrari, T. Bourdel, J. Cubizolles, L. D. Carr, Y. Castin, and C. Salomon, Science **296**, 1290 (2002).
- [25] P. K. Shukla, and F. Verheest, Astron. Astrophys. **401**, 849 (2003).
- [26] I. Ballai, J. C. Thelen, and B. Roberts, Astron. Astrophys. **404**, 701 (2003).
- [27] J. M. Ivanov, and L. V. Terentieva, Nucl. Phys. B, Proc. Suppl. **124**, 148 (2003).
- [28] L. S. Brizhik, and A. A. Eremko, Electromagn. Biol. Med. **22**, 31 (2003).
- [29] A. Wallraff, A. Lukashenko, J. Lisenfeld, A. Kemp, M. V. Fistul, Y. Koval, and A. V. Ustinov, Nature **425**, 155 (2003).
- [30] G. P. Agrawal, *Nonlinear Fiber Optics* (Academic Press, San Diego, 1995).
- [31] J. McEntee, Fibre Systems Europe, January 2003, p. 19.
- [32] V. E. Zakharov and V. S. Synakh, Sov. Phys. JETP **41**, 62 (1974).
- [33] V. E. Zakharov and A. M. Rubenchik, Sov. Phys. JETP **38**, 494 (1974).
- [34] Y. Silberberg, Opt. Lett. **15**, 1282 (1990).
- [35] L. Bergé, Phys. Rep. **303**, 260 (1998).
- [36] P. M. Goorjian and Y. Silberberg, J. Opt. Soc. Am. B **14**, 3253 (1997).
- [37] A. L. Dyshko, V. N. Lugovoi, and A. M. Prokhorov, Sov. Phys. JETP **34**, 1235 (1972).
- [38] K. J. Blow and D. Wood, IEEE J. Quantum Electron. **25**, 2665 (1989).
- [39] R. J. Hawkins and C. R. Menyuk, Opt. Lett. **18**, 1999 (1993).
- [40] H. S. Eisenberg, R. Morandotti, Y. Silberberg, S. Bar-Ad, D. Ross D, and J. S. Aitchison, Phys. Rev. Lett. **87**, 043902 (2001).

- [41] F. W. Wise, P. Di Trapani, *Opt. Photonics News*, **13**, 28 (2002).
- [42] Y. Chen, *Opt. Lett.* **16**, 4 (1991).
- [43] D. Edmundson, R. H. Enns, *Opt. Lett.* **17**, 586 (1992).
- [44] D. Edmundson, R. H. Enns, *Phys. Rev. A* **51**, 2491 (1995).
- [45] R. McLeod, K. Wagner, and S. Blair, *Phys. Rev. A* **52**, 3254 (1995).
- [46] A. Desyatnikov, A. Maimistov, and B. Malomed, *Phys. Rev. E* **61**, 3107 (2000).
- [47] B. A. Malomed, L.-C. Crasovan, and D. Mihalache, *Physica D* **161**, 187 (2002).
- [48] M. Quiroga-Teixeiro and H. Michinel, *J. Opt. Soc. Am. B* **14**, 2004 (1997).
- [49] I. Towers, A. V. Buryak, R. A. Sammut, B. A. Malomed, L. C. Crasovan, and D. Mihalache, *Phys. Lett. A* **288**, 292 (2001); B. A. Malomed, L.-C. Crasovan, and D. Mihalache, *Physica D* **161**, 187 (2002).
- [50] R. L. Pego and H. A. Warchall, *J. Nonlinear Sci.* **12**, 347 (2002).
- [51] D. Mihalache, D. Mazilu, L.-C. Crasovan, I. Towers, A. V. Buryak, B. A. Malomed, L. Torner, J. P. Torres, and F. Lederer, *Phys. Rev. Lett.* **88**, 073902 (2002).
- [52] J. E. Bjorkholm and A. Ashkin, *Phys. Rev. Lett.* **32**, 129 (1974).
- [53] M. Segev, B. Crosignani, and A. Yariv, *Phys. Rev. Lett.* **68**, 923 (1992).
- [54] G. C. Duree, Jr., J. L. Schultz, G. J. Salamo, M. Segev, A. Yariv, B. Crosignani, P. Di Porto, E. J. Sharp, and R. R. Neurgaonkar, *Phys. Rev. Lett.* **71**, 533 (1993).
- [55] C. Etrich, F. Lederer, B. A. Malomed, T. Pechel, and U. Peschel, *Progr. Optics* **41**, 483 (2000).
- [56] W. E. Torruellas, Z. Wang, D. J. Hagan, E. W. VanStryland, G. I. Stegeman, L. Torner, and C. R. Menyuk, *Phys. Rev. Lett.* **74**, 5036 (1995).
- [57] P. Di Trapani, D. Caironi, G. Valiulis, A. Dubietis, R. Danielius, and A. Piskarskas, *Phys. Rev. Lett.* **81**, 570 (1998).
- [58] X. Liu, K. Beckwitt, and F. W. Wise, *Phys. Rev. E* **62**, 1328 (2000).
- [59] A. Dubietis, E. Gaižauskas, G. Tamošauskas, and P. Di Trapani, *Phys. Rev. Lett.* **92**, 253903 (2004).

- [60] M. A. Porras, A. Parola, D. Faccio, A. Dubietis, and P. Di Trapani, physics/0404040.
- [61] M. A. Porras, G. Valiulis, and P. Di Trapani, Phys. Rev. E **68**, 016613 (2003).
- [62] J. M. Harbold, F. O. Ilday, F. W. Wise, J. S. Sanghera, V. Q. Nguyen, L. B. Shaw, and I. D. Aggarwal, Opt. Lett. **27**, 119 (2002).
- [63] J. M. Harbold, F. O. Ilday, F. W. Wise, and B. G. Aitken, IEEE Photon. Tech. Lett. **14**, 822 (2002).
- [64] T. D. Grow and A. L. Gaeta, private communication.
- [65] K. Beckwitt, Y.-F. Chen, and F. W. Wise, unpublished results.
- [66] C. J. Fecko, J. J. Loparo, and A. Tokmakoff, Opt. Commun. **241**, 521 (2004).